Radio-loud Active Galaxies in the Northern ROSAT All-Sky Survey III: New Spectroscopic Identifications from the RGB BL Lac Survey

S. A. Laurent-Muehleisen[1]
(slauren@igpp.llnl.gov)
University of California-Davis and
The Institute for Geophysics and Planetary Physics,
Lawrence Livermore National Laboratory
7000 East Ave., Livermore, CA 94550, USA

R. I. Kollgaard
(rik@fnal.gov)
Fermi National Accelerator Laboratory, Batavia, IL 60510, USA

R. Ciardullo, E. D. Feigelson
(rbc@astro.psu.edu, edf@astro.psu.edu)
Dept. of Astro. & Astrophys., The Pennsylvania State University,
University Park, PA 16802, USA

W. Brinkmann and J. Siebert
(wpb@rzg.mpg.de, jos@mpe.mpg.de)
Max-Planck-Institut für extraterrestrische Physik,
Giessenbachstrasse, D-85740, Garching, Germany

ABSTRACT

We present new spectroscopic identifications for 169 objects in the RASS-Green Bank (RGB) catalog of radio− and X-ray−emitting AGN. The data presented here significantly increase the fraction of bright RGB objects with classifications. Specifically, we report and discuss the classification of 66 radio-loud quasars, 53 BL Lacs, 33 Broad Line Radio Galaxies, 5 Narrow Line Radio Galaxies, 1 Seyfert I galaxy and 11 galaxies or galaxies in clusters. Over 78% of the identifications we present here are the first published classifications for these sources. The observations we report were undertaken as part of our targeted search program to identify a new, large unbiased sample of BL Lac Objects and we therefore discuss the BL Lac sample extensively. Unlike many previous surveys, we impose no selection criteria based on optical morphology, color or broadband spectral energy distribution. Our classifications

[1]Visiting Astronomer, Kitt Peak National Observatory, National Optical Astronomy Observatories, which is operated by the Association of Universities for Research in Astronomy, Inc. (AURA) under cooperative agreement with the National Science Foundation.

are based solely on a carefully defined set of self-consistent spectroscopic classification criteria. These criteria are then carefully evaluated and particular attention is paid to issues involving the classification and description of BL Lacs. The criteria yielded BL Lac classifications for 53 RGB objects, 38 of which were are newly discovered BL Lacs. We show these RGB BL Lacs exhibit transitional properties between normal galaxies and BL Lacs discovered in previous radio and X-ray surveys. We briefly discuss the broadband flux distributions of these new RGB BL Lacs and the range of Ca II H & K break contrasts (Br_{4000}) they exhibit. We show that there is no clear separation in Br_{4000} between BL Lacs and galaxies detected in the RGB survey, with the distribution of break strengths varying smoothly between 0% and 50%. We also present and use a simple method based on the break strength to estimate the contribution of both the host galaxy and AGN to the 4000 Å flux. We also show that the newly discovered RGB BL Lacs reside in a "zone of avoidance" in the $\log(S_x/S_r)$ vs. $\log(S_o/S_r)$ diagram. This has important implications for BL Lac search strategies since it shows that RASS BL Lac samples will be severely incomplete if candidates are chosen only from among those objects with the highest S_x/S_r flux ratios.

Subject headings: galaxies: active — BL Lacertae objects: general — quasars: general — radio continuum: galaxies — surveys — X-ray: general

Submitted for publication in the Astrophysical Journal Supplement Series

1. Introduction

The identification of X-ray and radio sources has proven to be an effective means of creating samples of quasars, Seyfert and radio galaxies, and BL Lacertae Objects (BL Lacs). The ROSAT All-Sky Survey (RASS) is an unusually large flux-limited survey which contains thousands of previously unidentified AGN. The original catalog created from it consists of over 60,000 soft X-ray (0.08−2.4 keV) sources with a flux limit that varies with ecliptic latitude from 1 to $5\times10^{-13}\,\mathrm{ergs\,s^{-1}cm^{-2}}$ (Voges, 1993). Our goal in the study of this catalog is to create a new, large unbiased sample of BL Lacs.

BL Lacs are relatively rare objects with only ∼250 known prior to the launch of the ROSAT satellite (Padovani & Giommi, 1995a). Although several samples exist, study of the BL Lac phenomena has concentrated on two main samples: the "1 Jy" radio−selected (Stickel et al., 1991) and the Einstein Extended Medium Sensitivity Survey (EMSS; Gioia et al., 1990; Stocke et al., 1991; Maccacaro et al., 1994) X-ray−selected samples. Study of these samples has shown that while radio− and X-ray−selected objects (RBLs and XBLs, respectively) generally share many observational characteristics, the two subclasses are statistically different in a variety of ways (Stocke et al., 1985; Morris et al., 1991; Perlman & Stocke, 1993; Laurent-Muehleisen et al., 1993; Kollgaard et al., 1996; Jannuzi et al., 1994). These results are also valid when more astrophysical classifications are made based on the frequency at which the synchrotron spectrum peaks. In this taxonomy, XBLs are essentially equivalent to "High frequency-peaked BL Lacs" (HBLs) and RBLs correspond well with "Low frequency-peaked BL Lacs" (LBLs; Padovani & Giommi, 1995b; Sambruna et al., 1996). Few objects with intermediate properties are known (see, e.g., Sambruna et al., 1996) and it is these transitional objects which likely hold important clues about the intrinsic nature of BL Lacs.

Creation of a large, unbiased sample of BL Lacs of any particular subclass is, however, a difficult problem because BL Lacs are so rare. They are therefore far outnumbered by other classes of objects in large area radio or X-ray surveys. Their identification in a catalog as large as the RASS therefore requires efficient selection criteria. Techniques based on the characteristic multiwavelength spectral energy distribution (SED) of BL Lacs discovered in EMSS (Gioia et al., 1990; Stocke et al., 1991; Maccacaro et al., 1994) have been used successfully in conjunction with the Einstein Slew Survey (Perlman et al., 1996) and the Hamburg Quasar Survey (Nass et al., 1996). The most common variant of the SED-based search criteria requires prior knowledge of the radio flux to identify candidates (Schachter et al., 1993). Although the requirement for detectable radio flux could theoretically introduce a bias, many studies have shown that radio silent BL Lacs either do not exist or are extremely rare (e.g., Nass et al., 1996; Tapia et al., 1977; Impey & Brand, 1982; Borra & Corriveau, 1984; Stocke et al., 1990; Jannuzi et al., 1993). Therefore, in order to increase our BL Lac search efficiency, we have chosen to study the correlation of the RASS with the Green Bank 6 cm radio survey of the northern sky (Gregory & Condon, 1991; Gregory et al., 1996). We then distinguish our dual radio and X-ray−selected BL Lacs from other emission-line AGN based on their optical spectra (see §4), imposing no other selection criterion

except the presence of a bright optical counterpart. We refer to the resulting BL Lac sample as the RASS-Green Bank or RGB BL Lac sample.

Sections 2 and 3 review the creation and followup VLA[2] observations of the RGB catalog. Section 4 presents the new spectroscopic data and classifications. Individual sources are discussed in §5. The final section presents the broadband characteristics of all the newly classified objects. A more complete discussion of the RGB BL Lac sample appears in a companion paper (Laurent-Muehleisen et al., 1998a). In what follows, we assume H_o=100 km s^{-1} Mpc^{-1}, q_o=0.5 and define spectral indices, α, such that $S_\nu \propto \nu^{-\alpha}$.

2. Selection of Candidate Objects

The RGB catalog was constructed by correlating the RASS with a new ∼150,000 source radio catalog created from the 1987 Green Bank (GB) survey maps (Gregory & Condon, 1991; Gregory et al., 1996). Details of the radio source detection and extraction procedure can be found in Neumann et al. (1994). The radio catalog consists of $\geq 3\sigma$ confidence sources and has a flux density limit of ∼15 mJy in the declination range from $30° - 75°$ and increases to ∼24 mJy at low declinations.

The cross-correlation of the RASS and the 3σ GB survey yielded 2,127 matches with angular separations $<100''$. The complete source lists are given in Laurent-Muehleisen et al. (1997). Because the positional accuracy of both the RASS and GB surveys is insufficient for unambiguous identification of optical counterparts, 5 GHz VLA observations were made of all 2,127 fields (Laurent-Muehleisen et al., 1997) and organized into two catalogs. The first consists of 1,861 sources for which new subarcsecond positions and core radio flux densities were obtained; the second consists of 436 sources for which only low resolution data (∼8″ positional accuracy) were obtained. We refer to this second catalog as the "low resolution VLA catalog". All sources whose radio/X-ray position difference was less than 40″ were compared with Automatic Plate Measuring (APM) scans of the high Galactic latitude (>25°) POSS I photographic plates (Kibblewhite et al., 1984). Optical counterparts within 3″ of RGB sources were identified and both the O (blue) and E (red) magnitudes measured (Laurent-Muehleisen, 1996; Brinkmann et al., 1997). A looser criterion of 5″ was used for sources in the low resolution VLA catalog. Approximately 80% of the high Galactic latitude RGB sources have optical counterparts brighter than the POSS I plate limit of O∼21.5 mag.

Given 1,567 RGB objects which satisfy our radio/X-ray position criterion of 40″ and a probability of ∼5% that a random optical counterpart will reside within 3″ of an RGB radio source (Brinkmann et al., 1997), we expect 78 spurious optical identifications in the RGB catalog.

[2]The NRAO is operated by Associated Universities, Inc., under a cooperative agreement with the National Science Foundation.

However, our spectroscopic observations are limited to objects brighter than O=18.5 mag. An analysis of random high Galactic latitude objects present on the POSS I plates shows that ∼18% of these are brighter than 18.5 mag (Laurent-Muehleisen, 1996). We therefore expect ∼14 spurious radio/optical associations among the optically bright RGB objects. Including the classifications presented in this paper, 80% of RGB sources meeting all the above criteria have been spectroscopically identified. Therefore, only 11 of the bright RGB objects with spectroscopic classifications (0.9%) are likely to be false coincidences.

Optical spectra were obtained for many of the RGB sources which lacked spectroscopic classifications (§4). Unlike other similar surveys, we select our candidate BL Lacs without imposing any criteria other than a limiting optical magnitude of O≤18.5 mag, required by our use of 2-m class telescopes. In particular, candidates were not selected based on their optical morphologly, color, or broadband SEDs. While this greatly increases the number of candidate objects which require spectroscopic classifications, it avoids any presumption that either radio− or X-ray−selected BL Lacs are restricted to particular regions of the $\alpha_{\rm ro}$ vs. $\alpha_{\rm ox}$ diagram where previous studies have found either RBLs or XBLs often reside (e.g., Stocke et al., 1985; Brinkmann et al., 1997, Figure 10). One of the principal results of this survey, discussed below and in Laurent-Muehleisen et al. (1998a), is that many of the characteristics of the RGB BL Lacs such as their broadband SEDs and distribution of Ca II break contrasts, differ significantly from those exhibited by previously compiled samples.

3. Spectroscopic Observations

We obtained low dispersion optical spectra of 171 objects in the RGB catalog over the course of six observing runs from February 1994 through September 1995 with two facilities: the McDonald 2.7-m telescope using the Large Cassegrain Spectrometer with the TI1 CCD and the Kitt Peak National Observatory's 2.1-m telescope using GoldCam and the F3KC Ford CCD (Table 1). While most of our observations were of previously unknown bright (O<18.5 mag) objects, some previously known BL Lacs and fainter unclassified objects were also observed as time and observing conditions allowed. Spectra were taken through a 2″ slit, resulting in a resolution of 10 Å for the McDonald and 14 Å for the Kitt Peak spectra. Table 1 gives the details of each run including date, wavelength coverage and resolution. The slit was not rotated during the night, but kept at a constant orientation. The effect of this should be small, however, since significant effort was made to observe objects as they crossed the meridian.

The goal of these observations is to distinguish BL Lacs from other kinds of radio− and X-ray−emitting objects. We therefore require spectra with sufficiently high S/N ratios to unambiguously detect emission lines characteristic of quasars, Seyfert and radio galaxies. Simulated spectra consisting of various line widths and strengths plus a Poisson noise contribution

show that a broad emission line of $W_\lambda \simeq 5$ Å can be detected at a $\sim 4\,\sigma$ confidence level in a 10 Å resolution spectrum when the S/N≈30. We therefore obtained spectra with S/N$\gtrsim$30 on all objects which we classify here as BL Lacs. Our observing strategy consisted of taking an initial exposure (nominally 20−30 minutes) after which the raw spectrum was examined. If no emission lines or galaxy aborption features were evident, the source was observed repeatedly until a S/N ratio of ≈30 was reached. For the brighter sources which had reached a S/N ratio greater than 30 in one exposure, we obtained a second exposure if the initial raw spectrum lacked any strong features in order to be able to unambiguously distinguish very narrow lines from cosmic rays (see Table 2).

The raw two-dimensional data were reduced following standard procedures using the IRAF (V2.10.4) analysis package. Wavelength calibration was carried out using Helium-Neon-Argon lamps taken at the beginning and end of the night. Comparison of our measured redshifts with published values for previously identified sources shows our redshifts are accurate to 0.001 for z<1.0 and 0.005 for z>1.0. The latter limit is more uncertain because the high redshift objects generally exhibit only broad emission lines.

Final calibrated spectra (including line identifications) for the 171 sources are shown in Figures 1.1−1.174. Many of the spectra were taken under nonphotometric conditions so that the flux density scale given in the figures should only be used as a rough guide to the brightness of the sources. The vast majority of the objects we observed (132 objects or 78%) have no previous reported classification in the literature and we report redshifts for 9 additional objects which previously lacked this information. We also looked at a small number of previously known objects. The majority these objects were previously known BL Lacs without known redshifts.

In Table 2 we give our observing log which consists of the (1) RGB Source Name; (2) Designation for the run on which the data were obtained (see Table 1); (3) Total Exposure Time (4) Number of Exposures per Source; (5) Spectroscopic Classification (see §4); (6) Redshift and (7) Notes. Individual spectra with notes too extensive to list in Table 2 are discussed in Section 5.

4. Results and Spectroscopic Classification

Although both optical and broadband multifrequency colors can yield approximate classifications for extragalactic objects (e.g., Stocke et al., 1991; McMahon, 1991; Schachter et al., 1993), unambiguous classification can only be achieved via spectroscopic observations. This is particularly true for BL Lacs which exhibit a wide range of optical colors and broadband spectral energy distributions, but whose main distinguishing characteristic is their featureless optical continuum (see Weedman, 1986; Padovani, 1992; Kollgaard, 1994; Urry & Padovani, 1995, and references therein). Below we present the results of spectroscopic observations of a large sample of bright, previously unidentified objects in the RGB catalog and our criteria used to classify these objects. Figure 2 summarizes these criteria and Table 2 (column 5) gives the results for the

individual sources.

4.1. Emission-line Objects

Most classes of AGN exhibit strong emission lines. Objects with strong broad permitted lines are classified as Type I AGN while those with only narrow lines are designated as Type II. Distinctions are also generally made between radio-loud and -quiet objects and between objects with high and low optical luminosities (e.g., quasars and Seyfert galaxies, respectively). While recent studies show transitional objects do exist and that these divisions are somewhat arbitrary, they do correlate with important differences between the various classes (e.g., Wilson & Colbert, 1995; Mas-Hesse et al., 1992, and references therein). We therefore classify objects with these divisions in mind. Specifically, we classify all emission-line AGN as follows:

- Following Kellermann et al. (1989), we define radio-loud objects as those having $\log(S_r/S_{opt})>1.0$ where the radio flux density is the core emission measured at 5 GHz and the optical flux density is measured from the POSS O plates. This parameter is then used to distinguish radio-quiet vs. radio-loud quasars and also Seyfert vs. radio galaxies. Alternately, radio luminosity can be used to define radio-loudness. These two methods produce nearly the same classification for the objects presented here, provided the limiting radio power is chosen to be $\log P_r=23.4\,W\,Hz^{-1}$, equivalent to the definition used by Ulvestad & Wilson (1989) and Miller et al. (1993), after converting to our choice of cosmology. The eight RGB objects whose classification is dependent on the differences in these two definitions are denoted in Table 2.

- The distinction between Type I and Type II low power AGN (the radio-quiet Seyfert I and II galaxies and the radio-loud Broad and Narrow Line Radio Galaxies) is based on the width of optical emission lines. Type I AGN exhibit both broad permitted and narrow forbidden lines. Type II AGN exhibit only narrow lines. We choose as a dividing point the presence of lines with FWHM velocity of $1000\,km\,s^{-1}$ (Osterbrock, 1989). This criterion conveniently matches our resolution which roughly corresponds to a FWHM of $1000\,km\,s^{-1}$.

- The division between quasars and low power AGN (Seyfert and radio galaxies) is traditionally based on the Johnson B magnitude (4400 Å effective wavelength) and lies between $-23.0<M_B<-21.0$ mag (Osterbrock, 1989). The uncertainties in the POSS O magnitudes are such that we consider them to be equivalent to B magnitudes and we choose $M_O=-22.0$ mag as the faintest absolute magnitude of RGB quasars. Using this definition, we find no "narrow-line" quasars in our sample, since our brightest narrow-line object (RGB J0207+295A) has $M_O=-20.9$ mag.

The classification of objects is then determined as follows (see Figure 2): Objects with $\log(S_r/S_{opt})\geq1.0$ are classified as radio-loud, and those objects which also have $M_O\leq-22.0$ mag

are classified as radio-loud quasars. Radio-loud objects with $M_O > -22.0$ mag are classified as radio galaxies, with the width of the lines distinguishing between Broad Line Radio Galaxies (BLRGs) and Narrow Line Radio Galaxies (NLRGs).

For radio-quiet objects ($\log S_r/S_{opt} < 1.0$), the optically luminous ($M_O \leq -22.0$ mag) objects would have been classified as radio-quiet quasars, but we found no such objects in our sample. The optically less luminous sources are either Seyfert I or II galaxies, depending on the line widths. We find only one such object of this type (RGB J1518+407) which, because it exhibits a broad (FWHM$\approx$1900 km s^{-1}) Hα line, we classify as a Seyfert I galaxy (also see §5).

We note that the ratio of quasars to low power emission-line AGN (1.7:1) is similar to that reported for other radio-/X-ray−selected samples which have flux limits similar to the RGB survey (Morris et al., 1991; Moran et al., 1996). The nearly complete absence of radio-quiet objects is also not surprising, given the radio flux limit of the RGB catalog ($\sim$20 mJy).

4.2. Galaxies and Clusters

The classification of galaxies has been made solely on the basis of the optical spectra presented in the figures. If the object lacked broad AGN-like emission lines and showed no indications of an underlying nonthermal powerlaw component (see §4.3), we classify the object as a galaxy (see Figure 2). However, these RGB galaxies exhibit both radio and X-ray emission far in excess of that expected from normal elliptical galaxies. It is possible the X-ray emission arises not from the radio source itself, but from a surrounding diffuse X-ray cluster. Unfortunately, available optical images are not deep enough to determine whether or not a cluster is present nor does our X-ray data have sufficient resolution to evaluate this hypothesis. However, because previously known clusters are associated with four of these galaxies, we classify them as "Clusters" in Tables 2 and 4.

The other eight objects with seemingly normal elliptical galaxy spectra (albeit with occasional weak emission lines; see Figures 1.8, 1.14 & 1.165), but very high X-ray and radio luminosties, may be as yet undetected clusters or they may be optically weak, but radio and X-ray luminous AGN. These RGB sources have log $P_r > 23.0$ W Hz^{-1} and log $L_X > 43.0$ erg s^{-1}. While radio luminosities of this magnitude are similar to those exhibited by bright B2 and 3CR radio galaxies (Fanti et al., 1978; Laing et al., 1983; Ulrich, 1989), the X-ray luminosity of these RGB sources is 1-3 orders of magnitude larger (Fabbiano et al., 1984; Morganti et al., 1988). There is precedent for this kind of object, including 3C 264 (Elvis et al., 1981; Baum et al., 1988) and the Einstein source J2310−43. Tanabaum et al. (1997) conclude the latter object is likely an AGN similar to BL Lacs which, either because of orientation or certain intrinsic properties of the AGN itself, lack both strong emission lines and significant nonthermal emission in the optical band.

Alternatively, it is also possible these objects are "optically passive X-ray galaxies" (Griffiths et al., 1995; Moran et al., 1996; Tanabaum et al., 1997), extraordinary early-type galaxies which

emit at least an order of magnitude more radio and X-ray luminosity than other galaxies with similar optical properties. Moran et al. (1996) found 8 such objects in the Einstein Two-Sigma catalog. They concluded, on the basis of followup radio observations, that the objects were unlikely to be hidden AGN whereas optical imaging showed that they may be members of previously unknown clusters or small groups of galaxies. Alternatively, these sources may be early type galaxies with an extraordinarily hot ISM. Similar objects have also been found in selected deep ROSAT PSPC fields and the study of them has led to the suggestion that a mini-cooling flow in a small cluster or group of galaxies may trigger AGN activity in these objects (Griffiths et al., 1995).

Without additional information, especially deep optical imaging, we cannot make any conclusions about the true nature of the galaxies presented here. We therefore assign the "Galaxy" classification to them, but note that these objects are not typical early-type galaxies and that followup observations are warranted.

4.3. BL Lacs

The classical definition of a BL Lac is an AGN with a highly variable, linearly polarized, nonthermal continuum which contains no optical emission lines (Stein et al., 1976). It is now generally recognized that objects which violate some of these criteria generally exhibit BL Lac-like properties and should be considered part of the class (see Kollgaard [1994] for a summary). For example, long-term, high S/N monitoring of BL Lacs has shown that many exhibit low luminosity emission lines with the most striking example being BL Lac itself (Miller & Hawley, 1977; Corbett et al., 1996). A standard definition is that BL Lacs are AGN with emission lines whose equivalent width does not exceed 5 Å (Stocke et al., 1991). However, many observational criteria exist which have added additional constraints to the classical definition (Remillard et al., 1986; Schwartz et al., 1989; Stickel et al., 1991; Stocke et al., 1991; Perlman et al., 1996; Nass et al., 1996).

While these new criteria originally delineated clear boundaries between BL Lacs and other classes of AGN, it is becoming clear that they are more arbitrary than originally suspected. The resulting selection affects are only now being addressed (e.g., Browne & Marchã, 1993; Padovani & Giommi, 1995a; Marchã et al., 1996; Scarpa & Falomo, 1997). Because X-ray−selected BL Lacs (XBLs/HBLs) typically exhibit properties intermediate between radio galaxies and radio-selected BL Lacs (RBLs/LBLs), the issues are particularly relevant in X-ray−selected samples which the RGB at least partially is. New spectroscopic observations also show the division between BL Lacs and weak-lined AGN and elliptical galaxies is becoming increasingly blurred (Marchã et al., 1996; Scarpa & Falomo, 1997). It is therefore necessary to develop a BL Lac definition which encompasses objects which exhibit the same *intrinsic* (not observed) characteristics. This is particularly difficult because much of the observed radiation in BL Lacs is dominated by orientation-dependent beamed radiation.

We consider the approach proposed by Marchã et al. (1996), who present a set of

self-consistent orientation-independent rules for discriminating BL Lacs from ordinary quasars, Seyfert, radio and elliptical galaxies. The Marchã et al. (1996) definition relies on the results of Dressler & Shectman (1987) who show that less than 5% of elliptical galaxies have a Ca II H&K ($\lambda\lambda$3933,3968) break contrast, Br_{4000}, below 0.4. Here, the term "break contrast" refers to the relative depression of the continuum blueward of the Ca II H&K lines (see below). It is therefore likely that any object with a weaker break contrast has an additional blue component present. It is also true that many objects with $\mathrm{Br}_{4000}\geq 0.4$ may have a similar continuum present, but it is impossible to determine this on the basis of the break contrast or any other property that correlates with it. This effect will obviously become more important for the intrinsically most luminous host galaxies with the weakest blue components, assuming that the two are uncorrelated. However, even modest host galaxy luminosities can be sufficient to obscure contributions from underlying blue continua (Halpern et al., 1997).

In addition to these complications, it is important to note that there are two possible sources of the additional component: an AGN or star formation. Ellipticals must be very young in order to have enough blue light present to significantly weaken the break contrast (González, 1993). The RGB objects with weak break contrasts are at redshifts that correspond to a lookback time of only $\sim$1 Gyr and it is therefore unlikely these objects constitute a young population of starforming ellipticals. Merger induced star formation is a far more plausible scenario. Carter et al. (1988) find that $\sim$15% of galaxies with abnormally weak break contrasts show significant evidence of star formation where up to 60% of the nuclear light at 4000 Å originates in hot young stars. However, these objects typically also show Balmer lines whose strength varies with the assumed contribution from hot young stars. We therefore assert that galaxies with weak break contrasts which lack spectral evidence for a burst of recent star formation in the form of Balmer lines, are likely old elliptical galaxies which harbor a weak BL Lac nucleus. The BL Lac classification is also strengthened by the presence of high luminosity radio and X-ray emission consistent with the AGN hypothesis.

We adopt the same definition of break contrast used by Dressler & Shectman (1987), namely:

$$\mathrm{Br}_{4000} = \frac{f^+ - f^-}{f^+}, \tag{1}$$

where f^+ is the average flux in the range 4050−4250 Å and f^- is the average flux in the range 3750−3950 Å. All wavelengths are in the rest frame. Two caveats deserve mention. First, f^+ and f^- are *average* fluxes which are good measures only if the slopes in each band are flat. For most sources this appears to be true. Second, the wavelength range for f^- includes the Ca II H, but not the Ca II K, line. This will decrease f^- slightly compared to the value it would have if the region around 3933 Å were excluded. However, this produces a change which is less than 1−2% in our reported break strengths and is less than the uncertainties introduced by observational effects. The value of the break strength in those objects for which we could detect it are given in the notes to Table 2 and we show a histogram of our measured break strengths in Figure 3. We note that the RGB objects observed here exhibit a continuous range of break contrasts, ranging from

0%-50%, and that no clear point exists where a division between BL Lacs and normal ellipticals can be made. Nevertheless, our formal definition presented in §4.3 makes an arbitrary cut at Br_{4000}=40%. We note that we are following up with optical polarimetry, high resolution (nuclear) optical imaging and X-ray and radio studies all RGB BL Lacs and galaxies *regardless* of break strength in order to determine the presence of any nuclear BL Lac component. It is therefore possible that some new RGB galaxies may be reclassified as BL Lacs in the future, but we have no definitive evidence at present to warrant such reclassification.

Break contrast alone is not enough to unambiguously distinguish BL Lacs from other types of low luminosity extragalactic objects. An emission line criterion must be established to exclude both radio and Seyfert galaxies which also show absorption features. A maximum permitted equivalent width has traditionally been set at W_λ=5 Å (Stickel et al., 1991; Stocke et al., 1991), although some definitions have used the rest and others the observed frame. In either case, there is mounting evidence that this may be too stringent a limit (e.g., Perlman et al., 1996; Marchã et al., 1996; Stocke & Rector, 1997) and that the only differences in the line properties of BL Lacs and highly polarized beamed quasars (HPQ blazars) are those introduced by the arbitrary 5 Å equivalent width criterion (Scarpa & Falomo, 1997). In both these cases, the measured equivalent width depends on the strength of beamed optical emission in the sense that an object very close to the line-of-sight will exhibit smaller equivalent widths than one further from the line-of-sight because continuum emission will be enhanced, but the intrinsic line luminosity will remain the same.

Marchã et al. (1996) suggest criteria which take this effect into account. Using examples from their '200 mJy' radio-selected sample and models which vary the orientation of 3C 371 (RGB J1806+698) to the line-of-sight, they simultaneously characterize the effects beaming produce in the break contrast − equivalent width plane (the $Br_{4000}-W_\lambda$ plane; see Figure 6 in Marchã et al., 1996). All objects which are more 'BL Lac-like" than 3C 371 (i.e., have weaker lines for a given break strength) and *also* have $Br_{4000}<40\%$ are considered BL Lacs. The Marchã et al. (1996) criteria encompass nearly all objects which would be classified as BL Lacs using the traditional criteria ($W_\lambda \leq 5$ Å and $Br_{4000} \leq 25\%$; Stocke et al., 1991) but cover a larger region of the $Br_{4000}-W_\lambda$ plane. While these criteria are arbitrary, they are a useful first step toward unambiguously defining the BL Lac class.

The RGB BL Lac classification criteria we adopt are summarized in Figure 2 and are as follows:

- If the spectrum is featureless or the only features observed are emission lines with $W_\lambda \leq 5$ Å, the object is classified as a BL Lac. All measurements of equivalent width are taken in the rest-frame.
- If absorption features are present and $Br_{4000}<25\%$, we classify the object as a BL Lac, provided any emission lines present have $W_\lambda \leq 5$ Å and no strong Balmer absorption lines are observed. Objects with strong Balmer absorption would have been classified as starforming

galaxies but no such objects were found. However, four RGB BL Lacs exhibit very weak Balmer absorption lines. They are RGB J0656+426, RGB J1516+293, RGB J2250+384 and RGB J2322+346 (Figures 1.23, 1.89, 1.162 & 1.173). All have been classified as "BL Lacs?".

- If the Ca II break contrast is between 25-40%, we classify the object as a possible BL Lac if any emission line present also has an equivalent width smaller than that required by the Marchã et al. (1996) criterion (specified by the symbol W_λ^M in Table 2) for that particular break strength. These tentative RGB BL Lacs are denoted by a question mark after their classification. As described above, any objects with strong Balmer absorption lines would have been classified as starforming galaxies. We note that because the spectroscopic setup was designed to obtain Br_{4000} for z$\simeq$0$-$0.5, many spectra do not extend far enough to the red to determine the Hα emission line strength. For this reason, the equivalent width criterion we use for classification is not as uniform as that employed by Marchã et al. (1996), whose equivalent width measurements are generally based on Hα. Followup spectroscopy in the region where Hα is expected would be useful in standardizing the classification of these objects. We therefore place the note "Hα useful" in Table 2 for these sources.

- If the Ca II break contrast is >40% we classify the object as a galaxy because of the lack of spectroscopic evidence for an AGN. We note, however, that a low luminosity BL Lac nucleus may be present in some of these objects. We again emphasize that the distribution of Ca II break contrasts shows no clear point at which the spectroscopic division between galaxies and BL Lacs should be made (Figure 3). We are pursuing higher S/N observations, studies which characterize the strength of Hα, optical polarimetry and spatially resolved spectroscopy of the core of these objects since they may help distinguish the two classes.

The formal RGB BL Lac definition is given by the above criteria. However, because of either poor quality data or variations in spectroscopic setup, we define two further criteria:

- When our spectra did not extend far enough to the blue to measure Br_{4000}, we made a tentative classification based the criteria defined above and, in the absence of Br_{4000}, on the O$-$E colors. Objects with weak (or no) emission lines and colors bluer than O$-$E=2.0 mag are tentatively classified as BL Lacs. In Table 2 we report both the colors and the note "Br_{4000} needed" for these objects which we then denote with the "BL Lac?" classification.

- We classify one object (RGB J1012+424) which appears to have two emission lines in its spectrum ($W_\lambda(\lambda4554)$=4 Å & $W_\lambda(\lambda4380)$=10 Å) and no measured Ca II break contrast as a possible BL Lac ("BL Lac?" in all tables). Although the lines violate the criteria given above, the measured wavelengths of the emission features correspond to no obvious emission line pairs and therefore may not be real. Further observations are required.

The variety of criteria used to classify BL Lacs raises concerns regarding the completeness of various surveys. Even catalogs which are completely identified may be missing BL Lacs because

of the misclassification of objects, or even contain additional objects which are not BL Lacs at all. This latter point was raised most recently by Stocke & Rector (1997) who suggest the 1 Jy RBL sample contains a number of lensed radio-loud quasars. On the other hand, there is evidence that differences in classification criteria have not led to serious errors in the characterization of the bulk properties of the XBL subclass (Laurent-Muehleisen et al., 1993), although existing samples may be incomplete, particularly at low luminositiies (Browne & Marchã, 1993; Halpern et al., 1997). Analyses which rely on the space density and shape of the luminosity function or LogN−LogS distribution will be particularly sensitive to these issues and care must therefore be taken to address them (Laurent-Muehleisen et al., 1998a).

5. Comments on Individual Sources

Before presenting the multiwavelength properties of the RGB sources, we briefly discuss some individual sources.

RGB J0044+193. − The presence of both broad Balmer lines and Fe emission at ∼5300 Å in this object is similar to that seen in Narrow-lined Seyfert I galaxies. Unlike this object, however, Narrow-lined Seyfert I galaxies are typically radio-quiet (Ulvestad et al., 1995). Therefore, because this object is both radio-loud and optically bright ($M_O \leq -22.0$ mag), we tentatively classify it as a radio-loud quasar, although it is unusual for radio-loud quasars to exhibit strong Fe emission (Boroson & Green, 1992). However, the subclass of radio-loud AGN which are also strong IRAS sources, as this object is, have been known exhibit extremly strong Fe emission (Lipari et al., 1993).

RGB J1248+514. − This object is an M4 (±1) star with an implied X-ray luminosity of $10^{29}-10^{30}$ erg s^{-1}. Stars of this type typically exhibit strong Balmer emission (Mullan & Fleming, 1996), but Figure 1.58 shows only aborption lines. Additionally, the implied radio luminosity of this source is a factor of $\sim 10^3$ larger than the most radio luminous dMe stars known (Caillault, 1989). We therefore believe the optical counterpart to this source is a spurious identification (§2).

RGB J1413+436. − This object may be a radio− and X-ray−luminous galaxy (§4.2) or a low luminosity AGN. Our spectrum does not extend far enough to the blue to measure Br_{4000}, making it difficult to determine the fraction of nonthermal emission. The FWHM of the Hα/[NII] blend is approximately 1900 km s^{-1}, which is too broad for a galaxy classification. We therefore classify this object as a BLRG.

RGB J1808+468. − The RASS and VLA positions of this source differ by 69″, greater than our 40″ radio/X-ray offset criterion (§2). However, new HRI observations show the radio and X-ray positions differ by only 2″ (Laurent-Muehleisen et al., 1998b).

RGB J1811+584. − The spectrum of this object is that of a K star or very low redshift elliptical galaxy (z=0.002). New data obtained at Lick observatory (not presented here) show that

this object has zero redshift and is therefore likely a spurious identification (see §2).

RGB J1922+691. – This object is notable for the strength of its forbidden O[II] and O[III] lines and concurrent lack of any detectable Balmer lines. Similar objects have been found in other surveys (e.g., the EMSS; Stocke et al., 1991). Observations of Hα would be useful to determine whether this object simply has a large Balmer decrement or if the Balmer lines are intrinsically weak.

6. Multiwavelength Properties

In Table 3 we reproduce for convenience the coordinates and multiband fluxes given in Laurent-Muehleisen et al. (1997) and Brinkmann et al. (1997). For those objects with measured break contrasts, we also estimate the separate contributions of the galaxy and AGN to the total optical flux (see below). Table 3 also lists the radio-loudness parameter ($\log \mathrm{S_r/S_{opt}}$), redshift and classification for all sources. The radio-loudness parameter has been K-corrected assuming $\alpha_{\mathrm{r,core}}$=0.0 and α_{opt}=1.0, although individual fluxes in Table 3 have not been K-corrected. Sources with unknown redshifts are K-corrected using the median redshift for the class (0.16 for BL Lacs, 0.770 and 0.231 for those quasars and BLRGs, respectively, for which a redshift could not be determined). These objects are all at high Galactic latitude (b>25°) and have not been corrected for extinction. Such corrections would be small compared with the ∼0.5 mag uncertainty in the POSS derived POSS O magnitudes (Laurent-Muehleisen, 1996). X-ray fluxes have been computed from the RASS count rates by assuming an average spectral index of α_{x}=1.2 and Galactic N_{H} absorption (Dickey & Lockman, 1990; Stark et al., 1992; Brinkmann et al., 1995).

Table 4 contains the multiband luminosities of the newly identified RGB objects grouped by spectroscopic class and lists the logarithm of the 5 GHz radio power, the absolute O magnitude and the logarithm of the X-ray luminosity for all objects which have a measured redshift. All luminosities have been K-corrected.

Decomposition of the optical magnitude into separate AGN and galaxy components was performed only for those sources for which a Ca II break contrast was measured. The separate contributions are estimated by assuming the host galaxy has an intrinsic break contrast of $\mathrm{Br_{4000}}$=50% and that contrasts smaller than this are a result of an underlying blue powerlaw continuum. The AGN magnitudes are therefore likely upper limits. Since the contrast is measured at ∼4000 Å and the effective wavelength of the POSS I O magnitude is ∼4400 Å, the true fraction of light originating in the galaxy does not change substantially in this 400 Å bandpass. We therefore calculate the AGN contribution as follows: the AGN continuum just redward and blueward of 4000 Å is assumed to be a constant, A (valid because the break at 4000 Å is very sharp). Then,

$$\frac{R-B}{R} \equiv 0.5 \quad \text{and} \quad \frac{R+A-(B+A)}{R+A} = s, \tag{2}$$

where A is the flux arising from the AGN component at 4000 Å, B is the flux of the galaxy component blueward of the break, R is the galaxy flux redward of the break, and s represents the measured break strength. The relative contribution of AGN to host galaxy light is then given by:

$$\frac{A}{R} = \frac{0.5}{s} - 1. \tag{3}$$

While not as accurate as a full spectral deconvolution, our method yields an AGN light fraction that differs by only 6% from that obtained by a full spectral deconvolution of the BL Lac object E 0336−248 (Halpern et al., 1997). This yields confidence that our estimates of the fraction of light arising from the AGN are accurate to ±10% or better. Generally we estimate that 30-60% of the total flux at 4000 Å is contributed by the AGN.

In Figures 4−6, we show histograms of the multiband luminosities of the various classes of sources. Because the samples presented here are incomplete (consisting only of those RGB objects which did not have a previous spectroscopic classification), a detailed analysis of these data is unwarranted. However the figures provide a useful evaluation of many of the classification criteria discussed here and we therefore limit our discussion to these issues. A full discussion of the properties of the all 118 RGB BL Lacs will be presented in Laurent-Muehleisen et al. (1998a).

The definitions of RGB BLRGs and quasars differ only by limits set on their optical luminosities (§4.1). Nevertheless, the RGB quasars constitute the most luminous class of objects in all three wavebands although both the radio and X-ray luminosities of the BLRGs (and NLRGs) overlap that of the quasars. The RGB classification criteria have the effect of abruptly truncating both distributions at M_O=−22.0 mag (Figure 5). However, a small discontinuity in the combined absolute optical magnitudes of the BLRGs and quasars exists at $M_O \simeq -22.0$ mag. Although it is not a well-defined break, this indicates that our criteria do correspond to some intrinsic difference in the quasar and BLRG populations. However, Figure 5 shows that many transition objects undoubtedly exist and that detailed study of the RGB sample would provide useful insight into the transition between these two AGN classes.

As noted in §4.2, the RGB galaxies are overluminous in both the radio and X-ray. As discussed above, the X-ray emission may (at least partially) originate in diffuse cluster emission, but the strength of the radio emission is difficult to explain. It is possible that many of these objects belong to the new class of optically passive X-ray galaxies, although other explanations exist (see §4.2).

The newly discovered BL Lacs show a wide range of radio, optical and X-ray luminosities.

The broadband spectral energy distribution of these objects is in fact much larger than expected, a point which will be discussed extensively in Laurent-Muehleisen et al. (1998a). Figure 5 also shows the distributions of both the nuclear and host galaxy absolute blue magnitudes for those 16 RGB BL Lacs with measured break contrasts (§6). Both the host galaxy and AGN absolute magnitudes peak near $M_O=-19.5$ mag and both distributions are smooth and well-behaved. Given an uncertainty of $\sim$0.5 mag in the apparent O magnitudes, the average estimated RGB BL Lac host galaxy luminosity of $\langle M_V\rangle=-23.5$ mag is consistent with more precise measurements obtained for samples of low redshift BL Lacs from the 1 Jy sample ($\langle M_V\rangle=-22.9$; Stickel et al., 1993) and Fanaroff-Riley Type I radio galaxies ($\langle M_V\rangle=-23.1$; Smith & Heckman, 1989), after converting to the same cosmology and assuming a typical host galaxy has a (B−V) color of $\sim$1.0. This supports our assertion that the method presented in §6 is reasonably sound.

The full RGB sample is large and flux-limited (in both the radio and X-ray) and as such can provide useful insight into the transitions between various classes of AGN. Of particular interest is the transition between RBLs and XBLs. Figure 7 shows the $\log(S_x/S_r)$ vs. $\log(S_o/S_r)$ diagram for the newly identified RGB objects (see Figure 11 in Brinkmann et al., 1997). As noted in Brinkmann et al. (1997), RGB objects generally span the intermediate region in this diagram between those regions populated by radio-loud quasars and RBLs at one end (low S_x/S_r ratio) and XBLs at the other (high S_x/S_r ratios). Figure 7 shows this "zone of avoidance" in which very few previously known BL Lacs reside. While it is clear the fraction of RGB BL Lacs increases with increasing S_x/S_r, more than 20% of the newly discoverd RGB BL Lacs reside in the region previously unpopulated by BL Lacs. This has important implications for BL Lac search strategies since it shows that RASS BL Lac samples will be severely incomplete if candidates are selected to have extreme S_x/S_r flux ratios.

7. Summary

We present spectra of 169 sources and their spectroscopic classifications. These sources belong to the RGB (RASS-Green Bank) sample which is based on spatial coincidences between the ROSAT All-Sky Survey, Green Bank 5 GHz, and APM POSS I catalogs. The criteria used to establish various classifications are discussed in detail. Of the 169 objects presented here, we find 53 BL Lacs, 66 radio-loud quasars, 33 BLRGs, 5 NLRGs, 1 Seyfert I galaxy and 11 galaxies or galaxies in clusters. (The optical counterparts of two objects are also identified as spurious; see §4.2). For the vast majority of the objects (83%), the data we present here yield for the first time a spectroscopic classification or a redshift for an object previously classified by other means.

Including the results of this work, approximately 70% of the RGB objects with POSS I counterparts and over 80% of the objects with counterparts brighter than O=18 mag now have reliable spectroscopic classifications (see Brinkmann et al. (1995) and Brinkmann et al. (1997) for the other identifications). The numerous quasars and radio galaxies in addition to the less numerous, but intriguing radio and X-ray luminous early-type galaxies, form a useful database

for further study, particularly since the RGB sample is simultaneously both an X-ray and radio flux-limited sample.

Our ultimate goal is the creation of a large unbiased sample of BL Lacs and in this study we report the discovery of 38 previously unknown BL Lacs. We also present and analyze our observations of 15 previously known BL Lacs, which were reobserved because they lacked redshift information. Particular attention is paid to the spectral information obtained for all BL Lac candidates. Many spectra show evidence for the underlying host galaxy. Following Marchã et al. (1996), we characterize the mixture of host galaxy and nuclear BL Lac light in terms of the Ca II H&K break contrast (Br_{4000}). Break strengths range from 0% to 50%, with those object with $Br_{4000}>40\%$ being classified as galaxies although no clear division between BL Lacs and galaxies exists. We present a simple method for decomposing blue optical magnitudes into separate contributions from the host galaxy and BL Lac. In the absence of high S/N spatially resolved spectra, we show this method gives reasonable upper limits to the optical AGN luminosity.

The RGB sample constitutes a new well-defined sample which is significantly larger and more sensitive than previous samples obtained from radio and X-ray−selected surveys. It thus has the potential to reveal new aspects of AGN populations and the astrophysics which govern radio-loud active galaxies. In particular, we show that the RGB sample includes many BL Lacs with properties between those of traditional radio− and X-ray−selected BL Lacs. In an associated paper (Laurent-Muehleisen et al., 1998a), we will present the full RGB sample of 118 BL Lacs and discuss their properties in detail in addition to implications this sample has for the unified scheme.

We extend our thanks to Dr. Richard McMahon who provided information on the RGB optical counterparts prior to publication, to Dr. Ed Moran for useful discussions on the spectroscopic classification of the emission line AGN presented here and to Dr. Joe Pesce for useful commentary on the manuscript. This work was partially supported by NASA Grant NAGW-2120 to EDF and partially by the Department of Energy at the Lawrence Livermore National Lab under contract W-7405-ENG-48. RIK acknowledges support from Fermi National Accelerator Laboratory. We have made use of the NASA/IPAC Extragalactic Database, operated by the Jet Propulsion Laboratory, California Institute of Technology, under contract with NASA. SALM also acknowledges partial support from the NASA Space Grant Consortium through their Space Grant Fellow program.

References

Baum, S. A., Heckman, T., Bridle, A., van Breugel, W., & Miley, G. 1988, ApJS, 68, 643

Boroson, T. A., & Green, R. F. 1992, ApJS, 80, 109

Borra, E. F., & Corriveau, G. 1984, ApJ, 276, 449

Brinkmann, W., Siebert, J., Reich, W., Fürst, E., Reich, P., Voges, W., Trümper, J., & Wielebinski, R. 1995, A&AS, 109, 147

Brinkmann, W., Siebert, J., Feigelson, E. D., Kollgaard, R. I., Laurent-Muehleisen, S. A., Reich, P., Voges, W., Trümper, J., & McMahon, R. 1997, A&A, 323, 739

Browne, I. W. A., & Marchã, M. J. M. 1993, MNRAS, 261, 795

Caillault, J.-P. 1989, AJ, 97, 163

Carter, D., Prieur, J. L., Wilkinson, A., Sparks, W. B., & Malin, D. F. 1988, MNRAS, 235, 813

Corbett, E. A., Robinson, A., Axon, D. J., Hough, J. H., Jeffries, R. D., Thurston, M. R., & Young, G. S. 1996, MNRAS, 281, 737

Dickey, J. M., & Lockman, F. J. 1990, ARAA, 28, 215

Dressler, A., & Shectman, S. 1987, AJ, 94, 899

Elvis, M., Schreier, E. J., Tonry, J., Davis, M., & Huchra, J. P. 1981, ApJ, 264, 20

Fabbiano, G., Miller, L., Trinchieri, G., Longair, M., & Elvis, M. 1984, ApJ, 277, 115

Fanti, R., Gioia, I., Lari, C., & Ulrich, M.-H. 1978, A&AS, 34, 341

Gioia, I., Maccacaro, T., Schild, R., Wolter, A., Stocke, J., Morris, S., & Henry, J. P. 1990, ApJS, 72, 567

González, J. 1993, PhD Thesis, University of California, Santa Cruz

Gregory, P. C., & Condon, J. J. 1991, ApJS, 75, 1011

Gregory, P. C., Scott, W. K., Douglas, K., & Condon, J. J. 1996, ApJS, 103, 427

Griffiths, R. E., Georgantopoulos, I., Boyle, B. J., Stewart, G. C., Shanks, T., & Della Ceca, R. 1995, MNRAS, 275, 77

Halpern, J. P., Eracleous, M. E., & Forster, K. 1997, AJ, To Appear

Impey, C. D., & Brand, P. W. J. L. 1982, MNRAS, 201, 849

Jannuzi, B. T., Green, R. F., & French, H. 1993, ApJ, 404, 100

Jannuzi, B. T., Smith, P. S., & Elston, R. 1994, ApJ, 428, 130

Kellermann, K. I., Sramek, R. A., Schmidt, M., Shaffer, D. B., & Green, R. F. 1989, AJ, 98, 1195

Kibblewhite, E. J., Bridgeland, M. T., Bunclark, P. A., & Irwin, M. J. 1984, Astronomical Microdensity Conference, NASA-2317, 277

Kollgaard, R. I. 1994, Vistas in Astronomy, 38, 29

Kollgaard, R. I., Palma, C., Laurent-Muehleisen, S. A., & Feigelson, E. D. 1996, ApJ, 465, 115

Laing, R. A., Riley, J. M., & Longair, M. S. 1983, MNRAS, 204, 151

Laurent-Muehleisen, S. A. 1996, PhD Thesis, The Pennsylvania State University

Laurent-Muehleisen, S. A., Kollgaard, R. I., Moellenbrock, G. A., & Feigelson, E. D. 1993, AJ, 106, 875

Laurent-Muehleisen, S. A., Kollgaard, R. I., Ryan, P. J., Feigelson, E. D., Brinkmann, W., & Siebert, J. 1997, A&AS, 122, 235

Laurent-Muehleisen, S. A., Kollgaard, R. I., Feigelson, E. D., & Brinkmann, W. 1998a, ApJ, (In Preparation)

Laurent-Muehleisen, S. A., Kollgaard, R. I., & Feigelson, E. D. 1998b, ApJ, (in preparation)

Lipari, S., Terlevich, R., & Macchetto, F. 1993, ApJ, 406, 451

Maccacaro, T., Wolter, A., McLean, B., Gioia, I. M., Stocke, J. T., Della Ceca, R., Burg, R., & R., F. 1994, ApJLett Commun., 29, 267

Marchã, M. J. M., Browne, I. W. A., Impey, C. D., & Smith, P. S. 1996, MNRAS, 281, 425

Mas-Hesse, J. M., Rodríguez-Pascual, P. M., de Córdoba, L. S. F., & Mirabel, I. F. 1992, ApJS, 92, 599

McMahon, R. G. 1991, in The Space Distribution of Quasars, ed. D. Crampton (ASP Conference Series), Vol. 21, p. 129

Miller, J. S., & Hawley, S. A. 1977, ApJLett, 212, L47

Miller, P., Rawlings, S., & Sanders, R. 1993, MNRAS, 263, 425

Moran, E. C., Helfand, D. J., Becker, R. H., & White, R. L. 1996, ApJ, 461, 127

Morganti, R., Fanti, R., Gioia, I. M., Harris, D. E., Parma, P., & de Ruiter, H. 1988, A&A, 189, 11

Morris, S. L., Stocke, J. T., Gioia, I. M., Schild, R. E., Wolter, A., Maccacaro, T., & Della Ceca, R. 1991, ApJ, 380, 49

Mullan, D. J., & Fleming, T. A. 1996, ApJ, 464, 890

Nass, P., Bade, N., Kollgaard, R. I., Laurent-Muehleisen, S. A., Reimers, D., & Voges, W. 1996, A&A, 309, 419

Neumann, M., Reich, W., Fürst, E., Brinkmann, W., Reich, P., Siebert, J., Wielebinski, R., & Trümper, J. 1994, A&AS, 106, 303

Osterbrock, D. E. 1989, in Astrophysics of Gaseous Nebulae and Active Galactic Nuclei, University Science Books (Mill Valley, CA), p. 318

Padovani, P. 1992, A&A, 256, 399

Padovani, P., & Giommi, P. 1995a, MNRAS, 277, 1477

Padovani, P., & Giommi, P. 1995b, ApJ, 444, 567

Perlman, E. S., & Stocke, J. T. 1993, ApJ, 406, 430

Perlman, E. S., Stocke, J. T., Schachter, J. F., Elvis, M., Ellingson, E., Urry, C. M., Potter, M., Impey, C. D., & Kolchinsky, P. 1996, ApJS, 104, 351

Remillard, R. A., Bradt, H. V., Buckley, D. A. H., Roberts, W., Schwartz, D. A., Tuohy, I. R., & Wood, K. 1986, ApJ, 301, 742

Sambruna, R. M., Maraschi, L., & Urry, C. M. 1996, ApJ, 463, 444

Scarpa, R., & Falomo, R. 1997, A&A, 325, 109

Schachter, J. F., Stocke, J. T., Perlman, E., Elvis, M., Remillard, R., Granados, A., Luu, J., Huchra, J. P., Humphreys, R., Urry, C. M., & Wallin, J. 1993, ApJ, 412, 541

Schwartz, D. A., Brissenden, R. J. V., Tuohy, I. R., Feigelson, E. D., Hertz, P. L., & Remillard, R. A. 1989, in BL Lac Objects, ed. L. Maraschi, T. Maccacaro and M.-H. Ulrich (Berlin: Springer Verlag), p. 209

Smith, E. P., & Heckman, T. M. 1989, ApJ, 341, 658

Stark, A. A., Gammie, C. F., & Wilson, R. W. 1992, ApJS, 79, 77

Stein, W. A., O'Dell, S. L., & Strittmatter, P. A. 1976, ARAA, 14, 173

Stickel, M., Padovani, P., Urry, C. M., Fried, J. W., & Kühr, H. 1991, ApJ, 374, 431

Stickel, M., Fried, J., & Kühr, H. 1993, A&AS, 98, 393

Stocke, J. T., & Rector, T. A. 1997, ApJLett, 489, L17

Stocke, J. T., Liebert, J., Schmidt, G., Gioia, I. M., Maccacaro, T., Schild, R. E., Maccagni, D., & Arp, H. C. 1985, ApJ, 298, 619

Stocke, J. T., Morris, S. L., Gioia, I., Maccacaro, T., Schild, R. E., & Wolter, A. 1990, ApJ, 348, 141

Stocke, J. T., Morris, S. L., Gioia, I. M., Maccacaro, T., Schild, R., Wolter, A., Fleming, T. A., & Henry, J. P. 1991, ApJS, 76, 813

Tanabaum, H., Tucker, W., Prestwich, A., & Remillard, R. 1997, ApJ, 476, 83

Tapia, S., Craine, E. R., Gearhart, M. R., Pacht, E., & Kraus, J. 1977, ApJLett, 215, L71

Ulrich, M.-H. 1989, in BL Lac Objects, ed. L. Maraschi, T. Maccacaro and M.-H. Ulrich (Berlin: Springer Verlag), p. 45

Ulvestad, J. S., & Wilson, A. S. 1989, ApJ, 343, 659

Ulvestad, J. S., Antonucci, R. R. J., & Goodrich, R. W. 1995, AJ, 109, 81

Urry, C. M., & Padovani, P. 1995, PASP, 107, 803

Voges, W. 1993, Adv. Space Res., Vol. 13, No. 12, 391

Weedman, D. W. 1986, in Quasar Astronomy, Cambridge University Press (Cambridge), p. 20

Wilson, A. S., & Colbert, E. J. M. 1995, ApJ, 438, 62

Fig. 1.— Figure 1 at end of paper.

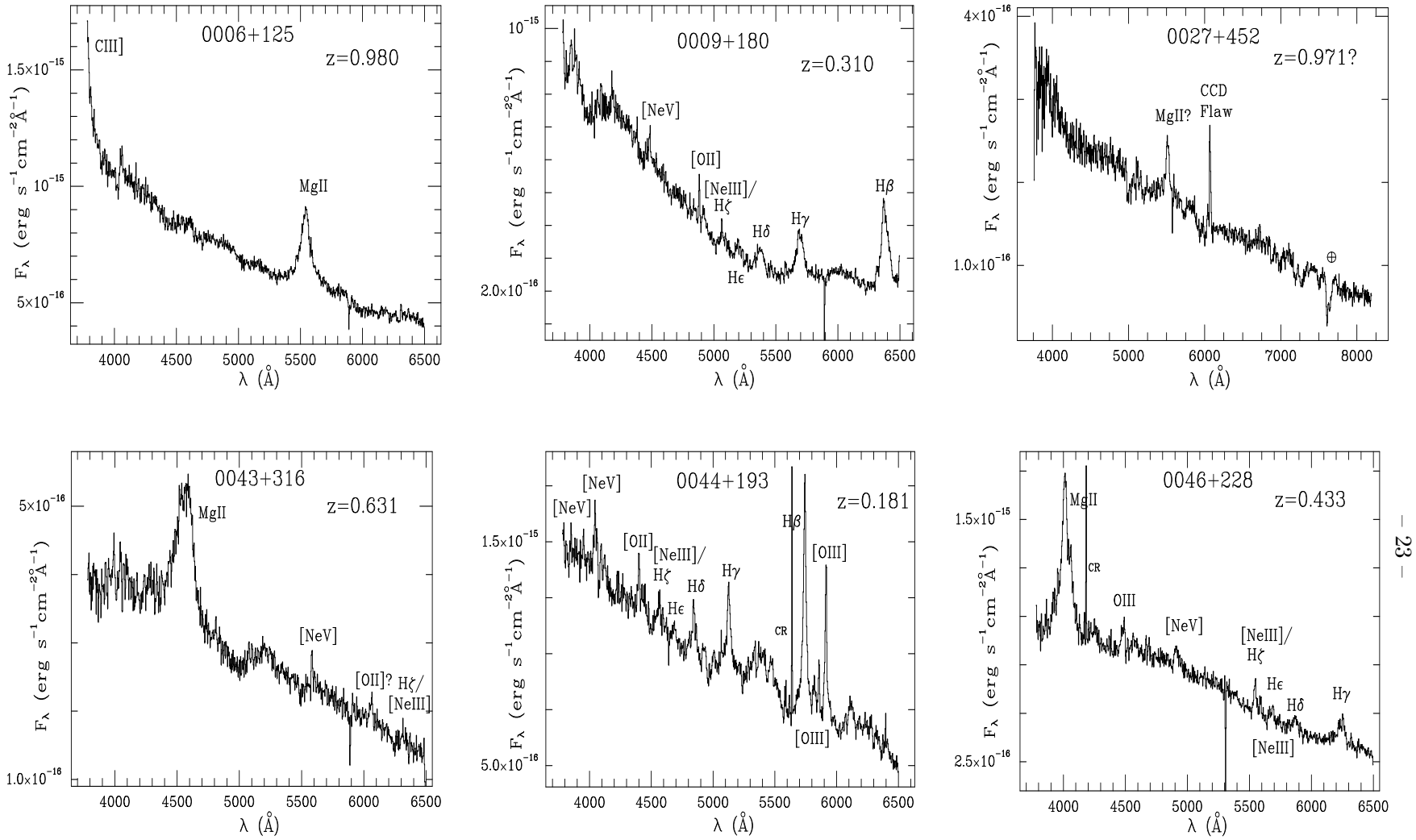

Figure 1.1 – 1.6: Spectra of RGB objects

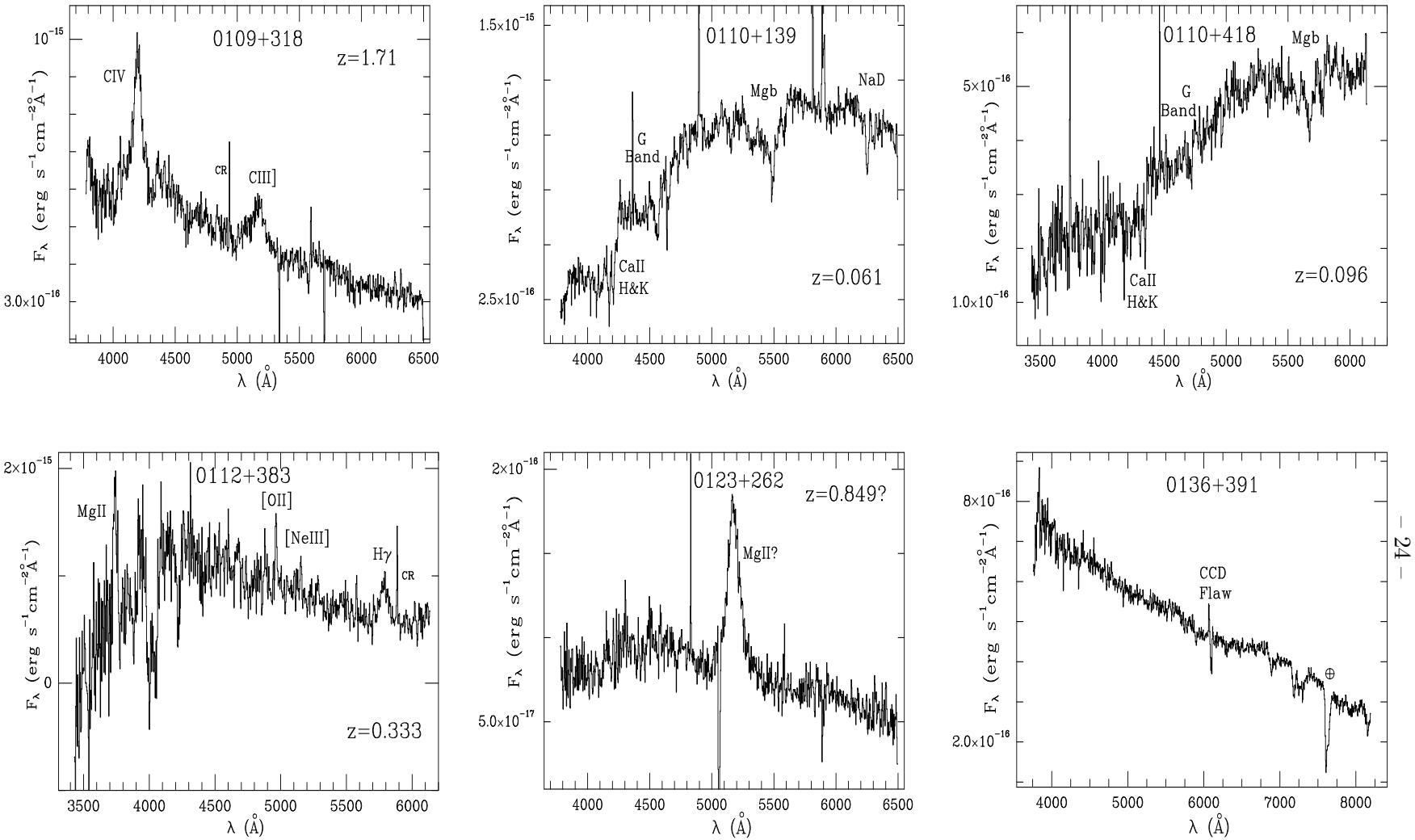

Figure 1.7 – 1.12: Spectra of RGB Sources (*continued*)

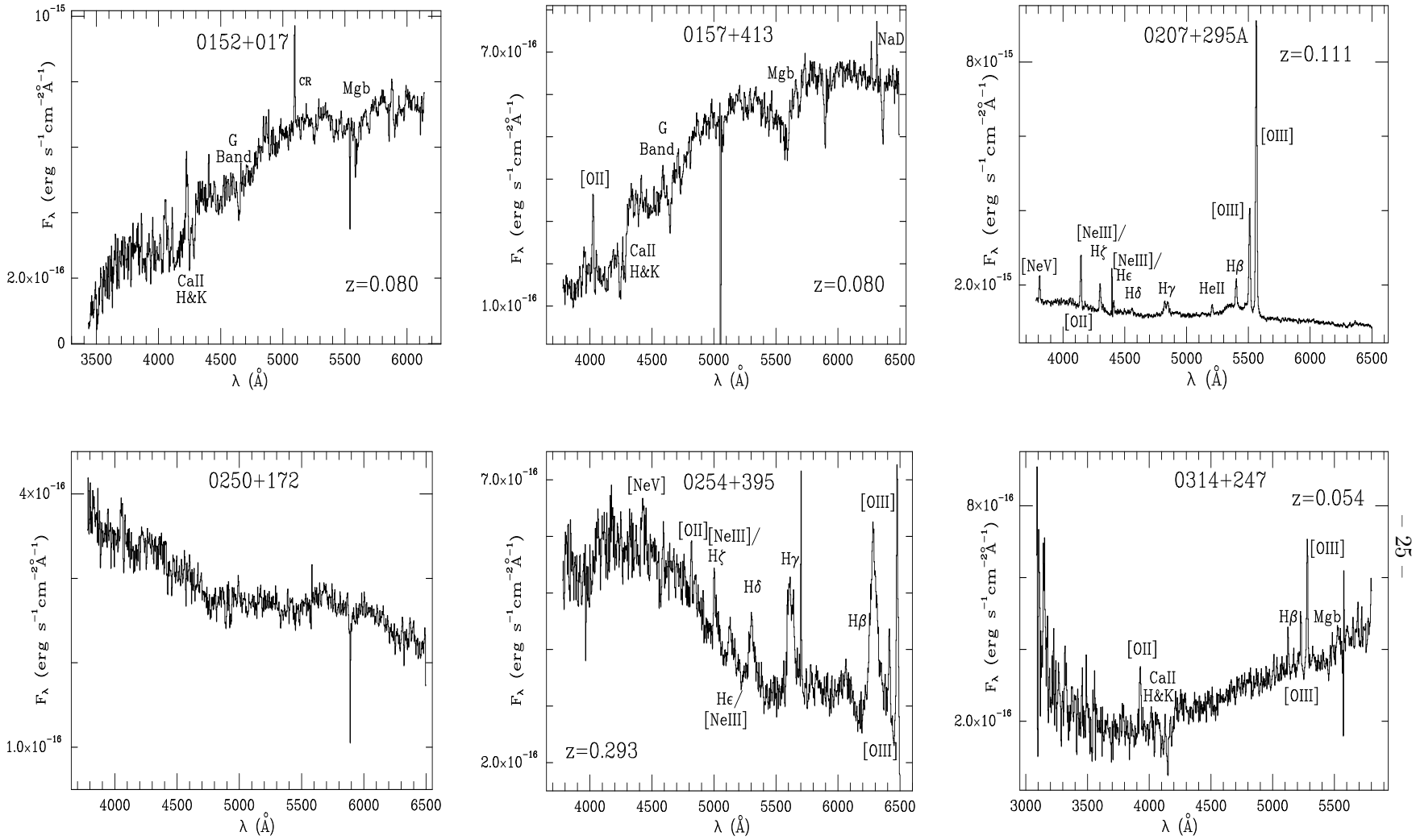

Figure 1.13 − 1.18: Spectra of RGB Sources (*continued*)

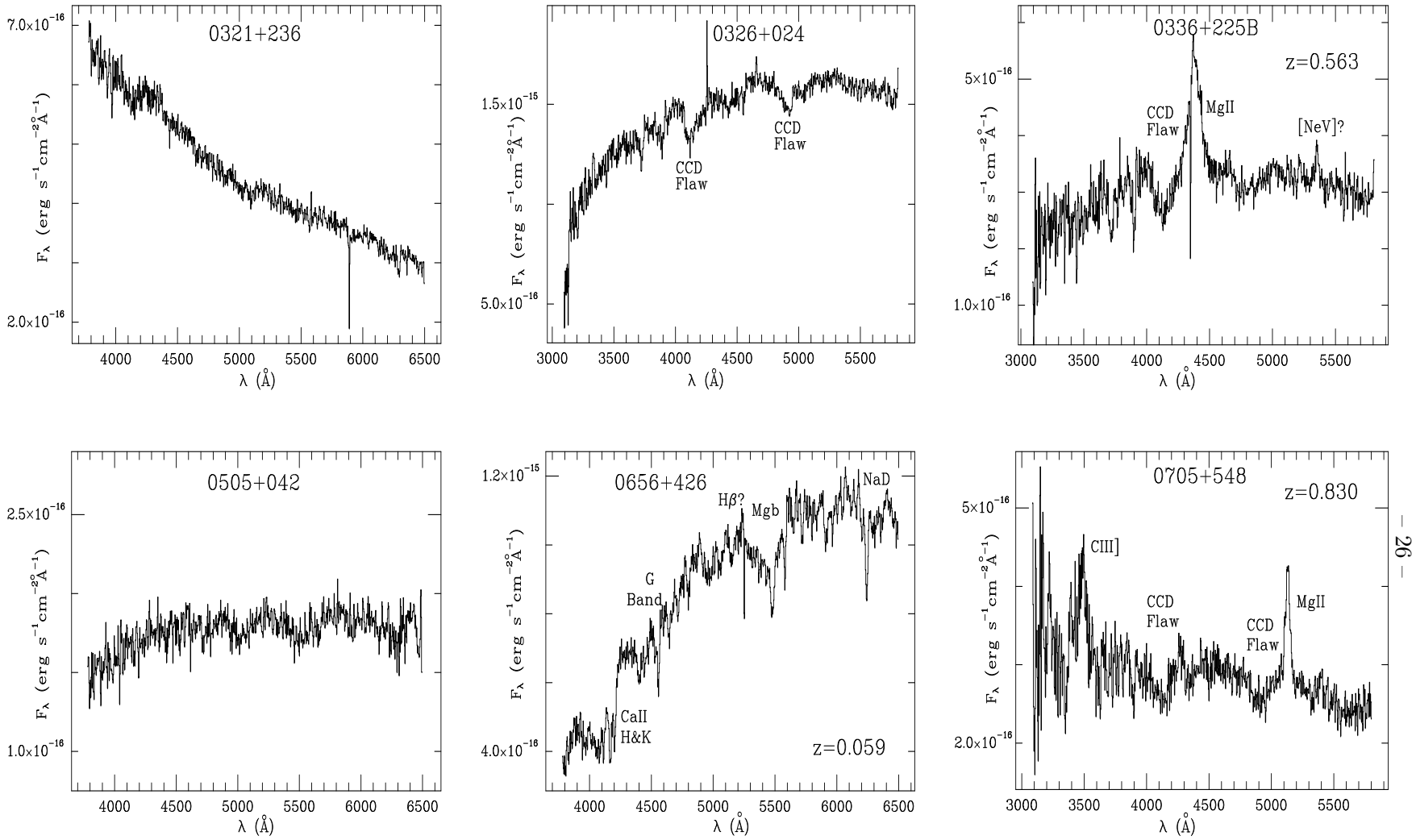

Figure 1.19 − 1.24: Spectra of RGB Sources (*continued*)

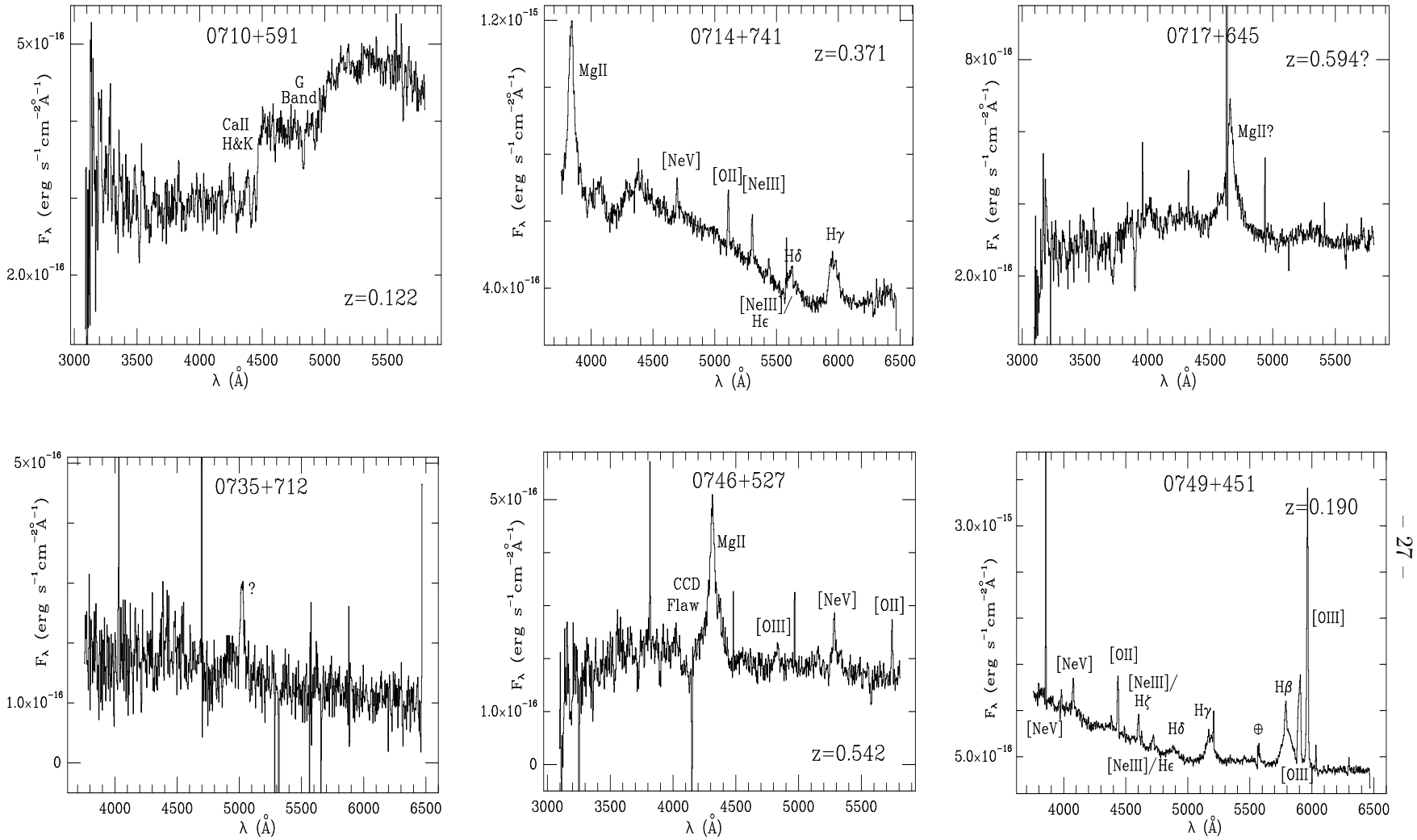

Figure 1.25 – 1.30: Spectra of RGB Sources (*continued*)

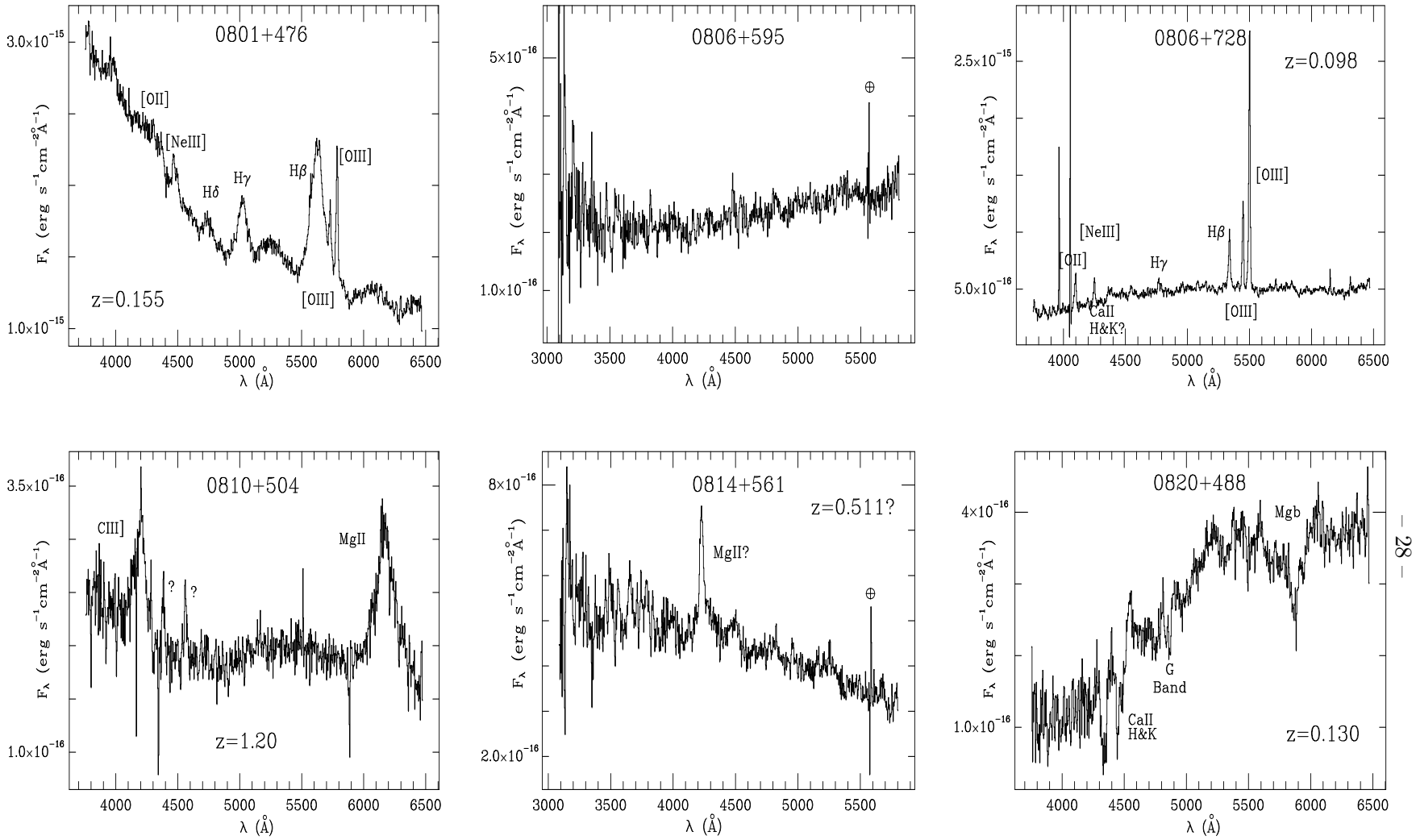

Figure 1.31 − 1.36: Spectra of RGB Sources (*continued*)

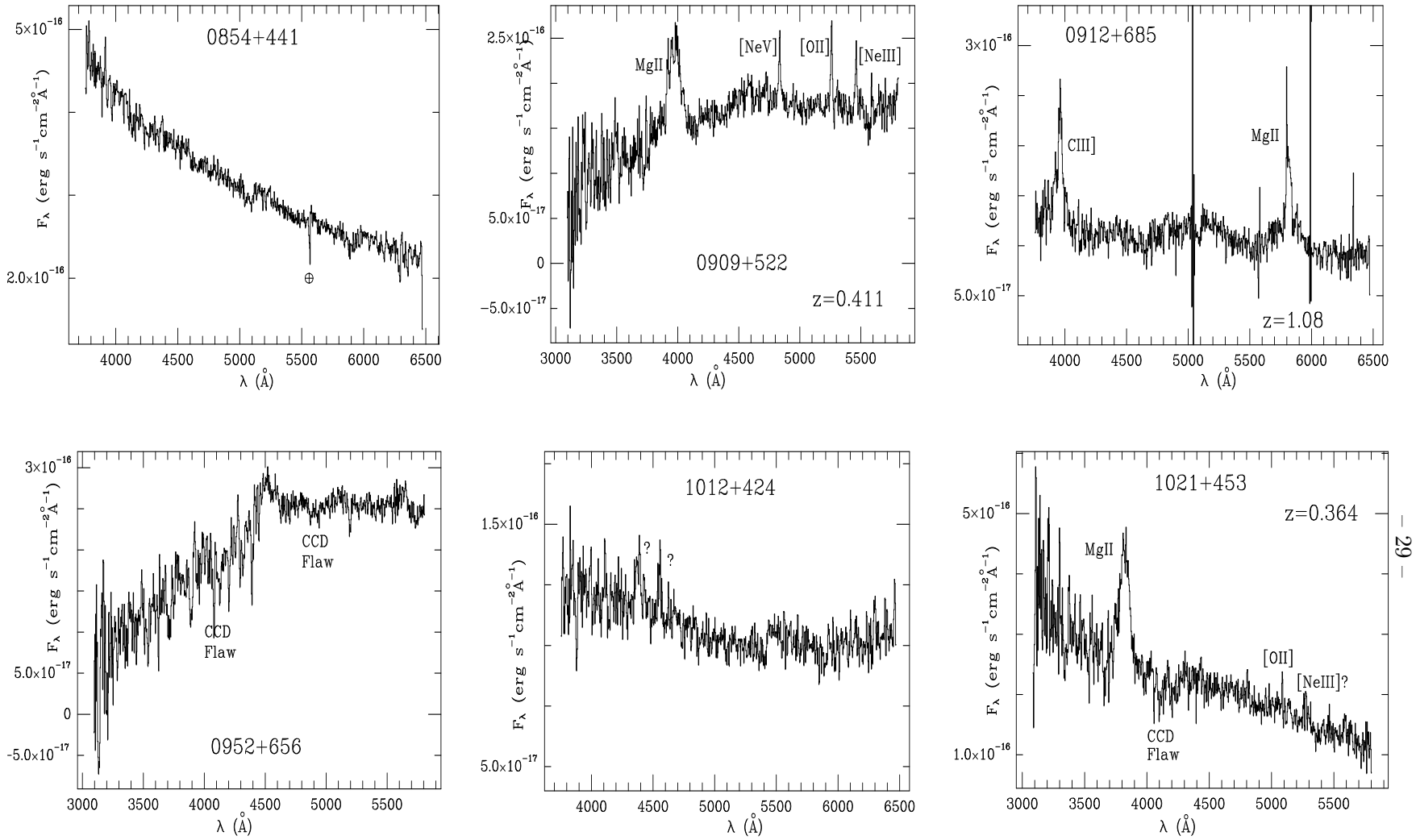

Figure 1.37 − 1.42: Spectra of RGB Sources (*continued*)

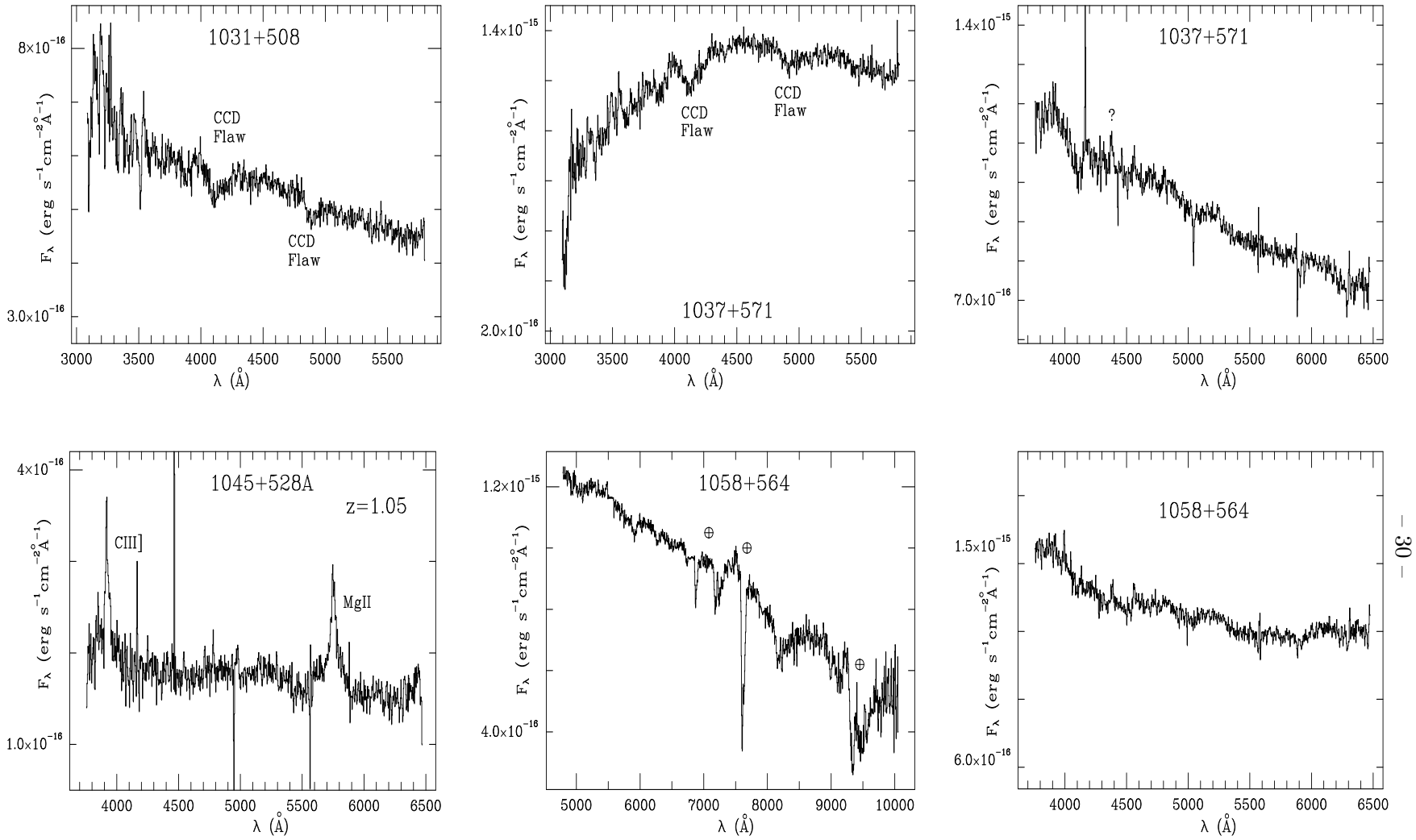

Figure 1.43 − 1.48: Spectra of RGB Sources (*continued*)

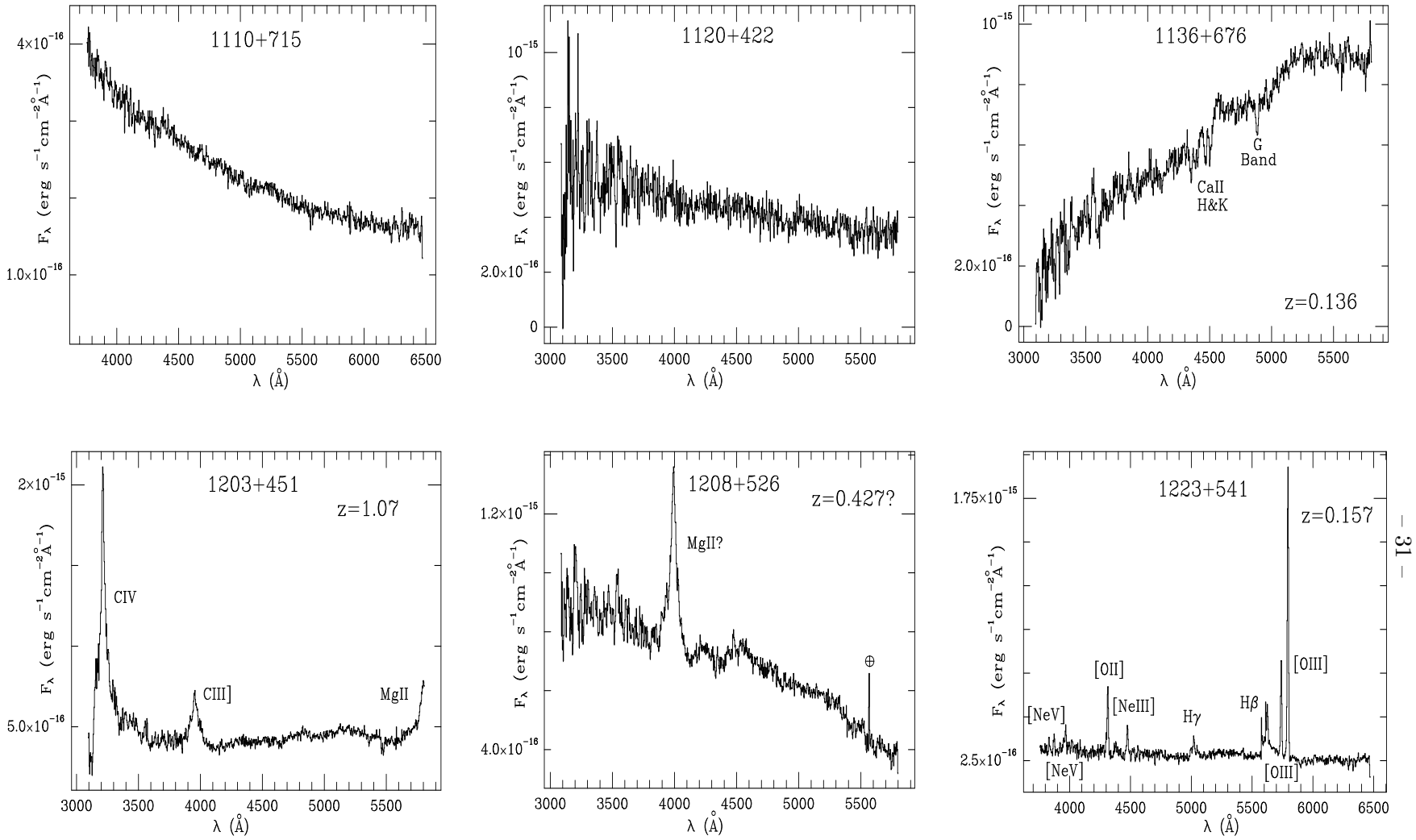

Figure 1.49 – 1.54: Spectra of RGB Sources (*continued*)

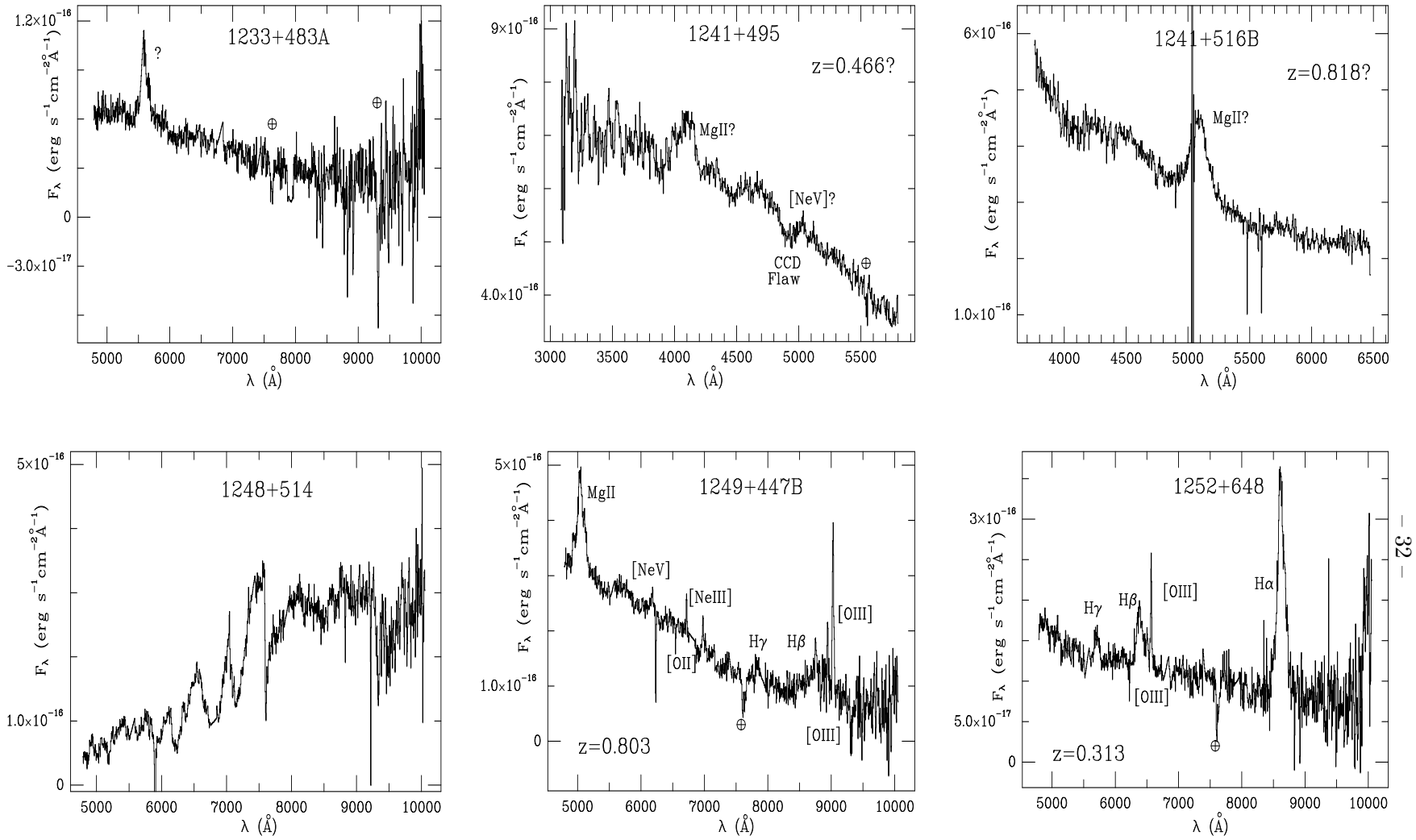

Figure 1.55 – 1.60: Spectra of RGB Sources (*continued*)

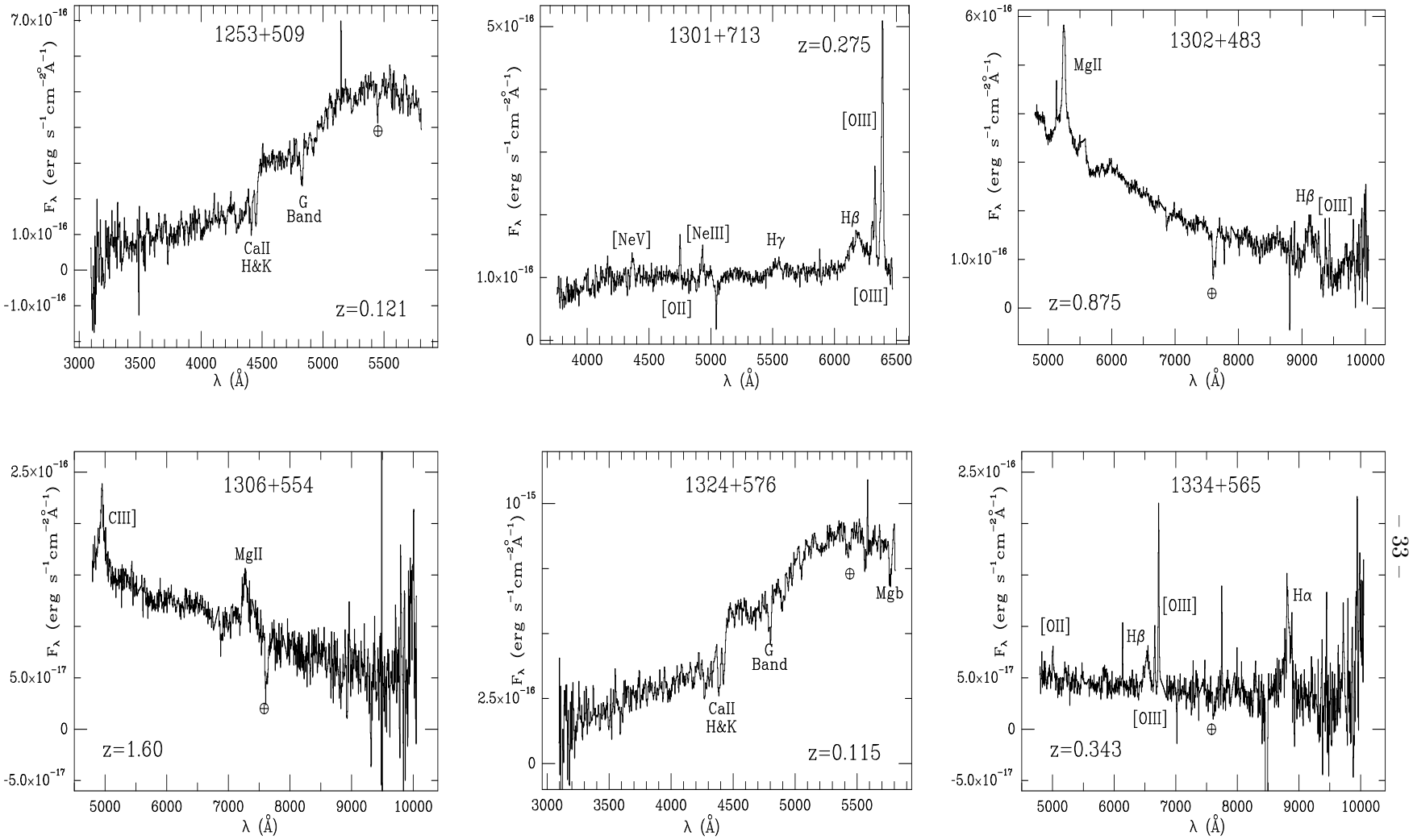

Figure 1.61 − 1.66: Spectra of RGB Sources (*continued*)

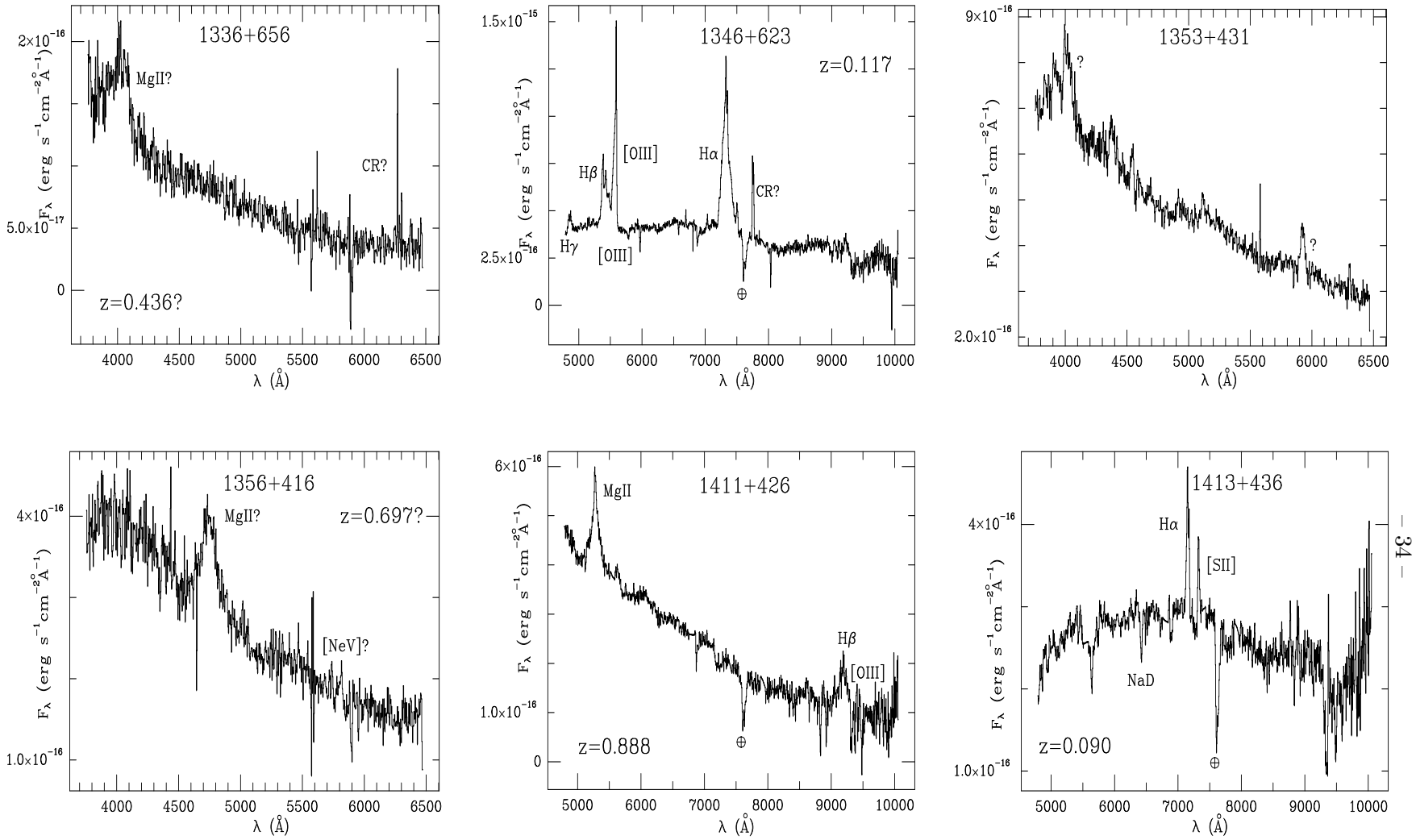

Figure 1.67 – 1.72: Spectra of RGB Sources (*continued*)

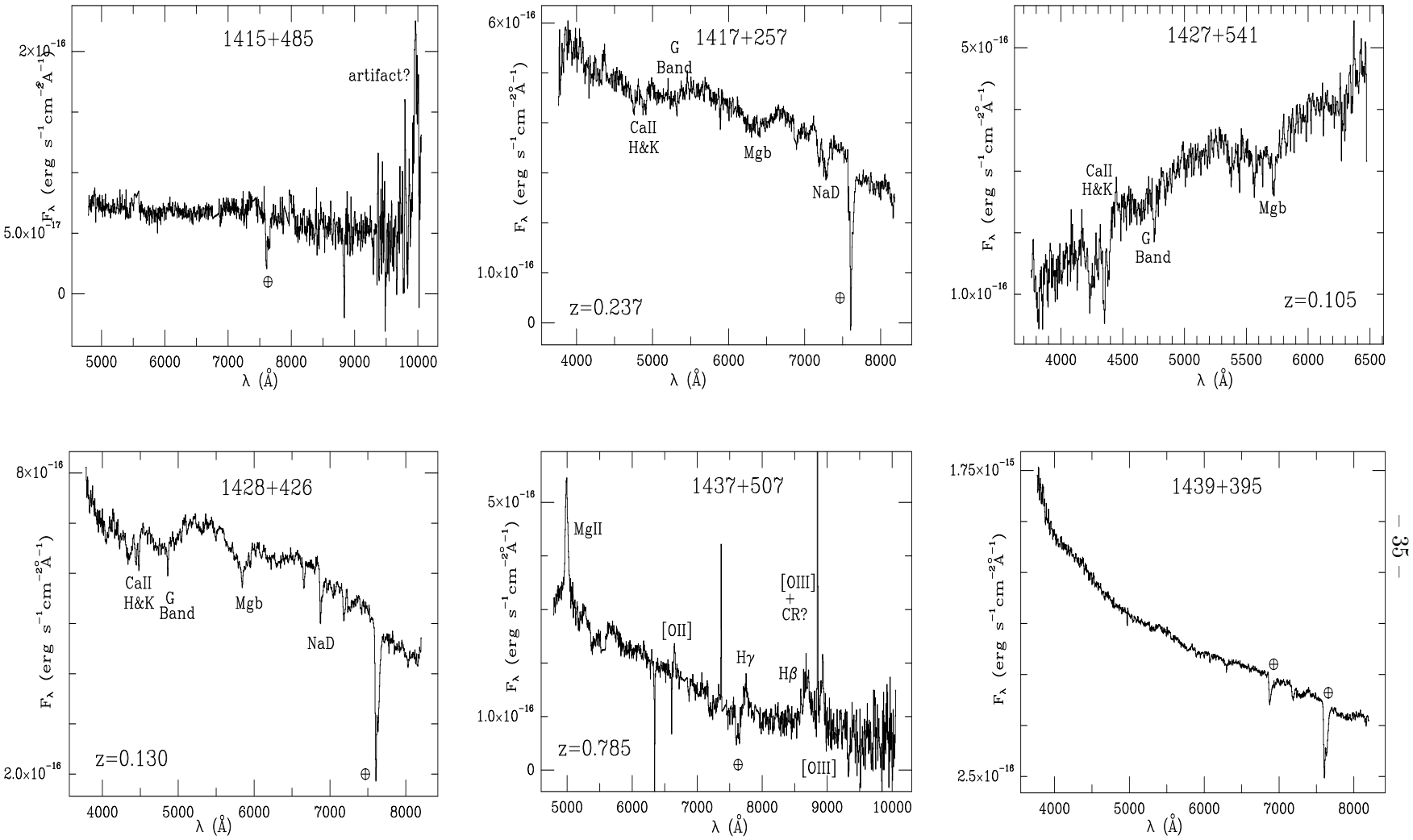

Figure 1.73 − 1.78: Spectra of RGB Sources (*continued*)

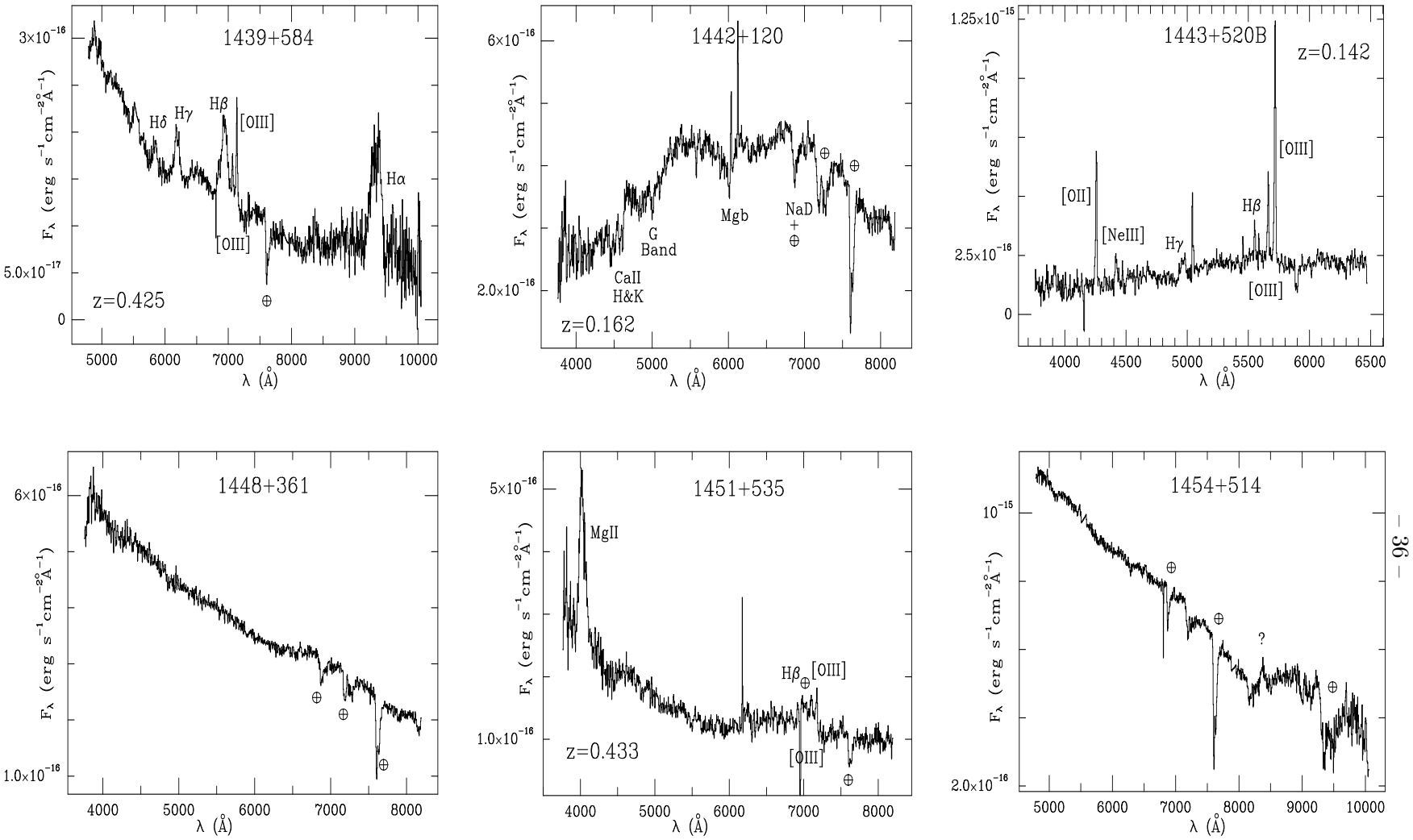

Figure 1.79 − 1.84: Spectra of RGB Sources (*continued*)

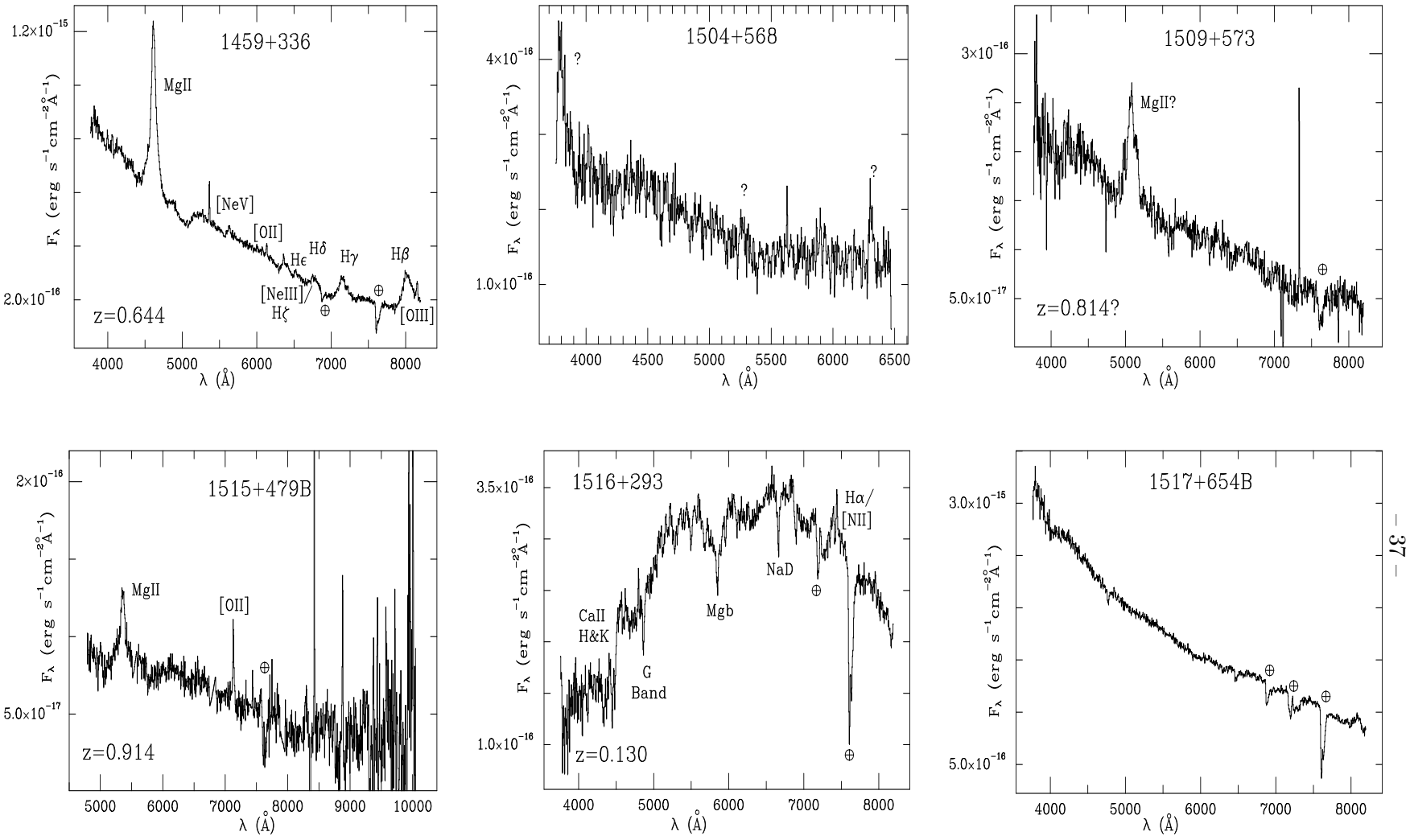

Figure 1.85 – 1.90: Spectra of RGB Sources (*continued*)

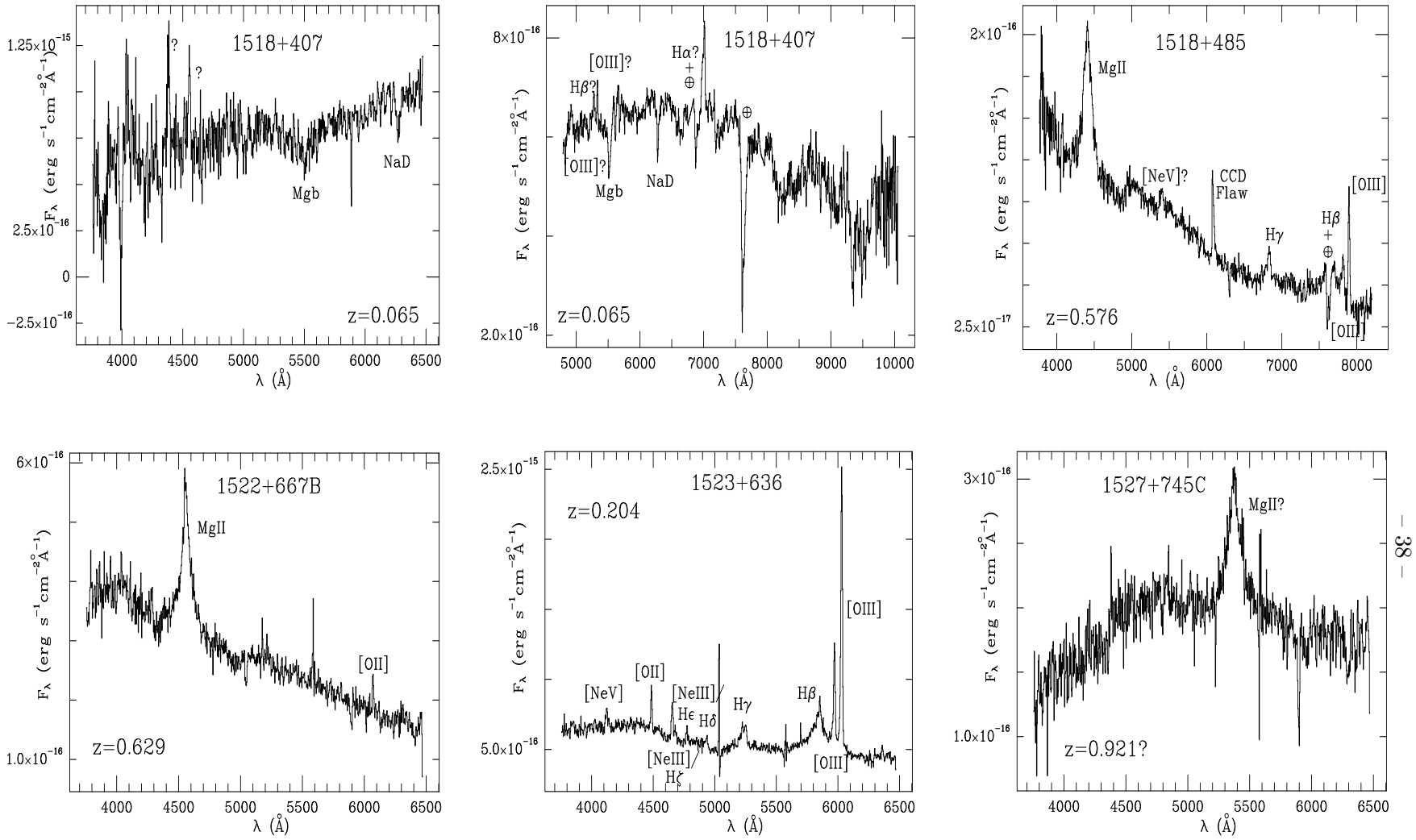

Figure 1.91 − 1.96: Spectra of RGB Sources (*continued*)

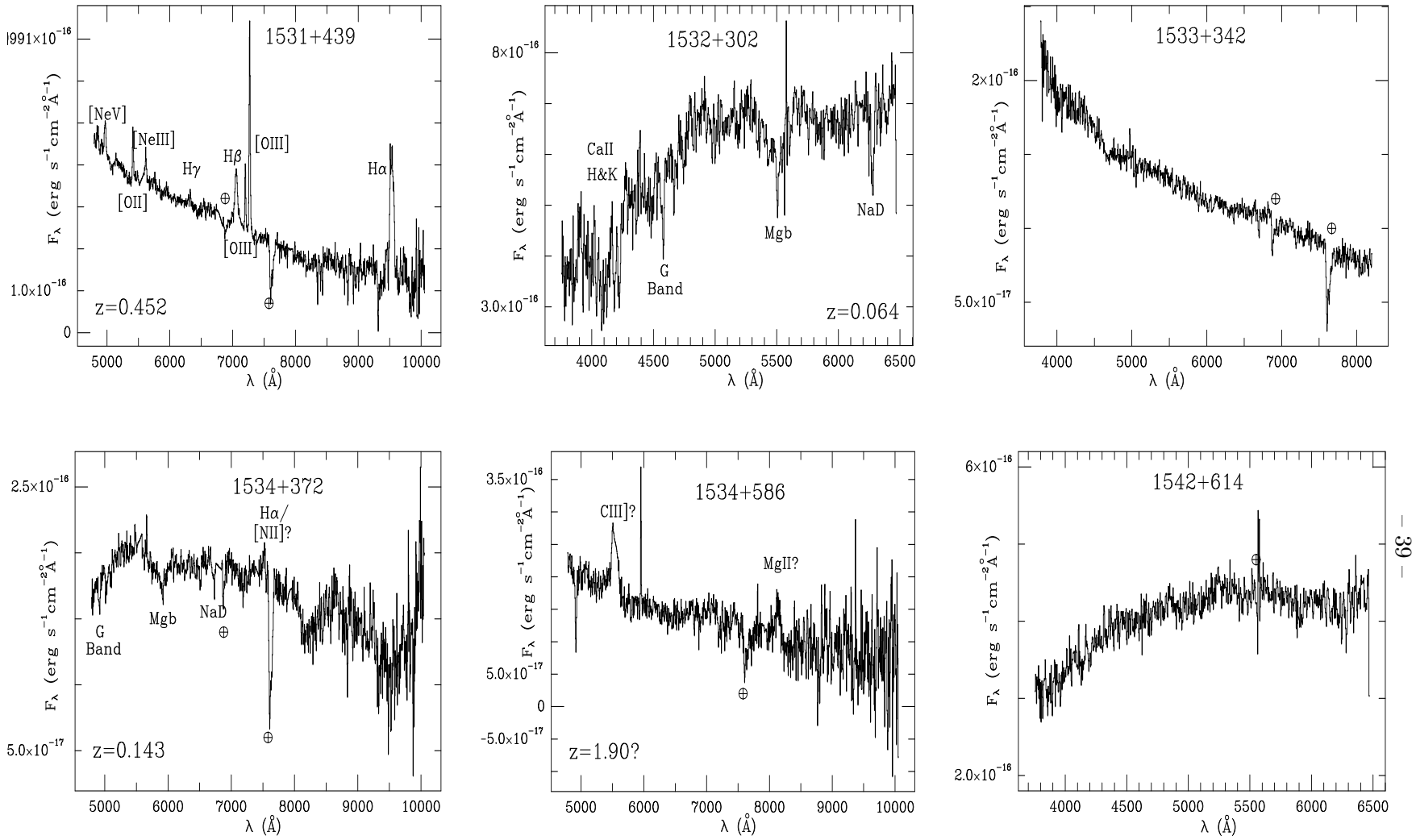

Figure 1.97 – 1.102: Spectra of RGB Sources (*continued*)

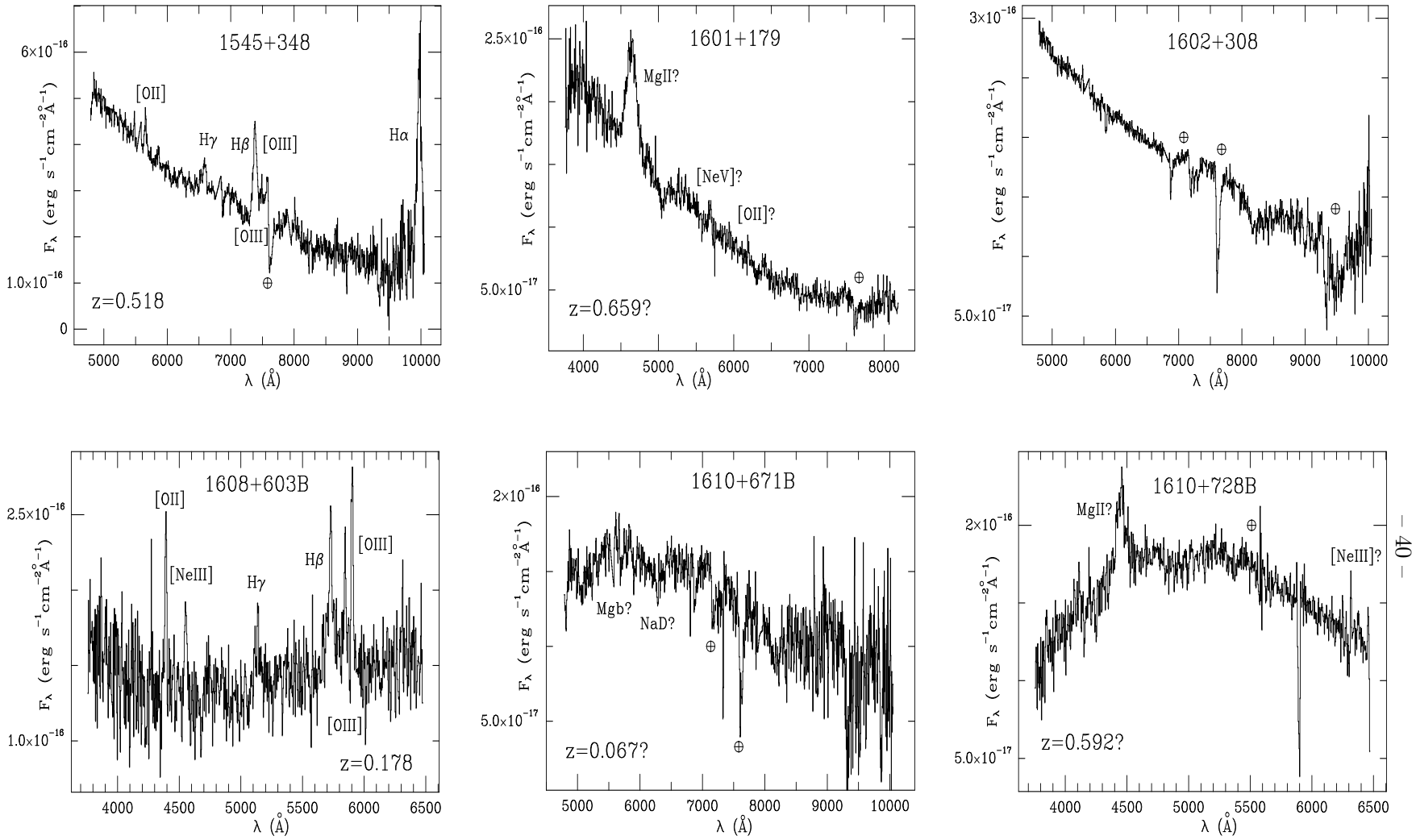

Figure 1.103 − 1.108: Spectra of RGB Sources (*continued*)

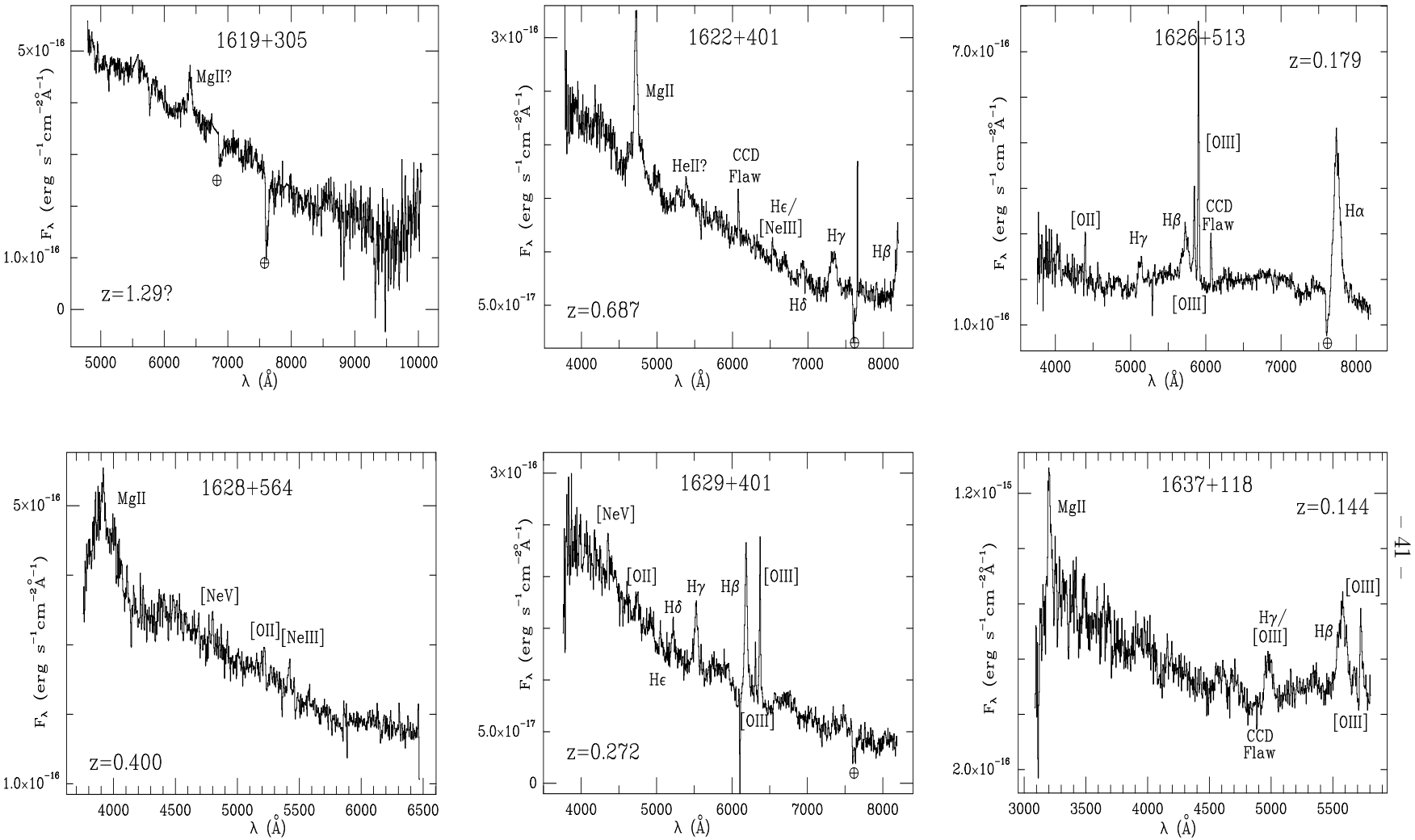

Figure 1.109 − 1.114: Spectra of RGB Sources (*continued*)

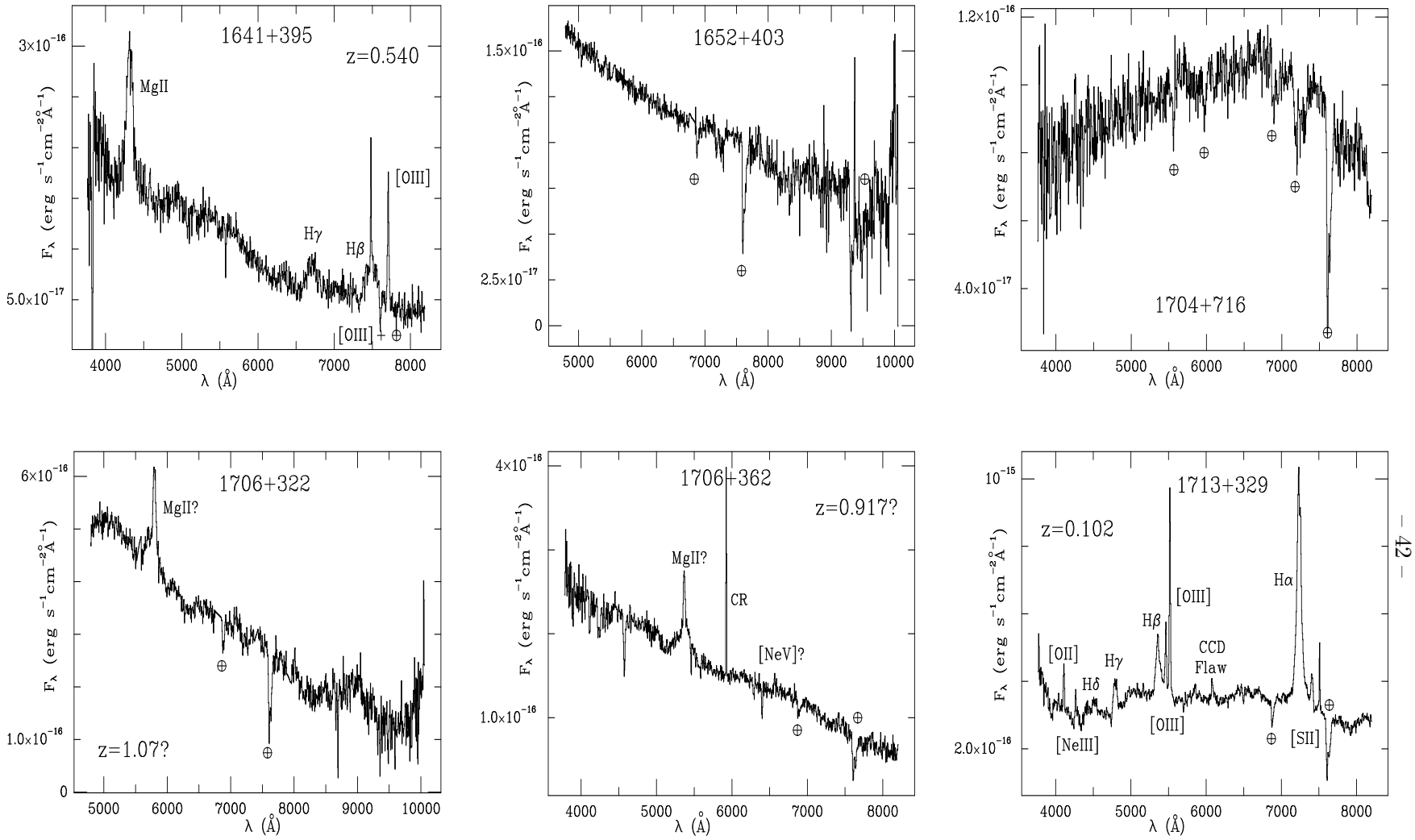

Figure 1.115 – 1.120: Spectra of RGB Sources (*continued*)

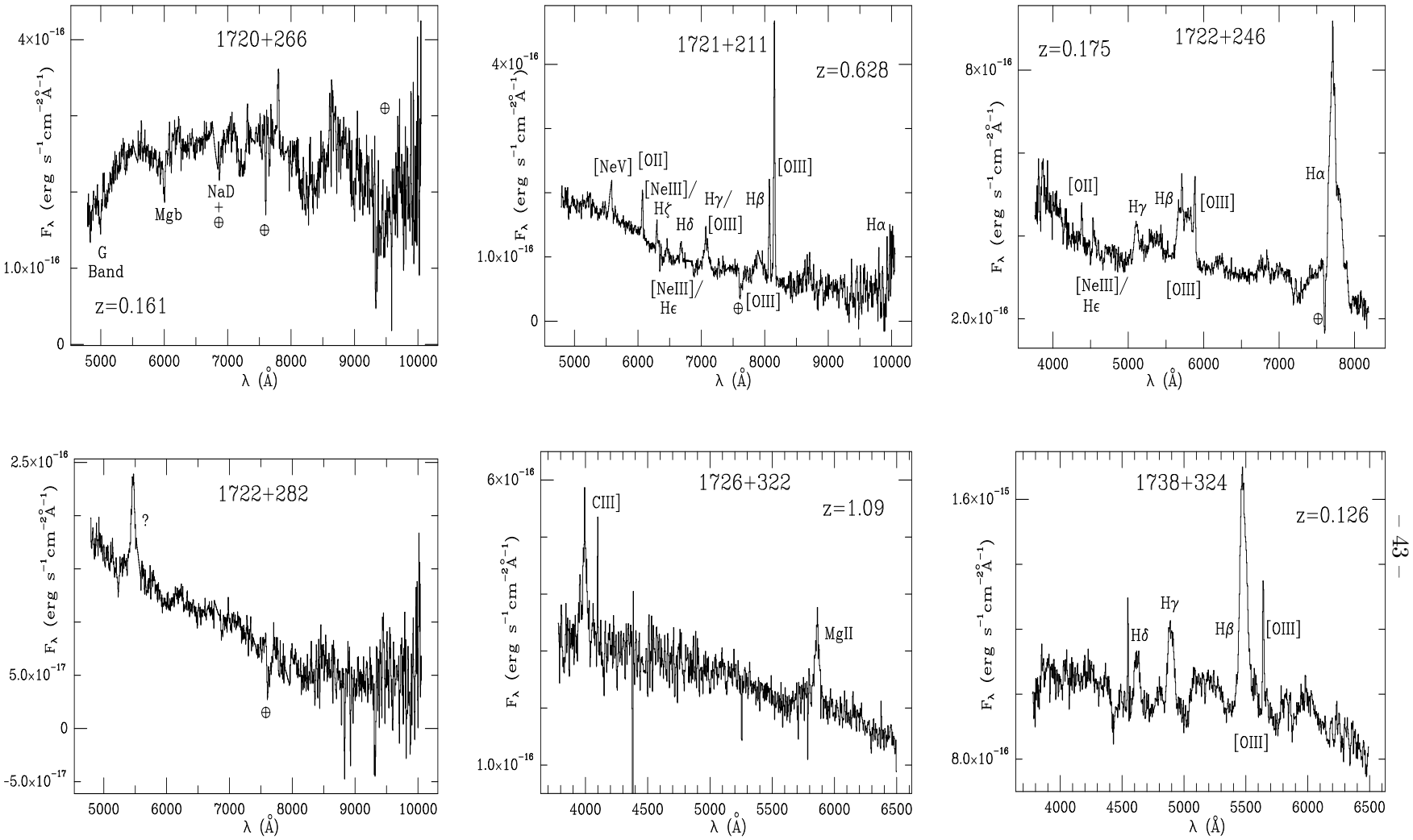

Figure 1.121 − 1.126: Spectra of RGB Sources (*continued*)

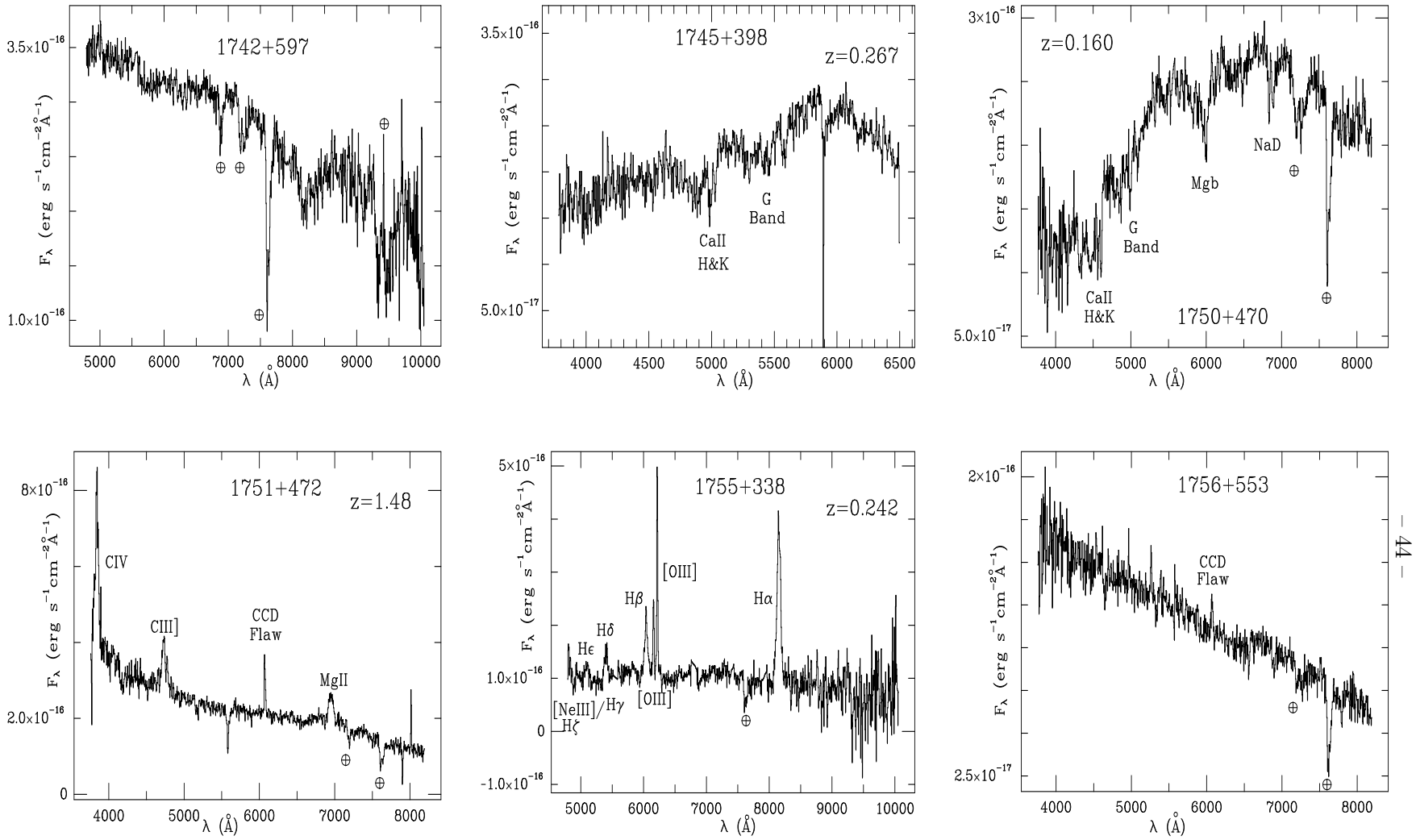

Figure 1.127 – 1.132: Spectra of RGB Sources (*continued*)

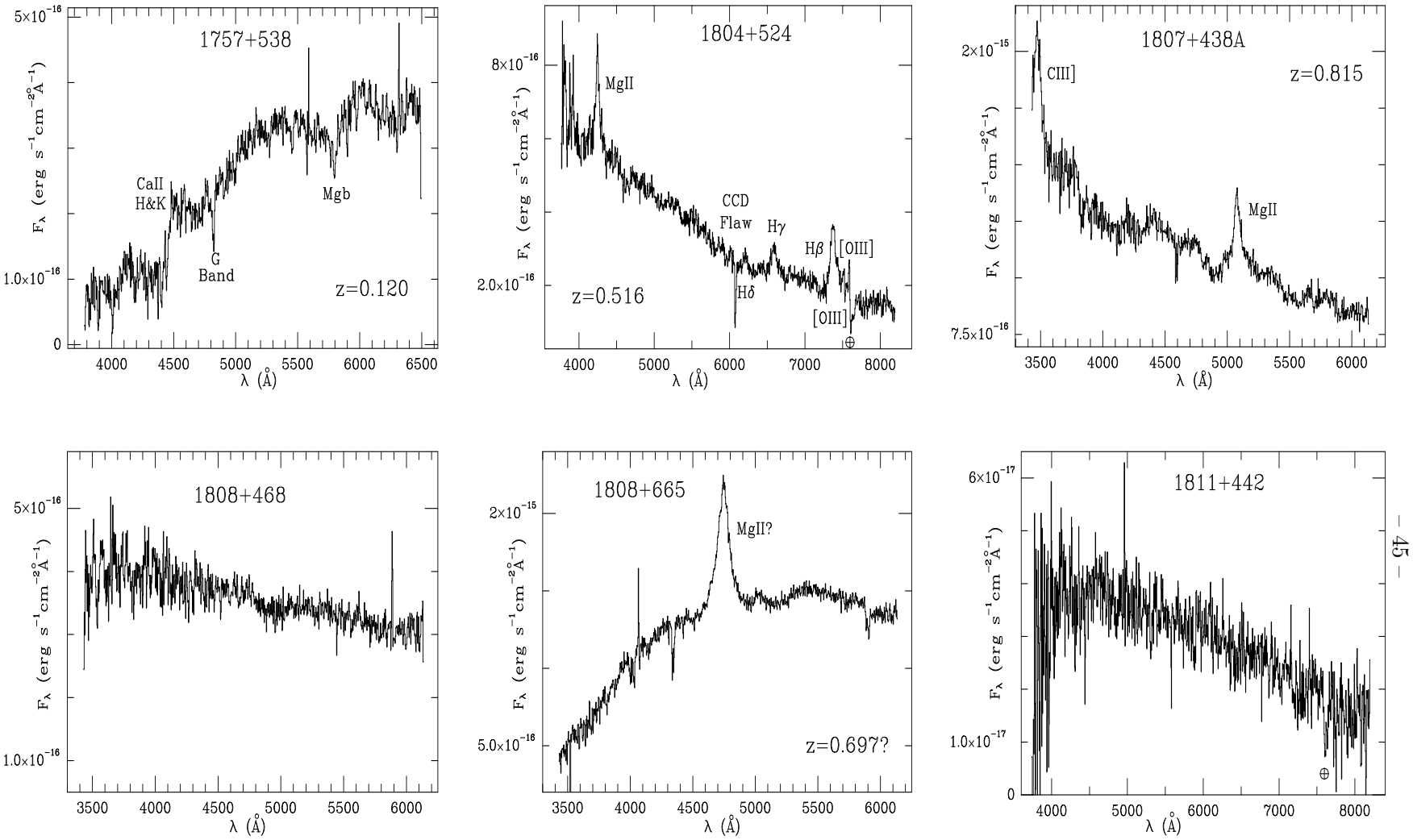

Figure 1.133 – 1.138: Spectra of RGB Sources (*continued*)

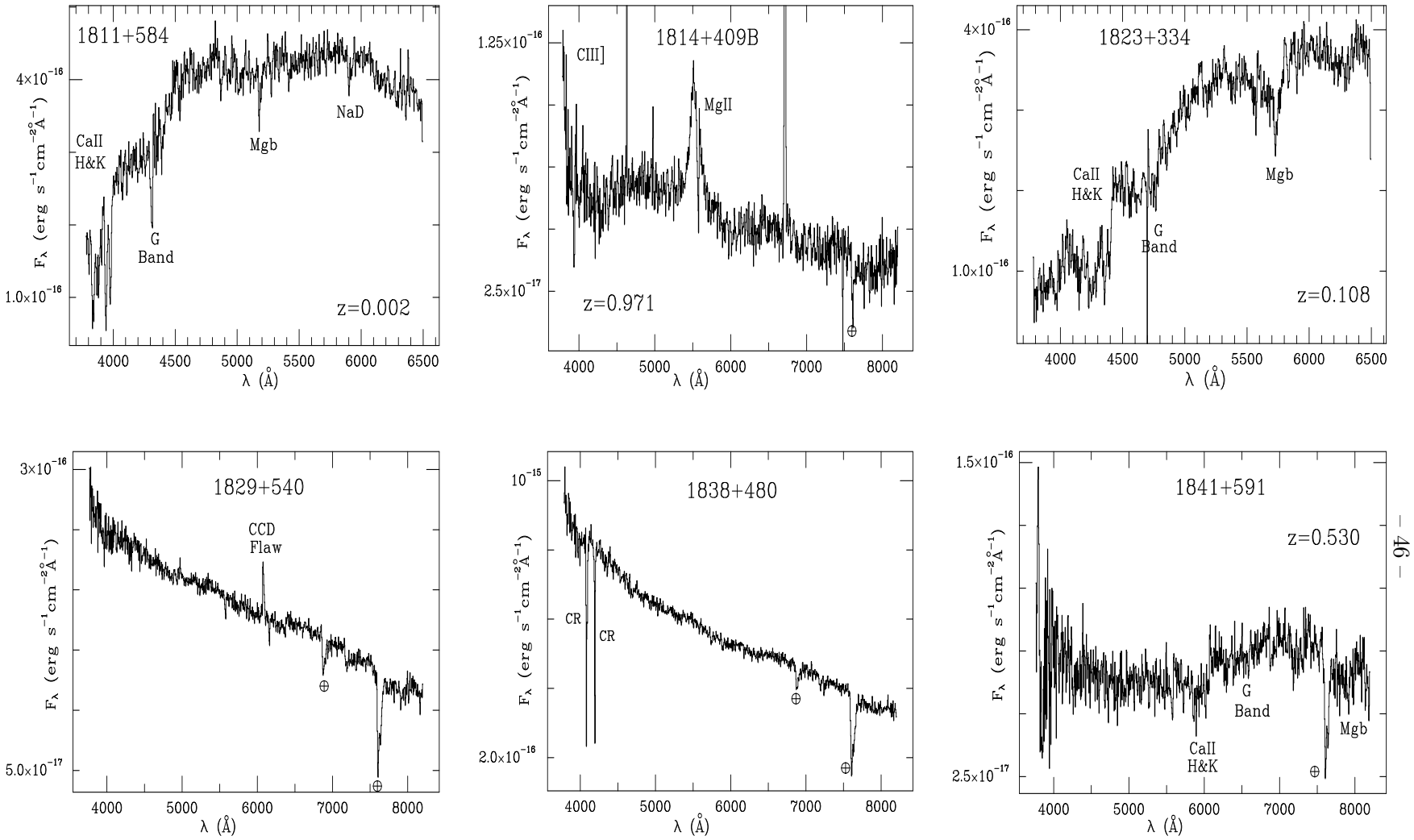

Figure 1.139 − 1.144: Spectra of RGB Sources (*continued*)

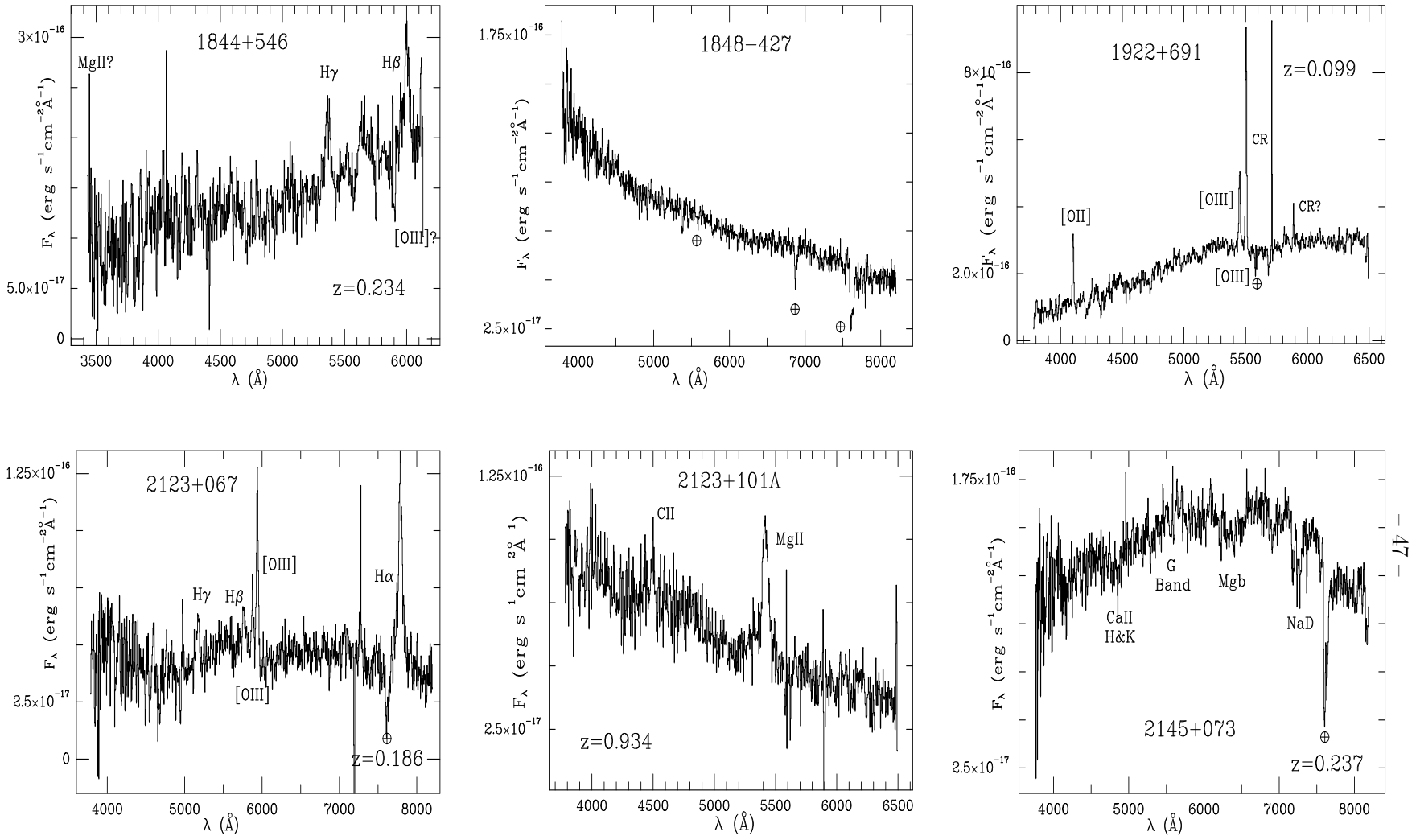

Figure 1.145 – 1.150: Spectra of RGB Sources (*continued*)

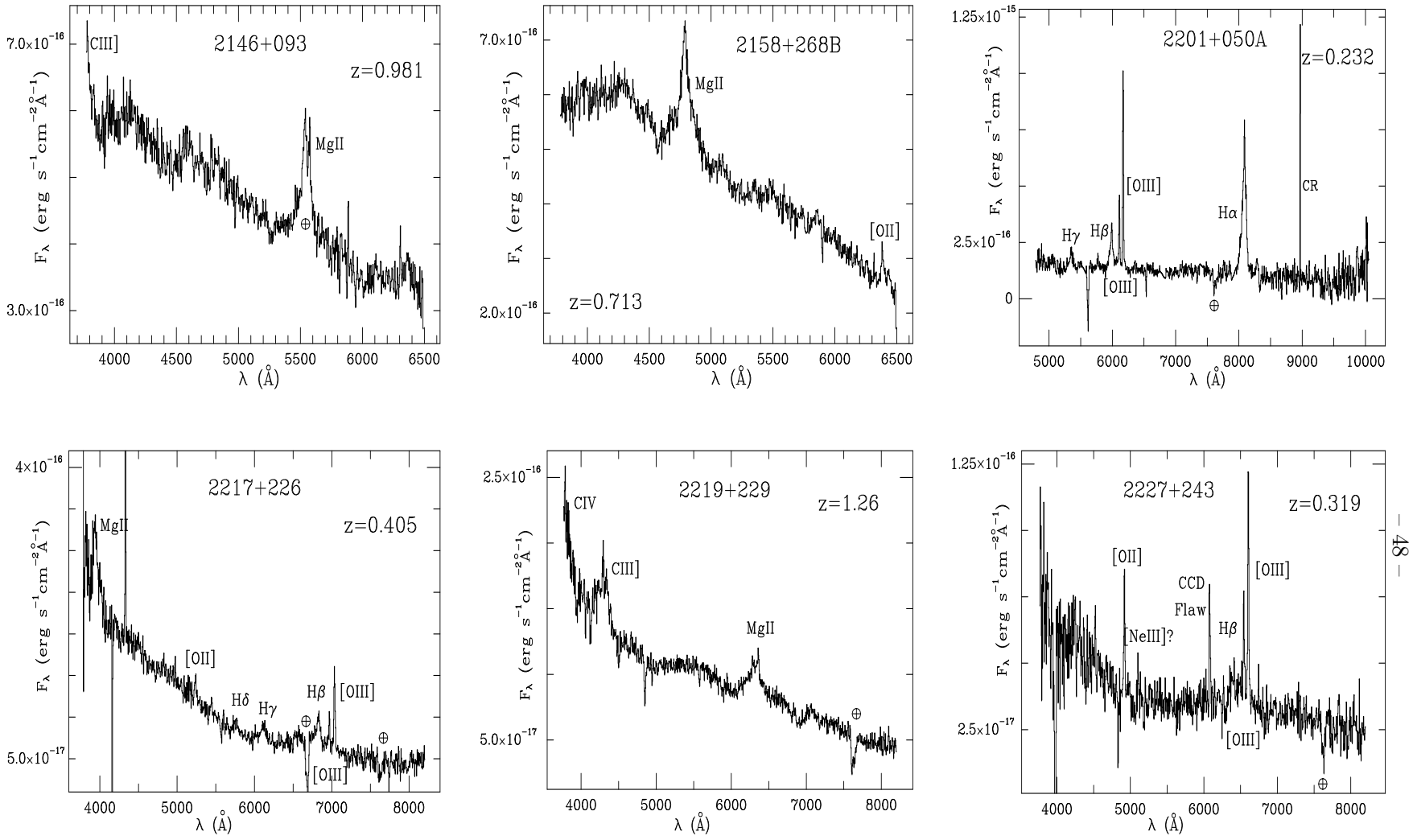

Figure 1.151 – 1.156: Spectra of RGB Sources (*continued*)

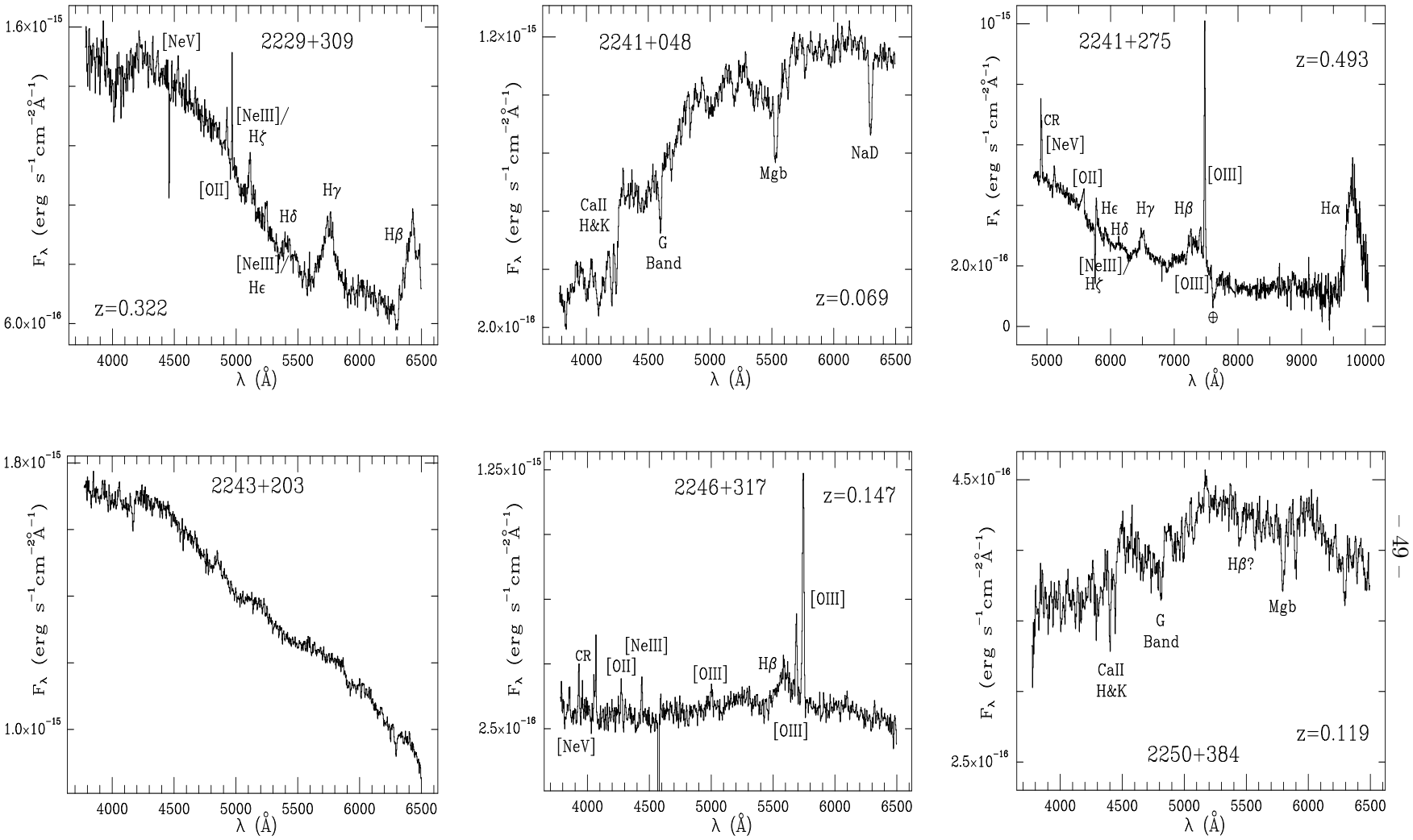

Figure 1.157 – 1.162: Spectra of RGB Sources (*continued*)

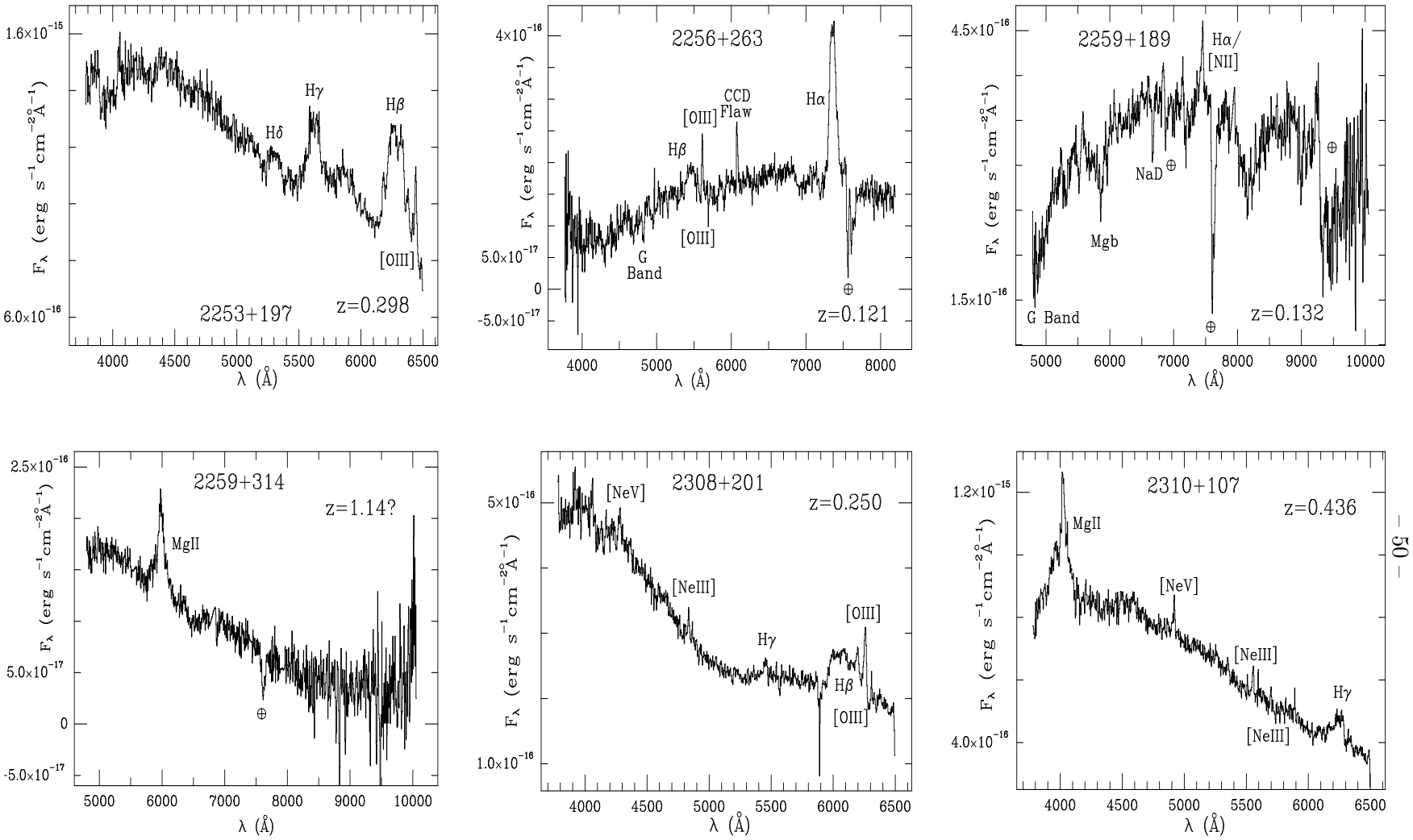

Figure 1.163 − 1.168: Spectra of RGB Sources (*continued*)

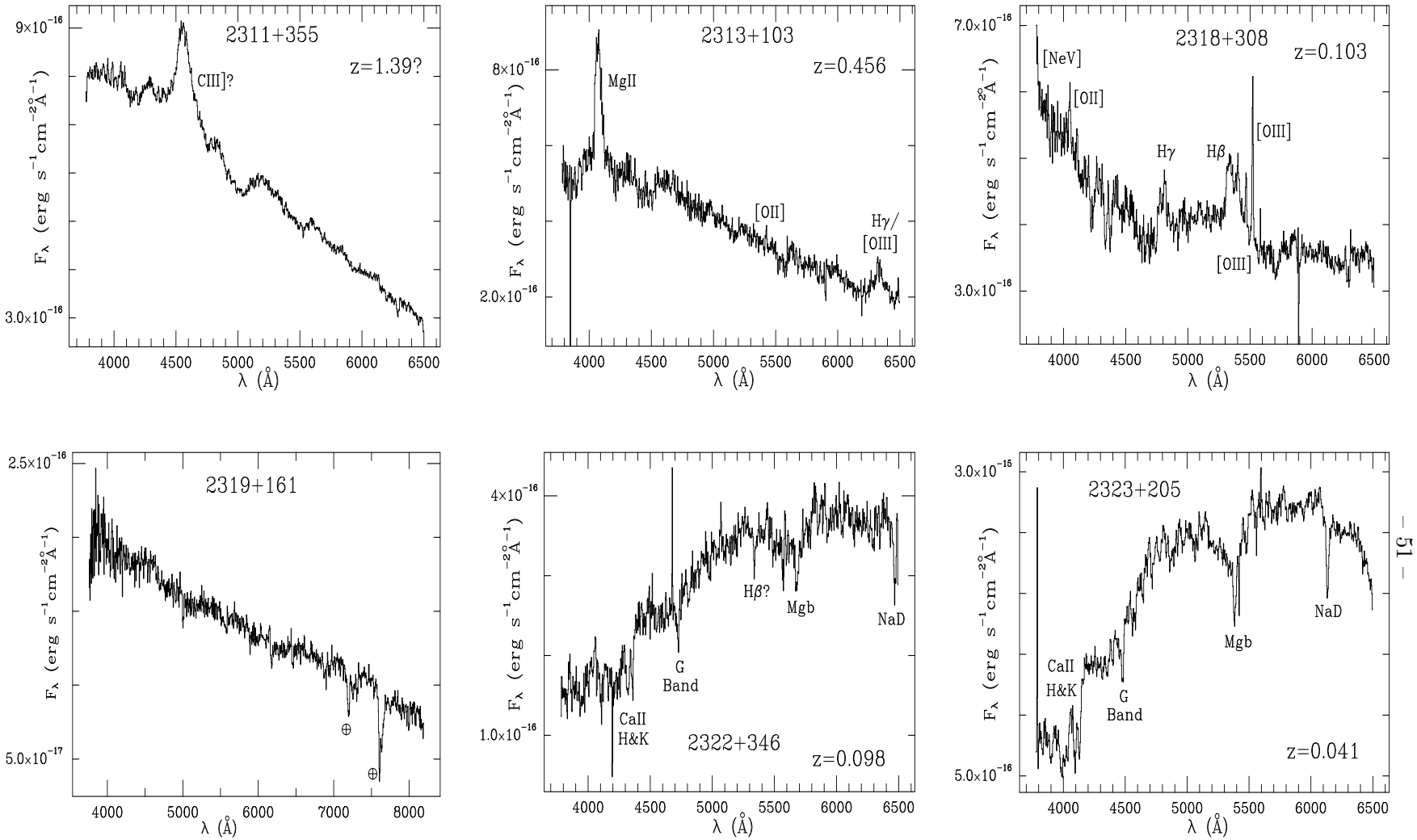

Figure 1.169 − 1.174: Spectra of RGB Sources (*continued*)

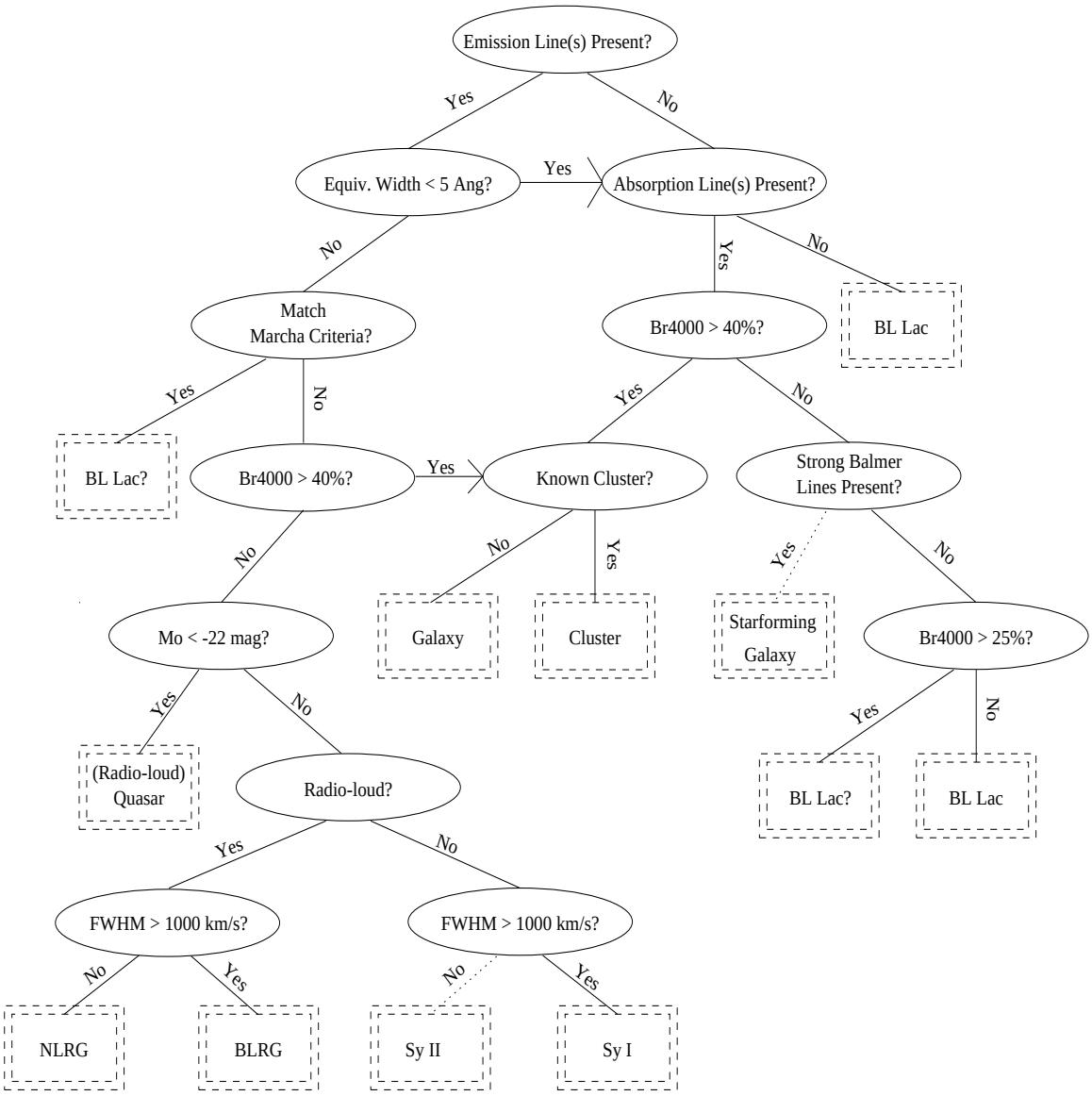

Fig. 2.— The RGB classification criteria used in this study. Dotted boxes represent the end point of a decision tree. Only radio-loud quasars are listed as no radio-quiet quasars were found, although we did allow for that possibility. Seyfert II and starforming galaxies are both listed, although we found none of these objects in this study. We therefore use dotted lines leading to the respective boxes.

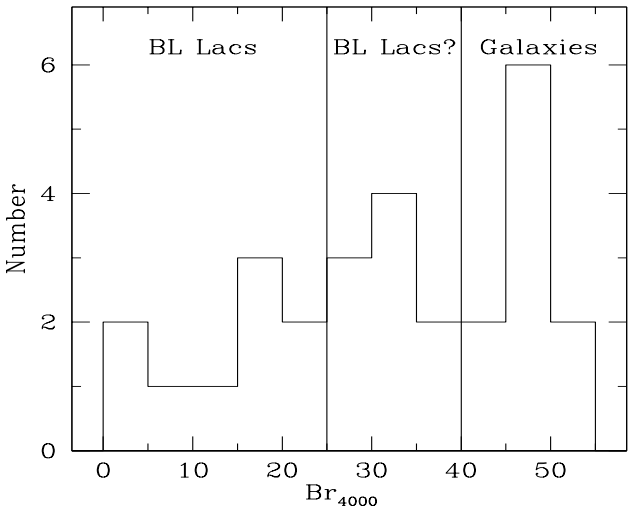

Fig. 3.— The distribution of Ca II break strengths (Br_{4000}) for the 28 objects for which it was measured. Objects with Br_{4000}>40% have been classified as galaxies while objects with Br_{4000}<25% have been classified as BL Lacs. Objects with intermediate break strengths have been classified as probable BL Lacs ("BL Lacs?").

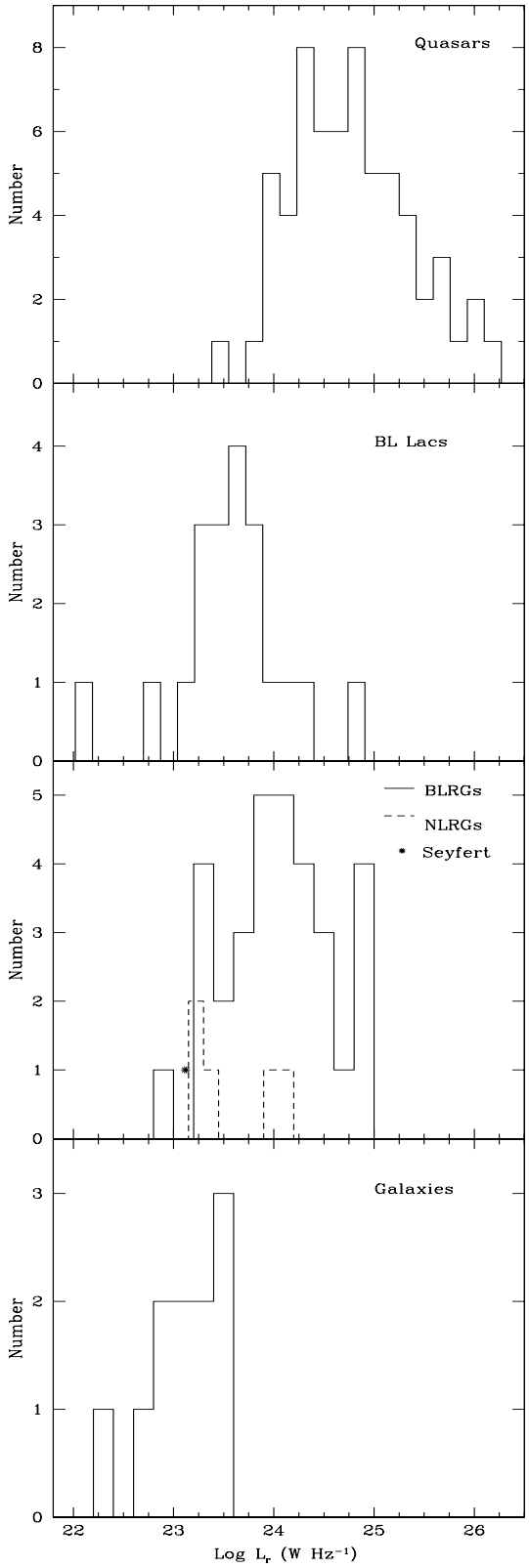

Fig. 4.— The distribution of the logarithm of the radio luminosities for the newly identified RGB sources. The panels show the distribution of the various spectroscopic classes: (1) radio-loud quasars, (2) BL Lacs, (3) Broad and Narrow line radio galaxies and the one object we classify as a Seyfert and (4) galaxies and galaxies in known clusters.

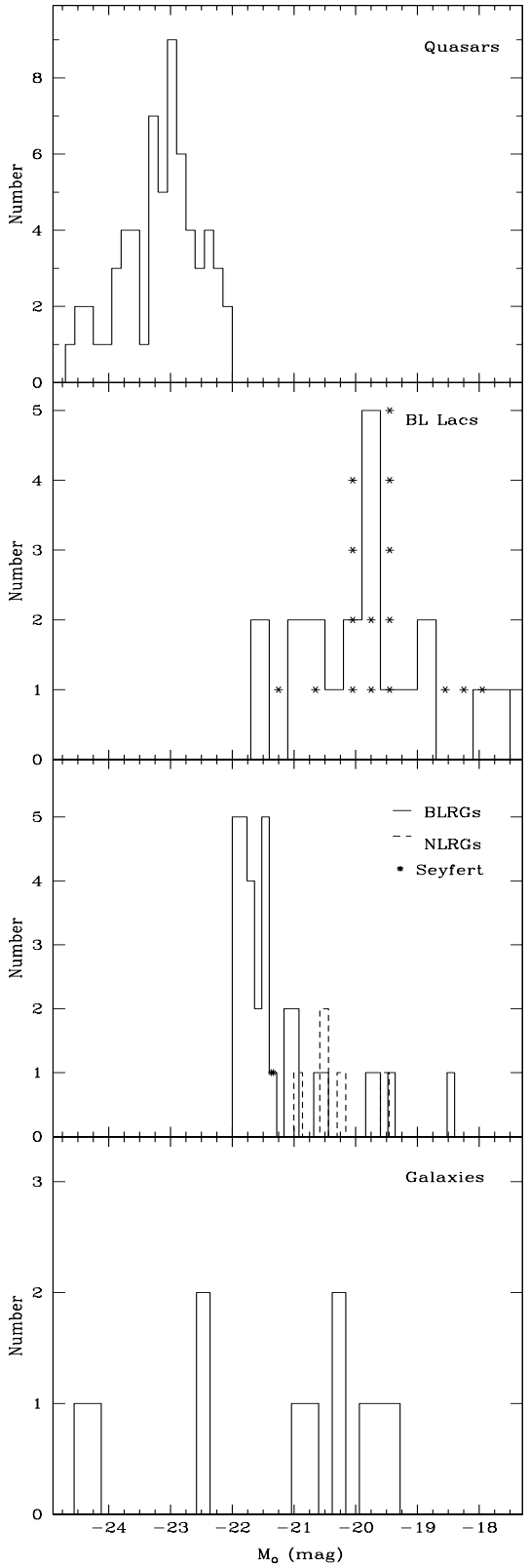

Fig. 5.— The distribution of absolute O magnitudes for the newly identified RGB sources, separated by spectroscopic class. The panels are in the same order and represent the same objects as described in Figure 4. The asterisks in second panel show the distribution of BL Lac host galaxy optical luminosities derived using our method described in §6.

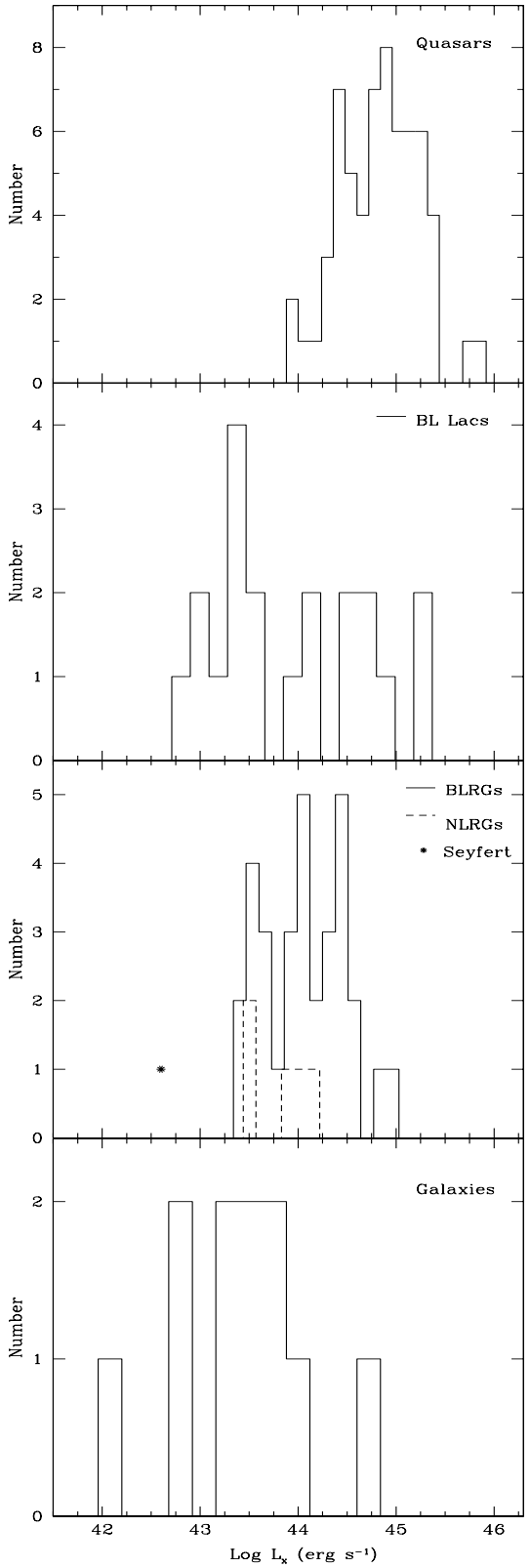

Fig. 6.— The distribution of the logarithm of the X-ray luminosity for the newly identified RGB sources. The panels show the distribution of the various spectroscopic classes (see Figure 4).

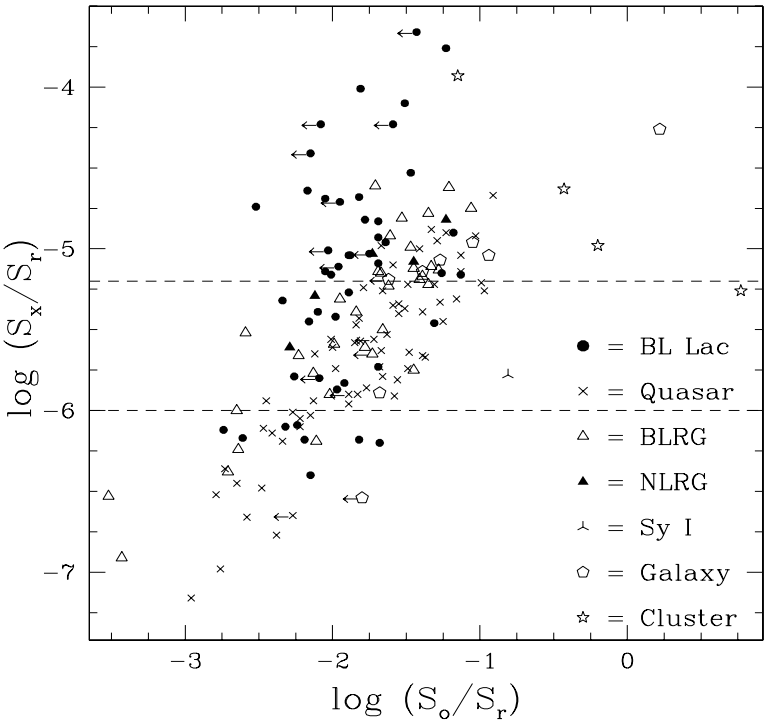

Fig. 7.— Log (S_x/S_r) as a function of log (S_o/S_r). Estimated optical fluxes of only the AGN component are used for those objects with measured break contrasts (§6). The ratio S_o/S_r is therefore formally an upper limit and left arrows in the figure denote this. While there is no clear separation of classes, the objects with the highest X-ray to radio flux density ratios are preferentially BL Lacs (see also Figure 11 in Brinkmann et al. 1997). However, BL Lacs are found throughout the diagram, including the region between log (S_x/S_r)=−6.0 and log (S_x/S_r)=−5.2 which represents a zone of avoidance in which few previously known BL Lacs resided.

TABLE 1
Spectroscopic Run Observing Parameters

Observatory			Instrument	Detector	Date	Range (Å)	Resolution (Å / 3pix)
McDonald	(mcd1)	2.7-m	LCS	TI1	2/12/94−2/14/94	3100−5800	10.2
Kitt Peak	(kp1)	2.1-m	GoldCam	F3KC	7/6/94 −7/10/94	3800−8200	14.4
McDonald	(mcd2)	2.7-m	LCS	TI1	8/5/94 −8/6/94	3450−6150	10.2
McDonald	(mcd3)	2.7-m	LCS	TI1	3/28/95−4/3/95	3750−6450	10.2
Kitt Peak	(kp2)	2.1-m	GoldCam	F3KC	5/30/95−6/2/95	4800−10000	14.4
McDonald	(mcd4)	2.7-m	LCS	TI1	9/18/95−9/24/95	3800−6500	10.2

TABLE 2

Observing log and Source Properties

Name	Run[a]	Exposure T_{tot} (hr)	Exposure #	Class	z	Notes
0006+125	mcd4	0.33	1	Quasar	0.980	
0009+180	mcd4	0.33	1	Quasar	0.310	
0027+452	kp1	0.67	2	Quasar	0.971?	Uncertain line ID
0043+316	mcd4	0.33	1	Quasar	0.631	
0044+193	mcd4	0.33	1	Quasar?	0.181	Possible Narrow-lined Sy I; See text
0046+228	mcd4	0.33	1	Quasar	0.433	
0109+318	mcd4	0.33	1	Quasar	1.71	
0110+139	mcd4	0.33	1	Cluster	0.061	Br_{4000}=50%
0110+418	mcd2	0.5	1	BL Lac?	0.096	Br_{4000}=32% ($W_\lambda^M \leq$25Å); Hα useful
0112+383	mcd2	0.5	1	Quasar	0.333	Low resolution VLA catalog
0123+262	mcd4	0.5	1	Quasar	0.849?	Uncertain line ID
0136+391	kp1	0.33	1	BL Lac	···	Low resolution VLA catalog
0152+017	mcd2	0.5	1	BL Lac?	0.080	Low resolution VLA catalog; Br_{4000}=29% ($W_\lambda^M \leq$38Å); Hα useful
0157+413	mcd4	0.33	1	Cluster	0.080	Br_{4000}=47%; W_λ([OII]λ3727)=12Å
0207+295A	mcd4	0.33	1	NLRG	0.111	Alternate radio-quiet classification possible
0250+172	mcd4	1.17	1	BL Lac	···	
0254+395	mcd4	0.33	1	Quasar	0.293	
0314+247	mcd1	1.5	3	BL Lac?	0.054	Low resolution VLA catalog; Br_{4000}=30%; W_λ([OII]λ3727)=14Å; W_λ([OIII]λ5007)=12Å
0321+236	mcd4	0.67	2	BL Lac	···	
0326+024	mcd1	1.0	2	BL Lac	···	Low resolution VLA catalog; Prev. known BL Lac
0336+225B	mcd1	0.5	1	Quasar	0.563	Low resolution VLA catalog
0505+042	mcd4	1.0	3	BL Lac	···	
0656+426	mcd4	0.25	1	BL Lac?	0.059	Br_{4000}=36% ($W_\lambda^M \leq$40Å); Star-Forming Elliptical?; Hα useful
0705+548	mcd1	1.0	2	Quasar	0.830	Δ_{rx}=52″
0710+591	mcd1	1.5	3	BL Lac	0.122	Br_{4000}=22% ($W_\lambda^M \leq$25Å); Hα useful
0714+741	mcd3	0.67	2	Quasar	0.371	
0717+645	mcd1	0.5	1	Quasar	0.594?	Uncertain line ID
0735+712	mcd3	0.5	1	Quasar	···	W_λ=27Å
0746+527	mcd1	0.5	1	BLRG	0.542	
0749+451	mcd3	0.25	1	BLRG	0.190	
0801+476	mcd3	0.25	1	BLRG	0.155	
0806+595	mcd1	1.75	4	BL Lac	···	
0806+728	mcd3	0.42	1	NLRG	0.098	Br_{4000}=16%; Alternate radio-quiet classification possible
0810+504	mcd3	0.5	1	Quasar	1.20	
0814+561	mcd1	1.0	2	Quasar	0.511?	Uncertain line ID
0820+488	mcd3	0.83	2	Galaxy	0.130	Br_{4000}=41% ($W_\lambda^M \leq$47Å); Hα useful
0854+441	mcd3	1.33	4	BL Lac	···	Previously known BL Lac
0909+522	mcd1	1.0	2	BLRG	0.411	
0912+685	mcd3	0.5	1	Quasar	1.08	
0952+656	mcd1	1.67	3	BL Lac	···	
1012+424	mcd3	2.0	4	BL Lac?	···	W_λ=10Å & 4Å
1021+453	mcd1	1.83	4	BLRG	0.364	
1031+508	mcd1	1.0	2	BL Lac	···	Previously known BL Lac
1037+571	mcd1	0.5	1	BL Lac	···	Previously known BL Lac
	mcd3	0.5	1			W_λ=2Å
1045+528A	mcd3	0.5	1	Quasar	1.05	
1058+564	kp2	0.5	2	BL Lac?	···	Δ_{rx}=69″; Prev. known BL Lac

TABLE 2—*Continued*

Name	Run[a]	Exposure T_{tot} (hr)	Exposure #	Class	z	Notes
	mcd1	0.5	1			
1110+715	mcd3	1.5	3	BL Lac	···	Δ_{rx}=55″
1120+422	mcd1	0.83	2	BL Lac	···	Previously known BL Lac
1136+676	mcd1	0.5	2	BL Lac	0.136	Br_{4000}=20% ($W_\lambda^M \leq$47Å); Hα useful; Prev. known BL Lac
1203+451	mcd1	0.5	1	Quasar	1.07	
1208+526	mcd1	0.67	2	Quasar	0.427?	Uncertain line ID
1223+541	mcd3	0.33	1	BLRG	0.157	
1233+483A	kp2	0.94	2	Quasar	···	
1241+516B	mcd3	0.5	1	Quasar	0.466?	Uncertain line ID
1241+495	mcd1	1.33	3	Quasar	0.818?	Uncertain line ID
1248+514	kp2	0.33	1	Star	···	See text
1249+447B	kp2	0.33	1	Quasar	0.803	
1252+648	kp2	0.33	1	BLRG	0.313	
1253+509	mcd1	0.5	1	Galaxy	0.121	Δ_{rx}=55″; Br_{4000}=49%
1301+713	mcd3	1.0	2	BLRG	0.275	
1302+483	kp2	0.5	1	Quasar	0.875	
1306+554	kp2	0.33	1	Quasar	1.60	
1324+576	mcd1	0.67	2	Galaxy	0.115	Br_{4000}=41%
1334+565	kp2	0.5	1	BLRG	0.343	
1336+656	mcd3	0.5	1	BLRG	0.436?	Uncertain line ID
1346+623	kp2	0.5	1	BLRG	0.117	Alternate radio-quiet classification possible
1353+431	mcd3	0.33	1	Quasar	···	Unidentified lines
1356+416	mcd3	0.33	1	Quasar	0.697?	Uncertain line ID
1411+426	kp1	0.33	1	Quasar	0.888	
1413+436	kp2	0.67	2	BLRG	0.090	FWHM(Hα)$\approx$ 1900 km s^{-1}; See text
1415+485	kp2	1.17	3	BL Lac	···	Calibration error at ∼9970?
1417+257	kp1	0.5	1	BL Lac	0.237	Low resolution VLA catalog; Br_{4000}=0%; Prev. known BL Lac
1427+541	mcd3	1.0	2	BL Lac?	0.105	Br_{4000}=39% ($W_\lambda^M \leq$37Å); Hα useful
1428+426	kp1	1.0	2	BL Lac	0.130	Br_{4000}=1%; Previously known BL Lac
1437+507	kp2	0.33	1	Quasar	0.785	
1439+395	kp1	0.75	2	BL Lac	···	Previously known BL Lac
1439+584	kp2	0.5	2	BLRG	0.425	
1442+120	kp1	0.5	1	BL Lac	0.162	Low resolution VLA catalog; Br_{4000}=18%; Hα & atmospheric A-band coincident; Prev. known BL Lac
1443+520B	mcd3	0.33	1	NLRG	0.142	
1448+361	kp1	0.83	2	BL Lac	···	
1451+535	kp1	0.5	1	BLRG	0.433	
1454+514	kp2	1.0	2	BL Lac?	···	Flat fielding error at ∼8380?
1459+336	kp1	0.5	1	Quasar	0.644	
1504+568	mcd3	1.5	3	Quasar	···	Unidentified lines; $W_\lambda(\lambda6309)$=22Å; $W_\lambda(\lambda3790)$>22Å
1509+573	kp1	0.5	1	Quasar	0.814?	Uncertain line ID
1515+479B	kp2	0.5	1	Quasar	0.914	
1516+293	kp1	0.83	2	BL Lac?	0.130	Br_{4000}=32%; W_λ(Hα, [NII])=9Å; Star-forming ellpitical?
1517+654B	kp1	0.5	2	BL Lac	···	Previously known BL Lac
1518+485	kp1	1.0	2	Quasar	0.576	
1518+407	kp2	0.42	2	Sy I	0.065	FWHM(Hα)$\approx$ 1900 km s^{-1}
	mcd3	0.33	1			
1522+667B	mcd3	0.33	1	Quasar	0.629	

TABLE 2—*Continued*

Name	Run[a]	Exposure T_{tot} (hr)	Exposure #	Class	z	Notes
1523+636	mcd3	0.33	1	BLRG	0.204	
1527+745C	mcd3	0.33	1	Quasar	0.921?	Uncertain line ID
1531+439	kp2	0.58	2	Quasar	0.452	
1532+302	mcd3	0.17	1	BL Lac?	0.064	Br_{4000}=29%
1533+342	kp1	1.0	2	BL Lac	···	
1534+372	kp2	1.0	3	BL Lac?	0.143	W_λ(Hα,[NII]??)=4Å; Br_{4000} needed; O−E=1.6
1534+586	kp2	0.5	1	Quasar	1.90?	Uncertain line ID
1542+614	mcd3	0.67	2	BL Lac	···	
1545+348	kp2	0.42	2	Quasar	0.518	
1601+179	kp1	0.5	1	Quasar	0.659?	Uncertain line ID
1602+308	kp2	1.5	3	BL Lac	···	Previously known BL Lac
1608+603B	mcd3	1.0	2	Quasar	0.178	
1610+671B	kp2	1.0	2	BL Lac?	0.067?	Uncertain line ID; Δ_{rx}=43″; Br_{4000} needed; O−E=1.54
1610+728B	mcd3	1.0	3	Quasar	0.592?	Uncertain line ID
1619+305	kp2	0.33	1	Quasar	1.29?	Uncertain line ID
1622+401	kp1	0.5	1	Quasar	0.687	
1626+513	kp1	0.33	1	BLRG	0.179	Δ_{rx}=42″
1628+564	mcd3	0.75	2	Quasar	0.400	
1629+401	kp1	0.5	1	BLRG	0.272	
1637+118	mcd1	0.92	3	BLRG	0.144	Δ_{rx}=56″; Alternate radio-quiet classification possible
1641+395	kp1	0.33	1	Quasar	0.540	
1652+403	kp2	2.0	4	BL Lac	···	
1704+716	kp1	1.0	2	BL Lac	···	Previously known BL Lac
1706+362	kp1	0.5	1	Quasar	1.07	
1706+322	kp2	0.33	1	Quasar	0.917?	Uncertain line ID
1713+329	kp1	0.5	1	BLRG	0.102	Alternate radio-quiet classification possible
1720+266	kp2	1.0	2	Cluster?	0.161	Br_{4000} needed; O−E=2.4
1721+211	kp2	1.33	3	BLRG	0.628	
1722+246	kp1	0.33	1	BLRG	0.175	
1722+282	kp2	0.83	2	BLRG	···	Unidentified line; W_λ>60Å
1726+322	mcd4	0.5	1	Quasar	1.09	
1738+324	mcd4	0.33	1	BLRG	0.126	
1742+597	kp2	1.33	4	BL Lac	···	
1745+398	mcd4	1.0	2	BL Lac	0.267	Br_{4000}=17% (W_λ^M≤21Å); Hα useful
1750+470	kp1	0.83	2	BL Lac?	0.160	Br_{4000}=29%; Hα & atmospheric A-band coincident
1751+472	kp1	0.33	1	Quasar	1.48	
1755+338	kp2	0.33	1	BLRG	0.242	
1756+553	kp1	0.83	2	BL Lac	···	
1757+538	mcd4	0.33	1	Cluster	0.120	Br_{4000}=50%
1804+524	kp1	0.5	2	Quasar	0.516	
1807+438A	mcd2	0.5	1	Quasar	0.815	Δ_{rx}=51″
1808+468	mcd2	1.0	2	BL Lac	···	See text
1808+665	mcd2	0.5	1	Quasar	0.697?	Uncertain line ID
1811+584	mcd4	0.33	1	Star	···	See text
1811+442	kp1	2.94	5	BL Lac	···	
1814+409B	kp1	0.5	1	Quasar	0.971	
1823+334	mcd4	0.33	1	Galaxy	0.108	Br_{4000}=49%
1829+540	kp1	1.0	2	BL Lac	···	

TABLE 2—*Continued*

Name	Run[a]	Exposure T_{tot} (hr)	#	Class	z	Notes
1838+480	kp1	0.5	1	BL Lac	···	
1841+591	kp1	1.5	3	BL Lac	0.530	Br_{4000}=17% ($W_\lambda^M \leq$10Å); Hα useful
1844+546	mcd2	0.5	1	BLRG	0.234	
1848+427	kp1	1.5	3	BL Lac	···	
1922+691	mcd4	0.33	1	NLRG?	0.099	Alternate radio-quiet class. possible;No Balmer lines; See text
2123+101A	mcd4	0.5	1	BLRG	0.186	
2123+067	kp1	0.5	1	Quasar	0.934	
2145+073	kp1	0.5	1	BL Lac	0.237	Br_{4000}=10% ($W_\lambda^M \leq$10Å); Prev. known BL Lac
2146+093	mcd4	0.33	1	Quasar	0.981	
2158+268B	mcd4	0.33	1	Quasar	0.713	
2201+050A	kp2	0.25	1	BLRG	0.232	
2217+226	kp1	0.5	1	Quasar	0.405	
2219+229	kp1	1.33	3	Quasar	1.26	
2227+243	kp1	0.5	1	NLRG	0.319	
2229+309	mcd4	0.33	1	Quasar	0.322	
2241+275	kp2	0.5	1	Quasar	0.493	
2241+048	mcd4	0.33	1	Galaxy	0.069	Br_{4000}=45%
2243+203	mcd4	1.17	3	BL Lac	···	
2246+317	mcd4	0.33	1	BLRG	0.147	Alternate radio-quiet classification possible
2250+384	mcd4	1.17	3	BL Lac?	0.119	Br_{4000}=7% ($W_\lambda^M \leq$10Å); Star-forming elliptical?; Hα useful
2253+197	mcd4	0.33	1	Quasar	0.298	
2256+263	kp1	0.5	1	BLRG	0.121	Br_{4000}=25%
2259+189	kp2	0.75	2	Galaxy?	0.132	(W_λ(Hα,[NII])=9Å); O−E=2.7
2259+314	kp2	0.5	1	Quasar	1.14?	Uncertain line ID
2308+201	mcd4	1.0	3	BLRG	0.250	
2310+107	mcd4	0.67	2	BLRG	0.436	
2311+355	mcd4	1.17	3	Quasar	1.39?	Uncertain line ID
2313+103	mcd4	0.5	1	BLRG	0.456	
2318+308	mcd4	0.5	1	BLRG	0.103	Alternate radio-quiet classification possible
2319+161	kp1	1.0	2	BL Lac	···	
2322+346	mcd4	0.33	1	BL Lac?	0.098	Br_{4000}=33% ($W_\lambda^M \leq$29Å); Star-forming elliptical?; Hα useful
2323+205	mcd4	0.25	1	Galaxy	0.041	Br_{4000}=48%

[a]See Table 1

TABLE 3

SOURCE FLUXES AND SPECTROSCOPIC CLASSIFICATIONS

RGB Name	RA (J2000)	Dec	S_r (mJy)	O (mag)	$\log \frac{S_r}{S_{opt}}$	F_X ($10^{12} \frac{erg}{s\ cm^2}$)	z	Class
0006+125	00 06 23.06	12 35 53.1	156	17.6	2.88	0.61	0.980	Quasar
0009+180	00 09 34.86	18 03 43.1	70	16.6	1.95	1.58	0.310	Quasar
0027+452	00 27 42.26	45 14 57.1	91	17.9	2.76	1.26	0.971?	Quasar
0043+316	00 43 59.83	31 37 20.3	16	16.8	1.48	1.33	0.631	Quasar
0044+193	00 44 59.12	19 21 40.8	7	16.8	1.09	2.63	0.181	Quasar?
0046+228	00 46 20.27	22 49 43.3	58	16.3	1.79	3.04	0.433	Quasar
0109+318	01 09 27.88	31 49 56.0	181	17.8	3.16	1.41	1.71	Quasar
0110+139	01 10 03.16	13 58 41.4	16	11.7	−0.77	1.56	0.061	Cluster
0110+418	01 10 04.81	41 49 50.7	18	18.4[a]/17.8[b]	2.00	2.46	0.096	BL Lac?
0112+383[c]	01 12 18.2	38 18 59	113	17.3	2.44	1.34	0.333	Quasar
0123+262	01 23 43.10	26 15 22.5	173	18.0	3.05	0.92	0.849?	Quasar
0136+391[c]	01 36 32.7	39 06 00	49	15.8	1.42	20.2	···	BL Lac
0152+017[c]	01 52 39.7	01 47 18	65	17.1[a]/16.7[b]	2.03	4.97	0.080	BL Lac?
0157+413	01 57 05.01	41 20 30.6	23	14.3[d]	0.45	9.50	0.081	Cluster
0207+295A	02 07 02.22	29 30 46.1	19	16.5	1.27	5.05	0.110	NLRG
0250+172	02 50 37.96	17 12 08.5	35	17.5	1.95	5.71	···	BL Lac
0254+395	02 54 42.63	39 31 34.8	273	16.4	2.45	3.10	0.293	Quasar
0314+247[c]	03 14 02.7	24 44 31	6	18.3[a]/17.9[b]	1.47	2.12	0.054	BL Lac?
0321+236	03 21 59.93	23 36 11.0	56	16.8	1.87	0.65	···	BL Lac
0326+024[c]	03 26 14.0	02 25 16	68	17.5	2.24	24.9	···	BL Lac
0336+225B[c]	03 36 04.9	22 35 35	64	17.8	2.47	1.10	0.563	Quasar
0505+042	05 05 34.78	04 15 54.7	90	17.6	2.40	7.61	···	BL Lac
0656+426	06 56 10.67	42 37 02.7	138	16.5[a]/15.4[b]	2.11	3.87	0.059	BL Lac?
0705+548	07 05 44.69	54 48 09.9	13	18.0	1.91	1.26	0.830	Quasar
0710+591	07 10 30.07	59 08 20.5	34	18.0[a]/18.3[b]	2.13	35.6	0.125	BL Lac
0714+741	07 14 36.19	74 08 10.2	65	17.1	2.14	2.85	0.371	Quasar
0717+645	07 17 54.04	64 30 48.4	8	17.7	1.51	1.89	0.594?	Quasar
0735+712	07 35 02.36	71 15 06.1	72	18.1	2.69	1.46	··· [e]	Quasar
0746+527	07 46 57.09	52 46 19.9	8	18.4	1.79	1.69	0.542	BLRG
0749+451	07 49 06.51	45 10 33.9	51	16.5	1.73	2.85	0.190	BLRG
0801+476	08 01 31.96	47 36 16.1	42	16.4	1.59	11.5	0.155	BLRG
0806+595	08 06 25.94	59 31 06.9	29	17.2	1.75	6.07	···	BL Lac
0806+728	08 06 38.97	72 48 20.6	20	17.7[a]/18.6[b]	1.77	3.31	0.098	NLRG
0810+504	08 10 02.70	50 25 38.6	12	17.8	1.88	0.98	1.20	Quasar
0814+561	08 14 32.12	56 09 56.8	49	17.7	2.30	1.94	0.511?	Quasar
0820+488	08 20 28.10	48 53 47.5	5	17.5	1.05	0.98	0.130	Galaxy
0854+441	08 54 09.88	44 08 30.3	31	17.6	1.93	4.97	···	BL Lac
0909+522	09 09 24.68	52 16 32.7	33	18.4	2.37	1.27	0.411	BLRG
0912+685	09 12 36.59	68 34 25.1	104	17.8	2.80	0.61	1.08	Quasar
0952+656	09 52 32.19	65 38 01.1	27	18.0	2.04	1.82	···	BL Lac
1012+424	10 12 44.30	42 29 57.2	29	18.1	2.11	10.4	···	BL Lac?
1021+453	10 21 06.04	45 23 31.9	23	18.2	2.12	1.06	0.364	BLRG
1031+508	10 31 18.52	50 53 35.8	23	16.3	1.28	71.5	···	BL Lac
1037+571	10 37 44.31	57 11 55.8	89	17.4	2.32	2.58	···	BL Lac
1045+528A	10 45 42.18	52 51 12.6	43	18.1	2.53	0.68	1.05	Quasar
1058+564	10 58 37.73	56 28 11.3	178	15.8	1.98	4.69	···	BL Lac?
1110+715	11 10 37.59	71 33 56.6	22	18.0	1.95	2.12	···	BL Lac
1120+422	11 20 48.07	42 12 12.5	19	17.1	1.51	10.0	···	BL Lac

TABLE 3—*Continued*

RGB Name	RA (J2000)	Dec	S_r (mJy)	O (mag)	$\log \frac{S_r}{S_{opt}}$	F_X ($10^{12} \frac{erg}{s\ cm^2}$)	z	Class
1136+676	11 36 30.08	67 37 04.4	40	18.0[a]/18.3[b]	2.21	27.4	0.136	BL Lac
1203+451	12 03 35.39	45 10 49.6	53	17.7	2.47	0.88	1.07	Quasar
1208+526	12 08 22.45	52 40 13.5	19	16.7	1.46	2.01	0.427?	Quasar
1223+541	12 23 13.10	54 09 07.8	42	16.2	1.51	1.33	0.157	BLRG
1233+483A	12 33 54.45	48 20 50.0	7	18.0	1.64	0.51	··· [e]	Quasar
1241+516B	12 41 16.49	51 41 30.0	20	17.9	1.97	0.95	0.466?	Quasar
1241+495	12 41 39.73	49 34 05.5	7	17.6	1.47	1.57	0.818?	Quasar
1248+514	12 48 34.30	51 28 07.9	61	18.4	···	0.67	···	Star[f]
1249+447B	12 49 23.56	44 44 50.5	12	17.7	1.75	0.90	0.803	Quasar
1252+648	12 52 23.81	64 51 38.0	26	17.7	1.96	1.88	0.313	BLRG
1253+509	12 53 26.16	50 54 28.2	7	17.7	1.27	1.06	0.121	Galaxy
1301+713	13 01 30.37	71 20 13.1	30	17.4	1.89	1.32	0.275	BLRG
1302+483	13 02 17.20	48 19 17.6	90	17.7	2.65	0.27	0.875	Quasar
1306+554	13 06 03.36	55 29 44.0	282	17.9	3.37	0.35	1.60	Quasar
1324+576	13 24 00.92	57 39 16.4	25	16.6	1.42	3.21	0.115	Galaxy
1334+565	13 34 37.49	56 31 47.9	36	17.8	2.15	0.81	0.343	BLRG
1336+656	13 36 55.53	65 41 16.1	6	18.0	1.45	0.83	0.436?	BLRG
1346+623	13 46 17.59	62 20 45.5	7	17.9	1.35	2.07	0.117	BLRG
1353+431	13 53 41.74	43 10 52.4	24	16.9	1.74	0.77	··· [e]	Quasar
1356+416	13 56 07.38	41 36 15.2	47	16.4	1.81	1.02	0.697?	Quasar
1411+426	14 11 59.74	42 39 50.4	46	17.2	2.16	0.90	0.888	Quasar
1413+436	14 13 43.72	43 39 45.1	34	16.0	1.32	4.47	0.090	BLRG
1415+485	14 15 36.82	48 30 30.5	58	17.6	2.21	0.41	···	BL Lac
1417+257[c]	14 17 56.7	25 43 25	40	17.5	2.04	25.3	0.237	BL Lac
1427+541	14 27 30.33	54 09 23.5	24	17.4[a]/16.1[b]	1.73	0.80	0.105	BL Lac?
1428+426	14 28 32.62	42 40 21.1	21	16.9	1.56	80.8	0.130	BL Lac
1437+507	14 37 26.17	50 45 55.9	8	18.1	1.73	0.85	0.785	Quasar
1439+395	14 39 17.48	39 32 42.7	38	18.1	2.22	15.3	···	BL Lac
1439+584	14 39 42.86	58 27 59.1	16	18.5	2.09	1.39	0.425	BLRG
1442+120[c]	14 42 48.2	12 00 41	45	17.9[a]/18.5[b]	2.23	11.0	0.162	BL Lac
1443+520B	14 43 02.76	52 01 37.3	65	17.4	2.18	5.92	0.142	NLRG
1448+361	14 48 00.59	36 08 31.0	29	17.2	1.75	7.54	···	BL Lac
1451+535	14 51 06.44	53 33 54.0	6	18.3	1.57	0.81	0.433	BLRG
1454+514	14 54 27.12	51 24 33.6	80	18.4	2.67	0.95	···	BL Lac?
1459+336	14 59 58.45	33 37 01.6	105	17.6	2.62	1.34	0.644	Quasar
1504+568	15 04 55.57	56 49 20.3	6	17.1	1.21	0.58	··· [e]	Quasar
1509+573	15 09 40.69	57 18 11.9	10	18.3	1.92	0.42	0.814?	Quasar
1515+479B	15 15 12.02	47 55 09.0	9	18.4	1.94	0.26	0.914	Quasar
1516+293	15 16 41.59	29 18 09.2	34	18.2[a]/17.6[b]	2.21	2.15	0.130	BL Lac?
1517+654B	15 17 47.58	65 25 23.3	19	17.4	1.63	19.9	···	BL Lac
1518+485	15 18 30.95	48 32 14.4	5	18.4	1.55	0.89	0.576	Quasar
1518+407	15 18 38.91	40 45 00.1	29	15.0	0.82	0.85	0.065	Sy I
1522+667B	15 22 58.94	66 45 06.7	61	17.5	2.34	1.25	0.629	Quasar
1523+636	15 23 45.87	63 39 24.3	14	16.8	1.27	5.93	0.204	BLRG
1527+745C	15 27 12.08	74 31 50.8	8	17.5	1.52	0.50	0.921?	Quasar
1531+439	15 31 02.49	43 56 37.6	21	16.8	1.54	0.81	0.452	Quasar
1532+302	15 32 02.23	30 16 28.9	47	15.6[a]/17.9[b]	1.29	5.87	0.064	BL Lac?
1533+342	15 33 24.27	34 16 40.2	33	17.9	2.09	5.73	···	BL Lac

TABLE 3—*Continued*

RGB Name	RA (J2000)	Dec	S_r (mJy)	O (mag)	$\log \frac{S_r}{S_{opt}}$	F_X ($10^{12} \frac{erg}{s\ cm^2}$)	z	Class
1534+372	15 34 47.21	37 15 54.4	20	18.3	2.01	0.48	0.143	BL Lac?
1534+586	15 34 57.24	58 39 23.5	150	18.1	3.23	0.28	1.90?	Quasar
1542+614	15 42 56.94	61 29 55.3	102	17.2	2.30	1.46	···	BL Lac
1545+348	15 45 10.95	34 52 46.8	7	17.1[g]	1.19	1.49	0.518	Quasar
1601+179	16 01 51.56	17 54 09.9	7	18.4	1.75	0.49	0.659?	Quasar
1602+308	16 02 18.04	30 51 09.3	20	18.5[g]	2.11	2.59	···	BL Lac
1608+603B	16 08 20.55	60 18 28.2	26	16.0	1.22	2.25	0.178	Quasar
1610+671B	16 10 04.07	67 10 26.4	13	18.4	1.78	4.83	0.067?	BL Lac?
1610+728B	16 10 49.94	72 50 46.4	5	17.7	1.27	0.65	0.592?	Quasar
1619+305	16 19 02.48	30 30 51.5	38	17.1	2.13	0.94	1.29?	Quasar
1622+401	16 22 29.32	40 06 43.7	30	17.9	2.21	0.97	0.687	Quasar
1626+513	16 26 11.62	51 20 38.3	14	17.3	1.47	1.61	0.179	BLRG
1628+564	16 28 50.41	56 29 29.2	18	17.4	1.71	0.50	0.400	Quasar
1629+401	16 29 01.32	40 08 00.0	21	17.6	1.80	9.05	0.272	BLRG
1637+118	16 37 46.50	11 49 49.0	11	17.4	1.39	1.19	0.144	BLRG
1641+395	16 41 47.51	39 35 03.2	47	18.0	2.41	0.67	0.540	Quasar
1652+403	16 52 49.94	40 23 10.2	11	17.3	1.35	0.68	···	BL Lac
1704+716	17 04 46.98	71 38 17.6	17	16.5	1.23	3.79	···	BL Lac
1706+362	17 06 34.11	36 15 08.0	15	18.3	2.16	0.91	1.07	Quasar
1706+322	17 06 48.05	32 14 22.8	20	16.8	1.65	0.76	0.917?	Quasar
1713+329	17 13 22.58	32 56 27.9	25	16.8	1.50	4.50	0.102	BLRG
1720+266	17 20 09.92	26 37 31.1	7	17.4	1.21	14.6	0.161	Cluster?
1721+211	17 21 33.25	21 11 02.0	42	19.2[g]	2.86	0.75	0.628	BLRG
1722+246	17 22 41.25	24 36 19.1	28	16.5	1.45	3.33	0.175	BLRG
1722+282	17 22 42.16	28 15 00.1	150	20.0	3.61	0.78	··· [e]	BLRG
1726+322	17 26 35.13	32 13 23.0	183	17.6	2.97	1.14	1.09	Quasar
1738+324	17 38 40.50	32 24 09.0	209	16.1	2.16	2.40	0.126	BLRG
1742+597	17 42 32.00	59 45 06.8	77	17.4	2.26	0.91	···	BL Lac
1745+398	17 45 37.76	39 51 30.8	118	18.3[a]/18.9[b]	2.84	1.59	0.267	BL Lac
1750+470	17 50 05.00	47 00 43.7	10	19.0[a]/18.7[b]	2.01	3.47	0.160	BL Lac?
1751+472	17 51 31.63	47 13 22.6	34	17.1	2.11	1.67	1.48	Quasar
1755+338	17 55 11.27	33 50 59.7	158	17.9	2.80	1.16	0.242	BLRG
1756+553	17 56 15.89	55 22 18.1	10	17.9	1.55	14.1	···	BL Lac
1757+538	17 57 06.70	53 51 37.6	31	13.4[g]	0.24	5.77	0.120	Cluster
1804+524	18 04 52.74	52 24 29.4	7	17.0	1.15	0.76	0.516	Quasar
1807+438A	18 07 59.84	43 50 36.9	5	18.1[g]	1.14	1.00	0.815	Quasar
1808+468	18 08 01.20	46 49 41.0	41	18.4	2.38	0.58	···	BL Lac
1808+665	18 08 49.58	66 34 29.7	6	17.5	1.35	0.97	0.697?	Quasar
1811+584	18 11 33.92	58 25 15.6	3	17.8	···	0.49	···	Star[f]
1811+442	18 11 53.47	44 16 28.5	6	18.9[g]	1.69	0.87	···	BL Lac
1814+409B	18 14 34.48	40 57 46.4	7	18.7	1.94	1.30	0.971	Quasar
1823+334	18 23 09.84	33 24 39.1	3	14.9	−0.22	2.94	0.108	Galaxy
1829+540	18 29 24.29	54 02 59.8	18	17.6	1.69	3.51	···	BL Lac
1838+480	18 38 49.17	48 02 34.4	23	17.6	1.80	3.82	···	BL Lac
1841+591	18 41 20.31	59 06 08.2	6	19.7[a]/20.3[b]	2.17	0.74	0.530	BL Lac
1844+546	18 44 30.88	54 41 44.8	32	17.2	1.82	1.27	0.234	BLRG
1848+427	18 48 47.14	42 45 39.4	8	18.9	1.86	13.9	···	BL Lac
1922+691	19 22 14.65	69 11 12.4	20	17.0[d]	1.47	2.95	0.099	NLRG?

TABLE 3—*Continued*

RGB Name	RA (J2000)	Dec	S_r (mJy)	O (mag)	$\log \frac{S_r}{S_{opt}}$	F_X ($10^{12} \frac{erg}{s\ cm^2}$)	z	Class
2123+101A	21 23 13.34	10 07 54.9	301	19.0	3.50	0.65	0.186	BLRG
2123+067	21 23 19.33	06 46 22.9	11	18.0	1.87	1.55	0.934	Quasar
2145+073	21 45 52.30	07 19 27.2	37	19.0[a]/20.7[b]	2.61	11.9	0.237	BL Lac
2146+093	21 46 54.08	09 20 48.9	50	17.1	2.18	1.11	0.981	Quasar
2158+268B	21 58 25.60	26 52 41.4	24	17.8	2.08	1.11	0.713	Quasar
2201+050A	22 01 07.16	05 04 36.3	13	17.9	1.71	1.37	0.232	BLRG
2217+226	22 17 10.96	22 39 46.8	19	17.4	1.72	1.51	0.405	Quasar
2219+229	22 19 21.02	22 59 22.7	10	18.6	2.13	1.01	1.26	Quasar
2227+243	22 27 47.95	24 21 12.4	22	19.0	2.41	0.95	0.319	NLRG
2229+309	22 29 34.15	30 57 12.2	59	16.4	1.79	1.97	0.322	Quasar
2241+275	22 41 02.03	27 32 59.5	35	17.8	2.18	1.72	0.493	Quasar
2241+048	22 41 34.25	04 53 10.6	41	16.8[d]	1.70	0.94	0.069	Galaxy
2243+203	22 43 54.73	20 21 03.9	86	16.0	1.74	0.97	···	BL Lac
2246+317	22 46 21.68	31 42 08.0	13	16.5	1.09	4.13	0.147	BLRG
2250+384	22 50 05.77	38 24 37.3	60	16.0[g,a]/18.0[b]	1.17	7.36	0.119	BL Lac?
2253+197	22 53 07.37	19 42 34.8	254	16.3	2.38	1.01	0.298	Quasar
2256+263	22 56 39.17	26 18 43.8	40	19.1[a]/19.0[b]	2.64	2.14	0.121	BLRG
2259+189	22 59 19.16	18 57 30.3	17	17.6	1.67	1.96	0.132	Galaxy?
2259+314	22 59 50.77	31 24 52.1	13	18.4	2.14	0.85	1.14?	Quasar
2308+201	23 08 11.63	20 08 42.3	177	17.6	2.73	1.80	0.250	BLRG
2310+107	23 10 09.74	10 47 24.3	12	18.1	1.82	1.50	0.436	BLRG
2311+355	23 11 48.98	35 35 41.4	18	17.2	1.86	0.74	1.39?	Quasar
2313+103	23 13 55.67	10 19 09.8	35	18.1	2.29	1.06	0.456	BLRG
2318+308	23 18 36.90	30 48 37.0	22	17.5	1.73	2.85	0.103	BLRG
2319+161	23 19 43.44	16 11 50.1	17	18.0[g]	1.83	4.61	···	BL Lac
2322+346	23 22 44.01	34 36 14.0	30	18.2[a]/17.4[b]	2.14	2.16	0.098	BL Lac?
2323+205	23 23 20.35	20 35 23.6	114	16.0[d]	1.82	0.59	0.041	Galaxy

[a]Estimate of AGN magnitude
[b]Estimate of Galaxy magnitude
[c]Object from low radio resolution sample
[d]Converted from V to B mag assuming α_{opt}=1.0.
[e]Line identificaton unknown; Redshift undetermined
[f]Optical counterpart is likely a chance coincidence
[g]Converted from E to B mag assuming α_{opt}=1.0.

TABLE 4
SOURCE LUMINOSITIES

RGB Name	$\log P_{5GHz}$ (W Hz^{-1})	M_O[a] (mag)	$\log L_X$ (erg s^{-1})	z
		BL Lacs		
0110+418[b]	23.18	$-18.75_{(-19.35)}$	43.41	0.096
0152+017[b]	23.60	$-19.67_{(-20.07)}$	43.55	0.080
0314+247[b]	22.18	$-17.66_{(-18.06)}$	42.83	0.054
0656+426[b]	23.67	$-19.65_{(-20.74)}$	43.17	0.059
0710+591	23.68	$-19.68_{(-19.38)}$	44.80	0.125
1136+676	23.81	$-19.84_{(-19.54)}$	44.76	0.136
1417+257	24.24	-21.41	45.23	0.237
1427+541[b]	23.37	$-19.93_{(-21.23)}$	43.00	0.105
1428+426	23.49	-20.85	45.19	0.130
1442+120	24.00	$-20.29_{(-19.69)}$	44.52	0.162
1516+293[b]	23.71	$-19.55_{(-20.15)}$	43.62	0.130
1532+302[b]	23.27	$-20.71_{(-18.41)}$	43.42	0.064
1534+372[b]	23.54	-19.64	43.05	0.143
1610+671B[b]	22.75	-18.01	43.38	0.067?
1745+398	24.80	$-20.83_{(-20.23)}$	44.13	0.267
1750+470[b]	23.31	$-19.16_{(-19.46)}$	44.01	0.160
1841+591	23.86	$-20.60_{(-20.00)}$	44.44	0.530
2145+073	24.20	$-19.91_{(-18.21)}$	44.90	0.237
2250+384[b]	23.88	$-21.58_{(-19.58)}$	44.07	0.119
2322+346[b]	23.42	$-18.99_{(-19.79)}$	43.37	0.098
		Quasars		
0006+125	25.74	-23.60	44.93	0.980
0009+180	24.68	-22.80	44.27	0.310
0027+452	25.51	-23.28	45.24	0.971?
0043+316	24.47	-23.77	44.85	0.631
0044+193[b]	23.40	-22.04	44.21	0.228
0046+228	24.82	-23.67	44.86	0.433
0109+318	26.07	-24.06	45.84	1.71
0112+383	24.94	-22.22	44.26	0.333
0123+262	25.71	-23.00	44.98	0.849?
0254+395	25.23	-22.90	44.51	0.293
0336+225B	25.03	-22.60	44.66	0.563
0705+548	24.57	-22.97	45.09	0.830
0714+741	24.77	-22.61	44.69	0.371
0717+645	24.17	-22.78	44.95	0.594?
0810+504	24.70	-23.65	45.33	1.20
0814+561	24.86	-22.54	44.82	0.511?
0912+685	25.62	-23.52	45.03	1.08
1045+528A	25.20	-23.19	45.05	1.05
1203+451	25.32	-23.61	45.18	1.07
1208+526	24.32	-23.25	44.67	0.427?

TABLE 4—*Continued*

RGB Name	$\log P_{5GHz}$ (W Hz^{-1})	M_O[a] (mag)	$\log L_X$ (erg s^{-1})	z
1241+516B	24.39	−22.19	44.42	0.466?
1241+495	24.19	−23.35	45.17	0.818?
1249+447B	24.48	−23.22	44.91	0.803
1302+483	25.45	−23.34	44.47	0.875
1306+554	26.24	−23.89	45.17	1.60
1356+416	25.03	−24.32	44.83	0.697?
1411+426	25.16	−23.86	45.01	0.888
1437+507	24.29	−22.79	44.87	0.785
1459+336	25.33	−23.00	44.88	0.644
1509+573	24.41	−22.64	44.59	0.814?
1515+479B	24.40	−22.70	44.50	0.914
1518+485	23.92	−22.03	44.59	0.576
1522+667B	25.08	−23.07	44.82	0.629
1527+745C	24.41	−23.61	44.79	0.921?
1531+439	24.40	−23.24	44.33	0.452
1534+586	26.03	−23.87	45.24	1.90?
1545+348	23.97	−23.16	44.72	0.518
1601+179	24.15	−22.24	44.46	0.659?
1608+603B	23.84	−22.37	43.92	0.178
1610+728B	23.95	−22.77	44.48	0.592?
1619+305	25.26	−24.44	45.39	1.29?
1622+401	24.81	−22.80	44.80	0.687
1628+564	24.24	−22.44	44.00	0.400
1641+395	24.87	−22.33	44.41	0.540
1706+362	24.76	−23.01	45.19	1.07
1706+322	24.80	−24.31	44.97	0.917?
1726+322	25.87	−23.73	45.31	1.09
1751+472	25.27	−24.60	45.77	1.48
1804+524	23.96	−23.26	44.42	0.516
1807+438A	24.01	−22.85	44.97	0.815
1808+665	24.07	−23.22	44.81	0.697?
1814+409B	24.32	−22.48	45.25	0.971
2123+067	24.52	−23.13	45.29	0.934
2146+093	25.25	−24.10	45.20	0.981
2158+268B	24.76	−22.95	44.89	0.713
2217+226	24.28	−22.46	44.50	0.405
2219+229	24.64	−22.91	45.39	1.26
2229+309	24.63	−23.06	44.40	0.322
2241+275	24.69	−22.39	44.73	0.493
2253+197	25.21	−23.03	44.04	0.298
2259+314	24.74	−22.99	45.22	1.14?
2311+355	24.95	−24.43	45.35	1.39?
Broad Line Radio Galaxies				
0746+527	24.10	−21.94	44.82	0.542
0749+451	24.17	−21.99	44.08	0.190

TABLE 4—*Continued*

RGB Name	$\log P_{5GHz}$ (W Hz^{-1})	M_O[a] (mag)	$\log L_X$ (erg s^{-1})	z
0801+476	23.94	−21.70	44.50	0.155
0909+522	24.54	−21.49	44.43	0.411
1021+453	24.29	−21.48	44.24	0.364
1223+541	23.95	−21.93	43.58	0.157
1252+648	24.24	−21.71	44.35	0.313
1301+713	24.22	−21.78	44.08	0.275
1334+565	24.45	−21.78	44.07	0.343
1336+656	23.83	−21.98	44.30	0.436?
1346+623	22.92	−19.64	43.51	0.117
1413+436	23.41	−21.02	43.61	0.090
1439+584	24.25	−21.44	44.50	0.425
1451+535	23.82	−21.67	44.29	0.433
1523+636	23.65	−21.83	44.46	0.204
1626+513	23.54	−21.08	43.78	0.179
1629+401	24.05	−21.56	44.91	0.272
1637+118	23.27	−20.56	43.45	0.144
1713+329	23.37	−20.47	43.72	0.102
1721+211	24.91	−21.36	44.60	0.628
1722+246	23.84	−21.84	44.07	0.175
1738+324	24.47	−21.59	43.64	0.126
1755+338	24.85	−21.05	43.91	0.242
1844+546	24.12	−21.69	43.92	0.234
2123+101A	24.93	−19.45	43.42	0.186
2201+050A	23.72	−20.97	43.94	0.232
2246+317	23.38	−21.50	44.01	0.147
2256+263	23.72	$-18.51_{(-18.61)}$	43.55	0.121
2308+201	24.93	−21.41	44.13	0.250
2310+107	24.13	−21.88	44.56	0.436
2313+103	24.64	−21.96	44.45	0.456
2318+308	23.31	−19.79	43.53	0.103
Narrow Line Radio Galaxies				
0207+295A	23.32	−20.92	43.84	0.110
0806+728	23.25	$-19.49_{(-18.59)}$	43.55	0.098
1443+520B	24.05	−20.53	44.14	0.142
1922+691[b]	23.26	−20.21	43.51	0.099
2227+243	24.18	−20.45	44.07	0.319
Normal Galaxies and Clusters				
0110+139	22.76	−24.51	42.81	0.061
0157+413	23.15	−22.50	43.84	0.081
0820+488	22.83	−20.25	43.28	0.130
1253+509	22.95	−19.91	43.25	0.121
1324+576	23.47	−20.91	43.68	0.115

TABLE 4—*Continued*

RGB Name	$\log P_{5GHz}$ (W Hz^{-1})	M_O[a] (mag)	$\log L_X$ (erg s^{-1})	z
1720+266[b]	23.19	−20.77	44.64	0.161
1757+538	23.60	−24.20	43.97	0.120
1823+334	22.38	−22.48	43.59	0.108
2241+048	23.27	−19.67	42.70	0.069
2259+189[b]	23.42	−20.18	43.59	0.132
2323+205	23.28	−19.38	42.04	0.041
		Seyferts		
1518+407	23.12	−21.35	42.60	0.065

[a]Aboslute O Magnitude of AGN Component only; Estimate of host galaxy absolute O magnitude given in parentheses following, if available.

[b]Classification uncertain; See Table 2